THE MONITORING OF INDUCTION MACHINES USING ELECTRICAL SIGNALS FROM THE VARIABLE SPEED DRIVE

by

ABDULKARIM SHAEBOUB

A thesis submitted to the University of Huddersfield in partial fulfilment of the requirements for the degree of Doctor of Philosophy

September 2017

ABSTRACT

Induction motors are the most widely used industrial prime movers, mainly because of their simple yet powerful construction, ergonomic adaptability, rugged and highly robust structure combined with high reliability. However, under extreme and complex operations, such motors are subject to premature faults, which can be more significant when variable speed drive (VSDs) are used, due to the presence of more voltage harmonics, spikes and increases in operating temperature. In addition, VSD based systems also cause more noise in measured instantaneous current signals. These make it more difficult to investigate and accurately diagnose system faults in order to keep VSD based motors operating at an optimal level and avoid excessive energy consumption and damage to system.

However, insufficient work has been carried out exploring fault diagnosis using terminal voltage and motor current signals of VSD motors which are increasingly used in industry. To fill these gaps, this thesis investigates the detection of stator and rotor faults (i.e. shorted turn faults, open-circuit faults, broken rotor bars, and stator winding asymmetry combined with broken rotor bar faults) using electrical signals from VSDs under different loads and different speeds conditions.

Evaluation results show that under open loop control mode, both stator and rotor faults cause an increase in the amplitude of sidebands of the motor current signature. However, no changes were found that could be used for fault detection in the motor voltage signature with respect to open loop control mode. This is because, when the drive is in open-loop operation, there is no feedback to the drive and torque oscillations modulate the motor current only. The V/Hz ratio is kept constant even when the slip changes either due to the load or the fault.

On the other hand, the increase in the sideband amplitude can be observed in both the current and voltage signals under the sensorless control mode with the voltage spectrum demonstrating a slightly better performance than the motor current spectrum, because the VSD regulates the voltage to adapt changes in the electromagnetic torque caused by the faults. The comparative results between current and voltage spectra under both control modes show that the sensorless control gives more reliable diagnosis.

In order to monitor the condition of electrical drives accuratly and effectively, demodulation analysis such as modulation signal bispectrum (MSB) of the electrical signals from the VSDs has been explored extensively in this thesis to detect and diagnose different motor faults. MSB analysis has been shown to provide good noise reduction, and more accurate and reliable diagnosis. It gives a more correct indication of the fault severity and fault location for all operating conditions.

This study also examines detecting and diagnosing the effect of an asymmetric stator winding combined with broken rotor bar (BRB) faults under the sensorless operation mode. It examines the effectiveness of conventional diagnostic features in both motor current and voltage signals using power spectrum (PS) and MSB analysis. The obtained results show that the combined fault causes an additional increase in the sideband amplitude and this increase can be observed in both the current and voltage signals.

The MSB diagnosis based on the voltage signals is more sensitive to detect motor faults at lower loads compared with that of current signals. Moreover, this research presented a new method based on MSB sideband estimation (MSB-SE). It is shown that using MSB-SE, the sidebands due to weak fault signatures can be quantified more accurately, which results in more consistent detection and accurate diagnosis of the fault severity.

ACKNOWLEDGEMENTS

During my PhD study at University of Huddersfield, I have been fortunate to receive valuable suggestions, guidance and support from my supervisors, colleagues, family and friends.

First of all, I would like to express my deep appreciation and gratitude to my academic supervisors **Professor. Andrew Ball** and **Dr. Fengshou Gu** for their continuous support, encouragement, guidance, advice and making so many valuable experiences possible throughout the progress of this work.

Very special thanks and appreciation to my college friends at the Centre for Efficiency and Performance Engineering (CEPE) research group for their continuous support and for the unforgettable moments we spent together during last four years.

My thanks also go to the technical team for their kind help and continuous cooperation.

Last and always, special thanks extended to my family: my wife and my children: Ala, Reham and Rahma. Special and grateful thanks to my mother, brothers and sisters for their continuous support and encouragement.

Finally, I would like to thank all my relatives back home who supported me throughout my study and many thanks to all my friends back home.

Once again, thank you all very much from the bottom of my heart. without you, I could never have done it successfully.

STATEMENT OF ORIGINALITY

I hereby certify that all of the work described within this thesis is the original work of the author. Any published (or unpublished) ideas and/or techniques from the work of others are fully acknowledged in accordance with the standard referencing practices.

(***Abdulkarim Shaeboub***)

(*September 2017*)

LIST OF PUBLICATIONS

Journal Papers

1. Shaeboub, Abdulkarim, Gu, Fengshou, Lane, Mark, Haba, Usama, Wu, Zhifei and Ball, Andrew (2017). Modulation signal bispectrum analysis of electric signals for the detection and diagnosis of compound faults in induction motors with sensorless drives. *Systems Science & Control Engineering, 5 (1). pp. 252-267. ISSN 2164-2583.*

2. Lane, Mark, Shaeboub, Abdulkarim, Gu Fengshou and Ball, Andrew (2017). Investigation of reductions in motor efficiency and power factor caused by stator faults when operated from an inverter drive under open loop and sensorless vector modes. *Systems Science & Control Engineering,5(1).pp.361-379. ISSN 2164-2583.*

3. Haba, Usama, Feng, Guojin, Shaeboub, Abdulkarim , Peng, Xinyu, Gu, Fengshou and Ball, Andrew (2017). Motor current signature analysis for the compound fault diagnosis of reciprocating compressors. *International Journal of Condition Monitoring and Diagnostic Engineering Management. ISSN: 1363-7681*.

Conference Papers

4. Shaeboub, Abdulkarim, Abusaad, Samieh, Hu, Niaoqing, Gu, Fengshou and Ball, Andrew (2015). Detection and diagnosis of motor stator faults using electric signals from variable speed drives. *In: Proceedings of the 21st International Conference on Automation and Computing (ICAC). IEEE. ISBN 978-0-9926801-0-7*

5. Lane, Mark, Shaeboub, Abdulkarim, Gu, Fengshou and Ball, Andrew (2016). Investigation of reductions in motor efficiency caused by stator faults when operated from an inverter drive. In: Proceedings *22nd International Conference on Automation and Computing (ICAC). IEEE. ISBN 9781862181328*

6. Haba, Usama, Feng, Guojin, Shaeboub, Abdulkarim, Peng, Xinyu, Gu, Fengshou and Ball, Andrew (2016). Detection and diagnosis of compound faults in a reciprocating compressor based on motor current signatures. *In: COMADEM, the 29th International Congress on Condition Monitoring and Diagnostic Engineering Management, Empark Grand Hotel in Xi'an, China.*

7. Shaeboub, Abdulkarim, Lane, Mark, Haba, Usama, Gu, Fengshou and Ball, Andrew (2016). Detection and diagnosis of compound faults in induction motors using electric signals from variable speed drives. *In: Proceedings 22nd International Conference on Automation and Computing (ICAC). IEEE. ISBN 9781862181328.*

8. Haba, Usama, Shaeboub, Abdulkarim, Zainab Mones, Gu, Fengshou and Ball, Andrew (2017). Diagnosis of compound faults in reciprocating compressors based on modulation signal bispectrum of current signals. *Proceedings of 2nd International Conference on Maintenance Engineering, IncoME-II. The University of Manchester, UK.*

Awards

Best Student Paper Award in the *21st International Conference on Automation and Computing (ICAC) IEEE (2015).*

- Shaeboub, Abdulkarim, Abusaad, Samieh, Hu, Niaoqing, Gu, Fengshou and Ball, Andrew (2015) Detection and diagnosis of motor stator faults using electric signals from variable speed drives. *In: Proceedings of the 21st International Conference on Automation and Computing (ICAC). IEEE. ISBN 978-0-9926801-0-7*

TABLE OF CONTENTS

LIST OF FIGURES

LIST OF TABLES

LIST OF ABBREVIATIONS

AC	Alternating Current
ACIM	Alternating Current Induction Motor
AFD	Adjustable-Frequency Drive
AM	Amplitude Modulation
ASD	Adjustable Speed Drives
BRB	Broken Rotor Bar
CBM	Condition Based Monitoring
CF	Crest Factor
CM	Condition Monitoring
CSI	Current Source Inverter
DAS	Data Acquisition System
DC	Direct Current
EMF	Electro-Motive Force
Enc	Encoder
FDA	Frequency Domain Analysis
FFT	Fast Fourier Transforms
FI	Fault Indicator
FM	Frequency Modulation
FT	Fourier Transforms
HOS	Higher Order Spectra
Hz	Hertz
IAS	Instantaneous Angular Speed

IGBT	Insulated Gate Bipolar Transistor
IMs	Induction Machines
K	Kurtosis
kW	Kilo-Watt
Ls	Left Sideband
MCSA	Motor Current Signature Analysis
MMF	Magneto Motive Force
MRAS	Model Reference Adaptive System
MSB	Modulation Signal Bispectrum
MSB-SE	Modulation Signal Bispectrum and Sideband Estimator
NEMA	National Electric Motors Association
OP	Open Loop
PID	Proportional Integral Derivative Controller
PM	Preventive Maintenance
PPR	Pulse Per Revolution
PS	Power Spectrum
PV	Peak Value
PWM	Pulse Width Modulation
QPC	Quadratic Phase Coupling
RMS	Root Mean Square
RPM	Revolution Per minute
Rs	Right Sideband
SCR	Silicon Controlled Rectifier
SF	Stator Fault

SFOC	Sensorless Field Oriented Control
SL	Sensorless
TMD	Time Domain Analysis
VFD	Variable Frequency Drive
VSD	Variable Speed Drive
VSI	Voltage Source Inverter

LIST OF NOMENCLATURE

D_b	Ball diameter
D_p	Pitch diameter
L_{lr}	Rotor leakage inductance
L_{ls}	Stator leakage inductance
L_m	Motor mutual inductance
L_{ms}	Magnetising inductance for a stator winding
L_r	Rotor inductance
L_s	Stator inductance
p	Number of pole pairs
R_r	Rotor resistance
R_s	Stator resistance
T_e	Electromagnetic torque
T_l	Load torque
T_r	Rotor time constant
f_b	Ball fault frequency
f_c	Cage fault frequency
f_i	Inner race fault frequency
f_r	Rotor frequency
f_s	Fundamental supply frequency

f_F	Fault frequency
f_o	Outer race fault frequency
f_t	The frequency components due to the shorted turns
i_s	The stator current
i_r	The rotor current
i_{ds}	The *d* axis stator phase current
i_{qs}	The *q* axis stator phase current
m	The harmonic order
N_b	The number of rotor bars
n_r	Rotor speed
n_s	Synchronous speed
s	Motor slip
u_{sd}	The *d* axis stator phase voltage
u_{sq}	The *q* axis stator phase voltage
θ_r	Angular position of the rotor with respect to the stator reference
φ_m	The air gap flux
$\omega_s=2\pi f_s$	Supply angular speed
ω_b	The motor base angular frequency
ω_r	The rotor base angular frequency
σ	Motor leakage coefficient

α_I	The phase angle between voltage and current
α_Ψ	The phase angle between the stator flux and voltage
Ψ	The angular displacement
ψ_s	Stator flux
ψ_r	Rotor flux
β	Contact angle

Chapter 1

Introduction

This chapter provides an introduction to the research background in association with the work presented in this thesis. It describes the research background, introduces common techniques of condition monitoring and presents the motivation for pursuing this research. In addition, the aim and research objectives are given in detail. Finally, it outlines the organisation of the thesis.

1.1 Background and Motivation

Condition Monitoring (CM) began to be widely used during the 1960's and since then the technology has developed rapidly [1]. By using an online CM procedure, adequate warning of deterioration of plant and machinery can be given in order to plan maintenance needs [2]. CM is most frequently used as a predictive or condition based maintenance technique as this can provide early warning of potential failure with the opportunity of organising avoidance strategies to minimise lost time and unexpected costs, thus greatly improving manufacturing efficiency [3, 4].

Electrical drives are the majority of industrial prime movers and are the most popular because of their reliability and simplicity of construction. However, although AC induction motors are reliable, they are prone to various faults related to their functionalities and operational environments. According to published surveys induction motor failures include bearing failures, stator faults, broken rotor bars and end ring faults [5-9]. Such faults can cause not only the loss of production, but even catastrophic incidents and additional costs. Therefore, efficient and effective CM techniques are actively studied to improve the detection of faults at an early stage in order to prevent any major failure of the motors [10-12]. Different methods for fault identification have been developed and used effectively to detect machine faults at different stages using different machine variables, such as current, voltage, speed, efficiency, temperature and vibration.

The main target of fault detection and diagnosis is to ensure the success of the planned operations by providing information that recognizes and indicates anomalies of system behaviour. This information not only keeps the operators better informed of the status of the system, but also assists them in taking appropriate remedial actions to eliminate any abnormal system behaviour. The success of fault detection and diagnosis process is fundamentally related to the available information, the features contained in the information, and the technique with which those features are evaluated.

Many applications of induction motor driven systems require accurate speed regulation and good dynamic response to different loads and speed operational conditions. This generates a requirement for variable speed drives (VSDs) which are increasingly used in industry for obtaining better dynamic response, higher efficiency and lower energy consumption, but require more complex closed loop speed/torque control systems. Different speed control schemes are offered in the market [13, 14]. Options vary depending on the requirements of each application.

The control of induction machines can be divided into scalar and vector control. The most common scalar control method is the open loop (Volts/Hz) control. This control strategy yields inferior performance compared to the vector control strategy. However, scalar control is easily implemented. The fundamental idea of scalar control is to keep the ratio between voltage and frequency applied to the induction motor constant [15]. This constant ratio of Volts/Hz results in a constant air gap flux and consequently a constant torque for constant magnitudes of stator and rotor currents for operating frequencies from zero to the rated frequency.

On the other hand, closed loop schemes, with speed feedback measuring devices, provide accurate speed regulation. For some applications vector control schemes allow for optimum dynamic performance when necessary, with or without speed measuring, (sensorless), feedback devices [16]. Sensorless VSDs are widely utilised in many industrial applications. The sensorless drive is considered in this thesis as it is very commonly used in industry. However, closed loop and field oriented control, either with speed feedback sensors or sensorless, are all based on feedback regulation, and electrical faults in induction motor under closed control modes can have nearly the same effect on them [16]. VSD control provides accurate steady state and stable transient operation [17, 18].

Technological development has advanced CM making it more effective, i.e. electrical signal data collection and analysis using higher order spectra (HOS). HOS are useful signal processing tools that have shown significant benefits over traditional spectral

analyses. HOS have unique properties of nonlinear system identification, phase information retention and Gaussian noise elimination, thus HOS analysis has received substantial attention [19]. Studies such as [19] have researched the use of motor current signal analysis (MCSA) for the diagnosis of numerous different faults. Gu et al., have shown that in reciprocating compressors, suppressing random noise using the modulation signal bispectrum (MSB), which is an extension of CB for analysing modulation signals, has resulted in more accurate diagnosis than provided by the power spectrum (PS) [19].

Few reports have been found in the literature exploring the diagnostic performance of voltage and motor current signals using motors with VSDs. Possibly because VSD systems can induce strong noise components in voltage and current measurements. This research focuses on evaluating the data available from an AC three phase asynchronous squirrel cage induction motor control system and investigates the use of control parameters as a source for CM.

1.2 Research Scope

This research presents comparative results between the performance of motor current and voltage spectra in detecting induction motor faults with different degrees of severity under both the open loop and sensorless control (closed) modes. The results are obtained from common spectrum analysis applied to signals from a laboratory experimental setup operating under different loads and different speeds. Experimental tests are undertaken based on a 4 KW transmission system to replicate real common faults with different degrees of severity: open circuit fault, inter-turn short fault, broken rotor bar and a combination of faults. This research also examines the effect of asymmetric stator winding on the diagnosis of broken rotor bar faults under sensorless (closed-loop) operation mode. It examines the effectiveness of conventional diagnostic features in both motor current and voltage signals analysis using the MSB and PS.

1.3 Research Aim and Objective

1.3.1 Research Aim

The aim of this research is investigate the detection and diagnosis of induction motor faults using electrical signals from a variable speed drive system based on higher order spectra analysis.

1.3.2 Research Objectives

Objective 1. To develop a three phase induction motor test facility capable of simulating a range of motor faults of varying degrees of severity and obtain relevant experimental data. To change the open loop configuration of the test rig into a closed loop configuration in order to increase the system performance and accuracy of the test results.

Objective 2. To investigate the effect on the performance of a three phase squirrel cage induction motor with; broken rotor bar; stator faults; and stator winding asymmetry combined with a broken rotor bars. This will be achieved by reviewing the causes and effects of these faults up to and including failure mode.

Objective 3. To investigate the capability of electric signals from the VSD for detection and diagnosis of induction motor faults with a high degree of accuracy.

Objective 4. To apply and investigate the use of signal processing methods and techniques to collect data and attempt to detect, diagnose and assess the relative fault severity of the seeded faults.

Objective 5. To apply more advanced signal processing techniques to extract weak fault signals from noise contaminated current and voltage measurements using sensorless drives.

Objective 6. To present a new method for combined fault detection of stator winding asymmetry and broken rotor bar based on MSB-SE analysis of motor current and voltage signals with different degrees of severity and under sensorless control (closed) mode.

Objective 7. To provide useful information and guide lines for future research in this field.

1.4 Organization of the Thesis

This thesis is organised into nine chapters. The following is a brief overview of each chapter: The first chapter, this chapter, contains background, motivation and title of the research topic, the research aims and objectives and an outline of the thesis.

Chapter 2 - provides a review of literature relevant to this area of research. The literature review gives a brief background to induction motor electrical and mechanical construction, contains an overview of CM, describes the different types of CM systems and fault detection techniques used for AC induction motors. Fault detection techniques for AC induction motors with a variable speed drive system are presented in this chapter.

Chapter 3 - gives a brief background of the theory of the induction motor and its principles of operation; the motor's induced fields, motor slip and motor loads. Following this, operation of modern inverter control systems including open-loop and closed-loop will be detailed, from basic six-step inverters through to pulse-width-modulated sensorless vector units and then to devices operating in sensorless control mode using a model reference adaptive system.

Chapter 4- focuses on a review of different faults commonly occurring in three phase induction motors and the effects of those faults on the motor signals. Conventional diagnostic techniques such as time and frequency domain analysis are presented. Starting from an explanation of the basics of time domain analysis and this chapter discusses the uses of time domain analysis for data collection with respect to voltage and current, using such measures as: RMS, crest factor, kurtosis. The chapter also describes HOS techniques such as modulation signal bispectrum (MSB) and intruduces the modulation signal bispectrum based sideband estimation (MSB-SE) which leads to more consistent and accurate diagnosis of the fault and fault severity when applied to either motor current or voltage signals from a VSD.

Chapter 5 - starts with a detailed description of the experimental facilities required and the test rig. The details of control systems, measuring equipment and sensors,

data acquisition system and application software are presented. Finally, the chapter describes motor fault seeding by explaining each fault.

Chapter 6 **-** describes the use of open loop control and sensorless control applied to MCSA and voltage signature analysis, and then it presents the results of the measurements made both in the form of tables and graphs. Experiments are performed with variable load, with different motor conditions and data collected using a Sinocera YE6232B high speed data acquisition system (DAS). Signal processing and analysis techniques are applied to motor current and voltage signals with respect to Volt/Hz (open loop) control and sensorless control. The baseline data is compared with the corresponding data from tests of the motor with seeded faults, which include stator and rotor faults. The results for open loop and sensorless control are compared. It is shown that both current and voltage signatures from the sensorless control mode can be more effective and powerful in identifying the faults.

Chapter 7 - explains a method for detecting and diagnosing stator faults with different degrees of seveverities, based on MSB analysis of motor current and voltage signals under sensorless control mode. The results of motor current and voltage signals using MSB analysis are compared.

Chapter 8 **-** presents a new method based on MSB analysis of motor current and voltage signals for detection of a combination of faults; stator winding asymmetry and broken rotor bar with different degrees of severities, under sensorless control mode. The results of motor current and voltage signals analysis using PS and MSB methods are compared. The MSB has very effective noise reduction more than that of PS. In the PS the faults show as asymmetric sidebands around the supply frequency. These sidebands can be quantified more accurately using a new MSB-SE estimator, which results in more consistent detection and accurate diagnosis of the fault severity [20].

Chapter 9 **-** presents the conclusions for the research and provides an overview of the main achievements of the work described in the thesis. In addition, an explicit

summary of the novelty of the research conducted by the author is detailed. Finally, recommendations for future work on the CM of induction motor are given.

Figure 1.1 outlines the general structure of the research work and the scheme developed.

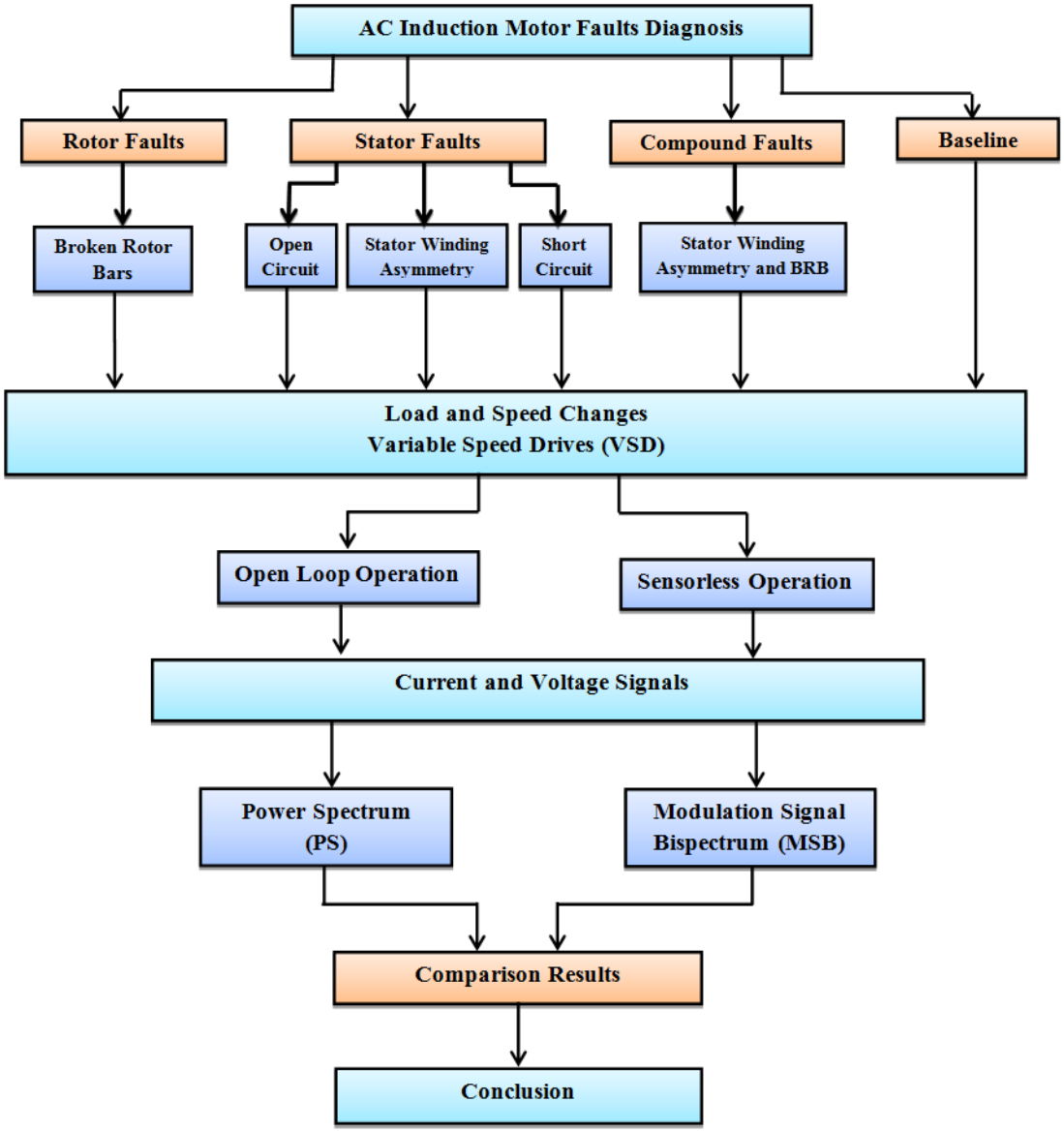

Figure 1.1 Research work scheme flowchart

Chapter 2

Condition Monitoring of Electric Motors

This chapter begins by introducing the AC induction motor, its components and common faults that arise in its operation. Then it provides a review of the literature on condition monitoring, describing the different types of condition monitoring systems and fault detection techniques that have been applied to AC induction motors, including those driven by variable speed drive systems.

2.1 Introduction to the Induction Motor

The three-phase electric induction motor is an electromechanical machine designed to convert electrical energy to rotational mechanical energy at its drive shaft. Induction motors have been, and still are used as the prime movers for many different kinds of equipment such as pumps, gearboxes, mills, fans, conveyors and compressors in industry at large [21]. The squirrel cage induction motor is simple, rugged, highly reliable, easy to maintain, acceptably efficient and relatively cheap, making it the most used machine in the manufacturing sector [22].

2.2 Induction Motor Components

2.2.1 The Stator

The stator is composed of three parts: frame, laminated core and windings as shown in Fig. 2.1. The frame mechanically supports the stator and the rotor shaft bearings. The windings are insulated copper wire and inserted into slots in the stator laminations and provide a route for the AC current which, in turn, produces the magnetic field that causing the rotor to rotate. The slots have insulation between the windings and the steel laminations [23]. The sequence and orientation with which the stator is wound determines the number of poles (stator magnets) and hence the speed of rotor shaft rotation [21]. The windings are designed to provide the output and speed required and to tolerate a large start up current for a short period of time during the motor's acceleration to full speed. The stator winding is always an asymmetric arrangement producing equal pairs of south and north magnetic poles. The ends of the winding are brought out through the motor casing to terminals inside a terminal box which is mounted on the frame. This is where the main leads are connected to the mains supply. The space between stator and rotor is termed ‘‘airgap’’ [23].

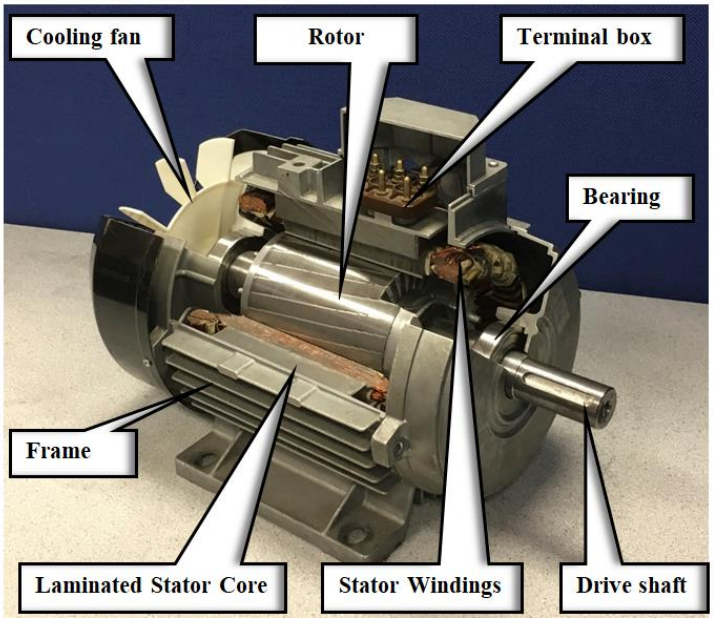

Figure 2.1 typical small induction motor

2.2.2 The Rotor

Rotor is the part that converts electrical energy to mechanical energy. Most electric power is distributed as three-phase AC. The main part of the rotor is the squirrel cage, which is composed of bars and two end rings as shown in Fig. 2.1. The electric current flows from one side to the other of the squirrel cage. The bars envelope by a laminated iron core, which concentrates the magnetic flux from the stator windings in the rotor. This lamination supports the rotor shaft mechanically. The bearings on both ends of the rotor shaft support the shaft and enable it to rotate and spin freely inside the stator [3].

2.3 Induction Motor Faults

The induction motor is commonly described as the workhorse of industry, mainly because of its simple yet powerful construction, ergonomically adaptable and, with a rugged and highly robust structure, it offers the valued characteristic of reliability. However, such motors are prone to various faults related to their functionalities and

operational environments and so efficient and effective CM techniques are required to detect the faults at an early stage to prevent any major failures on motors [10, 11].

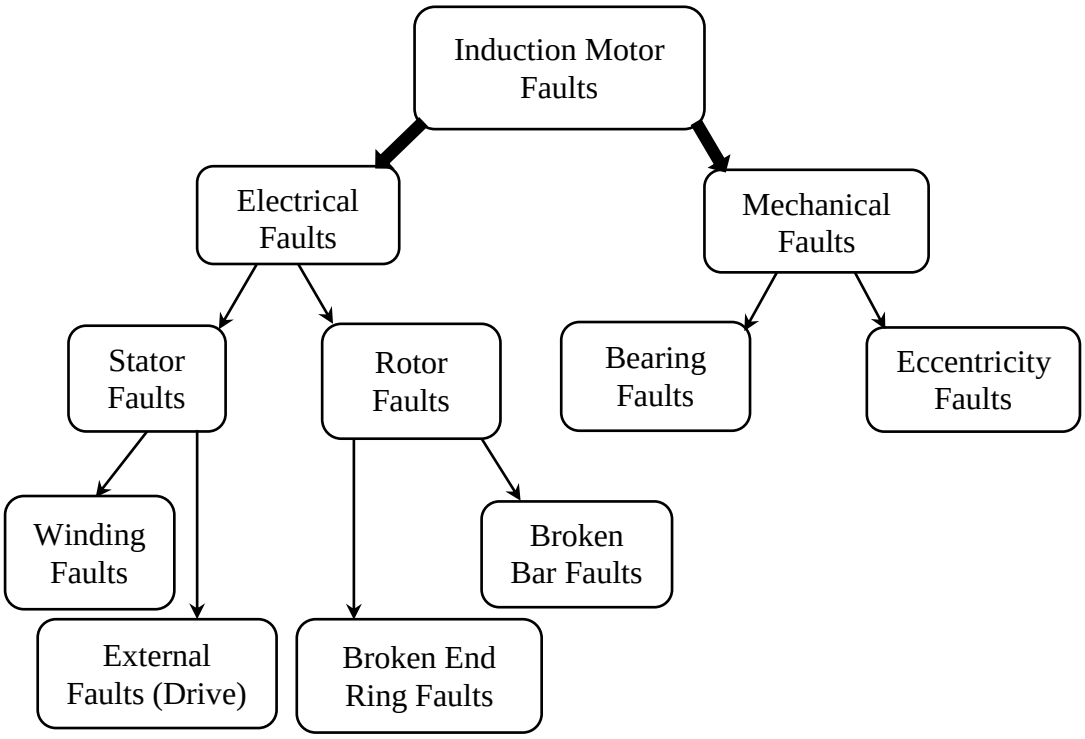

Figure 2.2 Classification of induction motor faults [24]

The taxonomy of the faults that occur in three phase induction motors has been divided into two major categories; Mechanical faults and Electrical faults. The diagram above shows the division and the hierarchy of the faults that occur in each highlighted category [24, 25].

It is necessary to know the relative impact of these faults in terms of real industrial scenario, so that any research emphasis can be concentrated where it would be most useful. The pie chart shown in Fig. 2.3 gives a brief but useful illustration of how the faults that occur in industry are divided. According to [7, 26, 27] bearing faults have been shown to be the most frequent faults in induction machines followed by stator faults and then rotor faults.

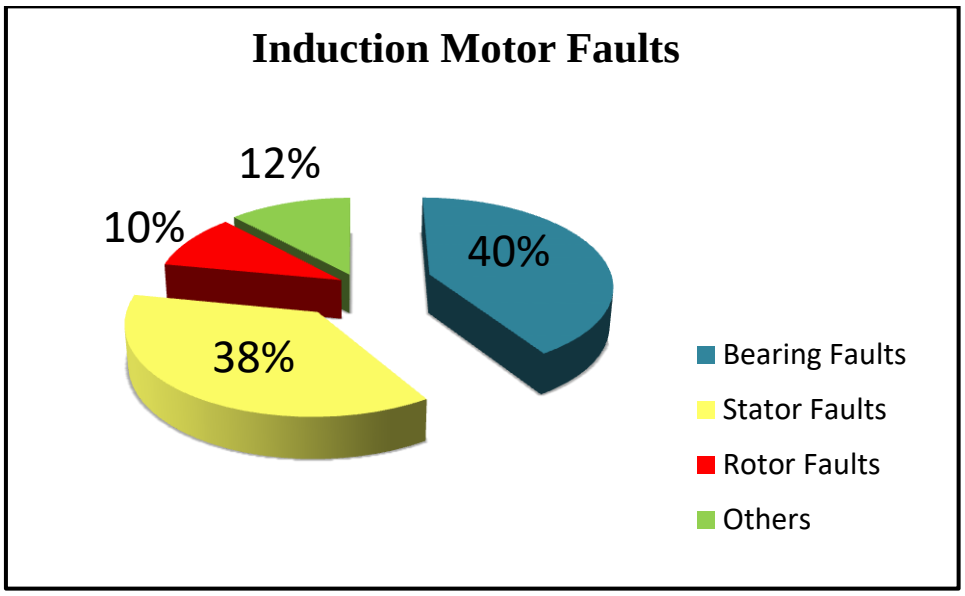

Figure 2.3 Motor faults distribution [7]

2.4 Condition Monitoring of Induction Machines

CM began to be widely used during the 1960's and since then the technology has developed rapidly [1]. CM is most commonly used as a predictive or condition-based maintenance technique. This technique can provide early warning of potential failure, thus it can provide opportunity of organising avoidance strategies to minimise lost time and unexpected costs, thus greatly improving manufacturing efficiency [3]. There are lots of publications, books and journal papers on CM [28].

CM is an observational activity, which can be performed both manually and automatically. CM is used to assess the condition of a machine's health and, potentially, predict when failure will occur. It should be applied only where the detection methods are reliable and the cost of monitoring is a fraction of the resulting plant reliability benefit. The most frequent used of CM as a predictive or condition-based maintenance technique. However, there are other predictive maintenance techniques that can also be used, including the use of the human senses (look, listen, feel and smell) [22].

CM of electric motors utilises the fact that every electric motor possesses a characteristic signature when operating normally and when this signature changes, even in a very small way, it may indicate the inception of a failure mode. Unfortunately, the small differences between normal and abnormal signatures may often be hidden in the noise in the system [29]. However, modern transducers and associated signal analysis techniques can now discriminate between truly random variations and significant trends. In this case the knowledge of the system parameters and normal characteristics are used to predict the likely time to failure [30].

The advantages of implementing a CM system in industry are; CM of machinery can make significant savings by allowing necessary repair/replacement work to be carried out at a convenient time. CM can enable the early detection and avoidance of potentially catastrophic faults, which could be extremely expensive if they occurred. CM allows the implementation of condition based maintenance rather than periodic or failure based maintenance, thus plant operating time can be saved. Modern CM techniques including advanced computerised signal processing and data acquisition systems have made monitoring and diagnostic systems accessible to all industrial production processes. These techniques are used to detect, diagnose and localise faulty operating conditions at an early stage in order to prevent system failure, and allow predictive and condition oriented maintenance [22]. A standard structure for engineering monitoring and diagnosis is shown schematically in Fig. 2.4.

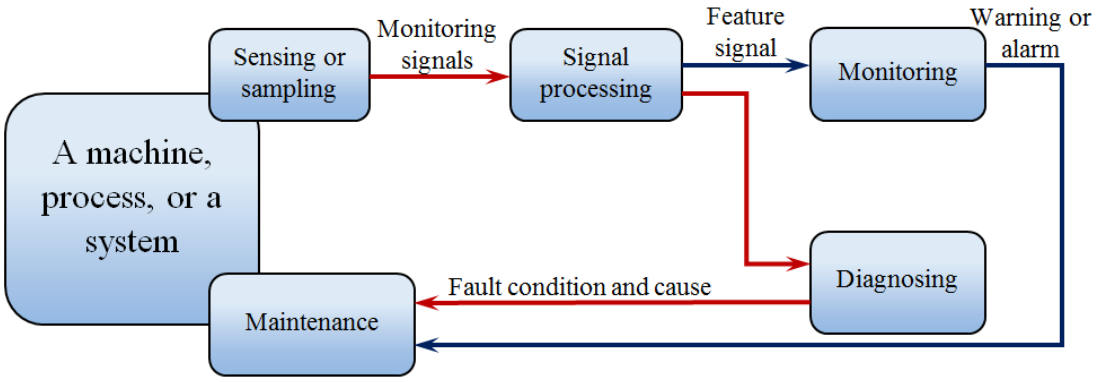

Figure 2.4 Schematic representation monitoring and diagnosis in process engineering [31]

Fig. 2.4 shows a system for health monitoring and diagnosis using the signals from sensors attached to, say, a process engineering machine. Sensor signals are invariably affected by noise, and signal processing techniques must be used to extract and capture the features from the signals. The signals come from the measurement of different features of the machine, these features can include surface vibration, sound pressure levels, acoustic emission, motor current, voltage, force, temperature and pressure.

Changes in the machine's condition are observed and diagnosed by determining variations in the sensor signal. For example, any change caused by electrical faults (such as a short-circuit) may results in unwanted increase in temperature of the machine cover or motor. However, it is also possible that the problem might be mechanical, such as a scratched bearing or misaligned shaft. Noise is not the only factor which affect sensor signals. working conditions also may have a large effect. Load and rotational speed of a motor are integral to the working conditions, and will invariable have a consideral impact on the measured sensor signals. power supply fluctuation can be also create noise disturbances [31, 32].

2.5 Condition Monitoring Techniques

2.5.1 Visual Inspection

Trained operatives use their human senses to monitor machines (e.g., visual inspection , listening to the machine and touching the machine) and can detect many indicators of a faulty condition (for example, machine temperature, level of vibration, etc). This technique is flexible and easy to use, and provides instant assessment of the general condition of a working system. However, the main drawback of using human senses is that it depends on the experience and skill of the individual inspector, and so different people can come to different conclusions. These basic skills can be enhanced by using devices such as stethoscopes [31, 33]. Generally, the cost of this method is

very low compared with alternative CM techniques and it has proved very useful for detecting simple faults like cracks, corrosion, overheating and leakage [34].

2.5.2 Vibration Analysis

Vibration generally exists in all rotating equipment, including even new and completely healthy machines [35]. Higher level and increasing vibration is usually linked to potential problems with the machine. Many researchers have performed much work using vibration analysis to detect faults occurring in electrical drives.

Ellison and Moore [36] performed research about the sources of noise and vibration in rotating electrical machines and demonstrated how different machine conditions influence the noise and vibration of the machine. They also discussed the measurement methods for machine noise and vibration and gave some suggestions on how to reduce machine noise.

In practice accelerometers are often used as the sensors to obtain vibration waveforms, the analysis of which may lead to detection of incipient fault conditions. These signals are analysed using different signal processing techniques, the simplest of which are the peak, root mean square (RMS) values and variance in the time domain, and power spectrum analysis in the frequency domain [37]. Time-frequency, wavelet and higher order spectral (HOS) analyses of the vibration signal are analysis procedures recently introduced to investigate machine conditions.

Rehab, et al., [38] studied mechanical faults in roller bearing using vibration measurements, under conditions of increasing radial clearance for the inner and outer race. This study used higher order statistical analysis. Results presented by [38] using the MSB confirmed that fault frequency amplitude not only changed with fault severity but was also influenced by the change of radial clearance as result of change in load zone angle.

Vibration monitoring is not adequate as an all-purpose tool for CM. Some types of machine faults may not produce significant changes in vibration signatures compared with the baseline vibration signal. The overall vibration signal from a machine is the sum of vibration in many components and even of the structures to which it may be coupled. However, mechanical defects generate vibration signals at particular frequencies, which can often be related to specific machine fault conditions [22]. In general, any type of machine fault results in variation in mechanical and electrical forces with the degree of variation dependent on the nature and intensity of the fault.

2.5.3 Instantaneous Angular Speed

A few machine components rotate at a notionally constant angular speed; their speed fluctuations can be detected by the use of an angular encoder. In theory changes in the instantaneous angular speed (IAS) of the rotor should reflect changes in the condition of the machine [39].

Ben Sasi, et al., [40] investigated the use of the IAS monitoring of electric motors. Results presented in [40] shown that, the power spectrum of the IAS signal could be used for the diagnosis of broken rotor bar. The key features in that case were the pole pass speed sidebands around the rotor speed components. These sidebands can be detected under higher load as in vibration signature monitoring. The main drawback of this technique is that it is complicated to use [41].

2.5.4 Acoustic Monitoring

Acoustic technology has been developed to include the field of CM. Acoustic analysis is now a recognised technique for non-destructive testing. This approach concentrates on the analysis of acoustic or noise waveforms produced by machinery processes. Microphones are often used to pick up acoustic signals to be compared against vibration-monitored waveforms. Microphones are sensitive, easy to mount and possess wide frequency response ranges that can give appropriate and comprehensive information [21]. However, because other similar machines in the vicinity also

generate airborne noise, the acoustic waveforms can be contaminated by noisy background signals. Other adverse effects include interference from other related sound sources such as the driving motor, loading generator and cooling fan, and reflecting surfaces [22].

2.5.5 Temperature Monitoring

Temperature is a basic and generic parameter used as a warning of motor fault conditions. It can be measured using simple and cheap thermocouples plugged into hand-held devices. Monitoring different signatures will provide machine thermal patterns which can indicate machine health. Thermography is a more advanced temperature-based monitoring technique that can be used to monitor the temperature of individual external and internal components using a special hand-held camcorder displaying real-time temperature maps [2].

Temperature at a signal sensor point, is usually easy to measure and will provide important local information. However, there is an important difficulty when monitoring the overall temperature of the machine, whole body temperature measurements run the risk of amalgamating local hot spots into a single, overall measurement [14].

2.5.6 Electrical Signature Analysis

Plant CM techniques including vibration monitoring, thermal analysis and acoustic monitoring; these techniques are often both capital and labour intensive [22, 42]. The high cost of implementing and operating these techniques frequently limits their use to critical machines within the factory. Motor current signature analysis (MCSA) presents a potential breakthrough with its ability to detect and quantify mechanical defects and degradations in electromechanical equipment, and unwanted changes in process conditions, without the need for special equipment to be installed on the motor or on the electro-mechanical equipment. The only requirement is access to the supply current carrying lines, thus money and time can be saved [43]. MCSA can be

used to analyse the driven load, the power supply, and perform a quick CM test of the motor or of the motor driven device [44].

MCSA uses available frequency analysis methods to diagnose current harmonic frequencies and their sidebands that can uniquely identify the presence of particular faults. MCSA has been found to be more effective and efficient in the monitoring of a number of motor faults including air-gap eccentricity, bearing damage, broken rotor bar and turn-to-turn shortage faults in the stator. Studies by Sharifi and Ebrahimi [45] combined MCSA with an examination of rotor slot harmonics to diagnose inter-turn-short circuit faults in motor stator windings on non-inverter driven motors. Vamvakari [46] and Kersting [47] have shown that the performance, efficiency and life of induction motors can be considerably affected by the quality of the power supply.

Messaoudi and Sbita [48] used MCSA for the diagnosis of multiple faults in an induction motor. These experiments [48] helped justify the claims that MCSA is one of the most efficient techniques for the diagnosis and the localization of multiple faults both electrical and mechanical, in which failures become apparent by harmonic modulations around the supply frequency. However, the signal amplitudes obtained from spectrum analysis include additive random noise and ignore phase information. Messaoudi and Sbita did not use HOS or other technique which allowed the retention of both amplitude and phase information while suppression of random noise.

HOS are useful signal processing tools that have shown significant benefits over traditional spectral analyses because HOS possess the unique property of nonlinear system identification, phase information retention and Gaussian noise elimination [19, 49]. Thus, HOS analysis has received a lot of attention from researchers. Gu, et al., [19] used bispectrum analysis to identify and quantify induction motor faults in a two stage reciprocating compressor. A modified bispectrum based on the amplitude modulation features of the motor current signal was developed to consider both lower and higher sidebands, and this was found to characterise the current signal more accurately. The result showed that conventional bispectrum analysis does not

adequately represent a motor current with amplitude modulation (AM) features because conventional bi-spectrum analysis cannot include two or more pairs of sidebands simultaneously, nor the random variation of sideband phase. MCSA has also been used to detect faults in downstream equipment such as gear transmission systems [50] by examining the supply current using a novel modulation signal bispectrum (MSB) method. Both gear faults and shaft misalignment have been detected using this technique.

Alwodi, et al., [51] provides details of the application of MSB analysis to motor current signals to diagnose and enhance feature components for the detection and diagnosis of stator faults. Although this work represents important progress, the effect of closed-loop VSD systems on the power supply parameters (i.e. both the current and voltage), were not examined in the case of stator faults.

More details on current signature analysis have been presented in [52] on a new, improved, method for broken rotor bar (BRB) diagnosis based on MSB analysis. The current signals obtained from a healthy machine and one with a BRB are described and explained. The theoretical electromagnetic relationships of the driving motor both healthy and with a BRB fault were examined. The results demonstrated that additional current with sinusoidal waveform at frequency $2sf_s$ was found in the case of the BRB. However, because the ratio between voltage and frequency was constant during the test there was no separate voltage signature analysis.

To conclude, MCSA research has attracted extensive interest recently, however significant works is still required to evaluate proposed techniques and test their applicability to real life. Moreover, further investigation is required to extract more and better information, and remove noise from the obtained current signal using less complicated calculations and fewer resources. Additionally, the studies reviewed showed that most research has been on directly fed or open-loop controlled induction motors.

2.6 Control System Based Condition Monitoring

Most conventional CM techniques, such as those highlighted in previous section, require additional equipment such as sensors, transducers, and data acquisition systems to gather information for monitoring. These can be very expensive. A relatively skilled and trained human resource is also required to perform critical associated tasks such as mounting sensors and wiring them, gathering, analysing and interpreting data. This way the process can become time consuming.

For effective control, AC induction motor drives, it is necessary to measure, calculate and estimate many parameters that affect the induction motor's speed; current and voltage (measured at the drive's terminals). These signals are then utilised with specific mathematical relationships to control the speed and torque. Regardless of the control techniques being used by the drive, most closed-loop drives need these signals to perform efficient control and maintain the required performance.

Any signal used within the controller may carry the feature of a certain fault. So, changes in control system behaviour can reflect the health of the system being controlled. In other words, any fault or defect in a mechanical system leads to a change in the system and the stability conditions, which appears as an observable response of the control system.

2.6.1 Fault Detection Techniques for Induction Motor Driven Systems

A large number of articles has been published on the use of different techniques and methods for the detection of mechanical and electrical faults in AC induction motor drives. All the works mentioned above focused on fault detection of induction motors directly connected to the power line supply and did not investigate the effects of closed-loop variable speed drive (VSD) systems. Little work has been found which explores the diagnostic ability of power supply parameters, i.e. current and voltage signals for induction motors with VSDs. Such investigations are doubly important,

however, because VSD systems can induce high levels of noise in voltage and current measurements.

Obaid, et al., [53] studied the detection of shaft misalignment and load unbalance based on the current in inverter driven induction motors using the open-loop control mode. The work presented in [53] also induced investigating the detection of mechanical faults using frequency harmonics present in the stator current. However, the study did not consider the case of changes in supply frequency while the induction motor was in operation.

Lin Wang [54] used motor terminal voltage and current for detecting and diagnosing bearing faults with a VSD. The main idea here was to detect changes in amplitude modulation between the spatial harmonics and the supply fundamental frequency caused by the bearing faults. This study found that the controller caused high levels of noise because the VSD provides a pulsed width modulated signal source, which masked small components at bearing characteristic frequencies. Further study of MCSA with advanced signal processing analysis is required.

Detection of BRBs in a pulse-width modulated voltage source-inverter-fed induction motor are discussed in [55]. Experimental results obtained from a 3kW three-phase squirrel cage induction motor are presented. Experimental results confirm the results predicted by a simple current signal model, that a fault in a BRB introduces a frequency component onto the current signal as a sideband to the excitation frequency, and which can be used as an effective and accurate feature for recognition of the fault. The method described works well under open loop control mode, but some difficulties appear with regard to closed loop control. The authors confirmed that further research needs to be carried out regarding features, advantages, limitations, and possible improvements of the proposed techniques.

Haram, et al., [56] investigated the use of the dynamic response of the electrical signals from variable frequency drives for mechanical fault diagnosis. They claimed

that load and speed oscillations arising from different types of mechanical faults could lead to a modulation in the supply components. However, the study found that it difficult to detect faults when the VSDs operating in a closed-loop mode.

Benghozzi, et al., [57] focused on developing a new sensorless method to monitor and diagnose different faults in a gearbox transmission system based on the parameters acquired from control systems. This work confirmed that it is possible to use existing control data for monitoring mechanical faults in gearbox transmission systems.

Lane, et al., [58] used signals from a sensorless vector control drive for detecting unbalanced motor windings in an induction motor. Initial results comparing baseline and faulty data sets for two resistance placements indicated that small increases in stator resistances can be detected by observing voltage and current signals. The change also led to a slight increase in motor efficiency in the speed range below the motor rated speed, whereas there is a reduction in efficiency at the rated speed. The authors decided that more tests are required under both open-loop and closed-loop modes to confirm this result.

Abusaad, et al., [59] showed that it is feasible to use signals from a sensorless flux vector control drive for detection of misalignment faults. The misalignments cause deviations in related variables such as torque, motor current, I_d and I_q. These variables are useful in developing a model based detection scheme and identifying the optimal variables. Applying the model based method to experimental data sets from a motor gearbox drive system found that the developed model and detection approach for the variables of interest can discriminate between different misalignment severities, showing that it is feasible to use any of the torque related variables for monitoring misalignments.

Hamad, et al., [60] investigated power supply parameters from VSDs for monitoring and diagnosing mechanical faults based on a two stage helical gearbox transmission system. The study found that the stator current, voltage and power spectra showed an

increase in sideband amplitude with increase in load and fault severity, under sensorless operating mode. However, an increase in fault severity also caused an increase in noise, which in turn will cause an overlap in the signals, and this will affects detection discrimination.

2.7 Summary

The articles reviewed contained descriptions and details of numerous methods for obtaining information about the health of machinery, these included sound and vibration, instantaneous angular speed, and thermal monitoring. In the case of induction motor driven systems, motor electrical signature analysis continues to receive attention as it is readily available, in most instances, at the motor's terminals and there is no need for additional measuring devices. Detailed information about the health of the monitored system, either electrical or mechanical, can be obtained from these signals.

The literature review also showed that the use of current and voltage signals from induction motors with VSDs, which are increasingly used in industry due to their effectiveness and lower energy consumption, has been relatively neglected. Very few publications contained reports of work on the detection of stator and rotor faults (such as inter-turn short-circuit, stator winding asymmetry and BRBs) for VSD systems. The benefits of detecting such faults using sensorless measurements with VSD systems, i.e. using the same information as used by the drive's control system, and without the need for complex calculations and consumption of extra resources, are obvious. Examination of the spectra of induction motor current and voltage, locating characteristic fault frequencies, can detect unwanted changes in a machine. The spectrum may be obtained using a FFT because the fault frequencies that occur in the motor current and voltage spectra are unique for the different motor faults, this method is commonly used for the detection and diagnosis of faults in induction motors.

No work has been found describing in any detail the effectiveness of motor current and voltage signature analysis for detection and diagnosis of motor stator faults with different loads and different speeds under Volt/Hz and sensorless control mode. Also, no previously published work has reported investigating the potential for detecting and diagnosing the effect of asymmetry in the stator winding with a BRB under sensorless operation mode. In addition, no work has been found that describes MSB analysis of electric signals from VSD systems.

This research work aims to address this gap and develop a CM scheme for detecting stator and rotor faults, such as open-circuit faults, inter-turn short-circuit and stator winding asymmetry combined with BRB using electrical signals obtained from VSD induction motors.

Chapter 3

Induction Motor Speed Control Using AC Drive

This chapter gives a brief background to the theory of the induction motor, and its principles of operation; the motor's induced fields, motor slip and motor loads. Following this, the operation of modern inverter control systems including open-loop and closed-loop, is presented from basic six-step inverters through to pulse-width-modulated sensorless vector units, and then to devices operating in sensorless control mode using a Model Reference Adaptive System (MRAS).

3.1 Principles of Motor Operation

The principle on which the induction motor operates is based on the synchronous rotating magnetic field [15]. The stator is composed of three windings, each shifted electrically 120º from its neighbours, as shown in Fig. 3.1.

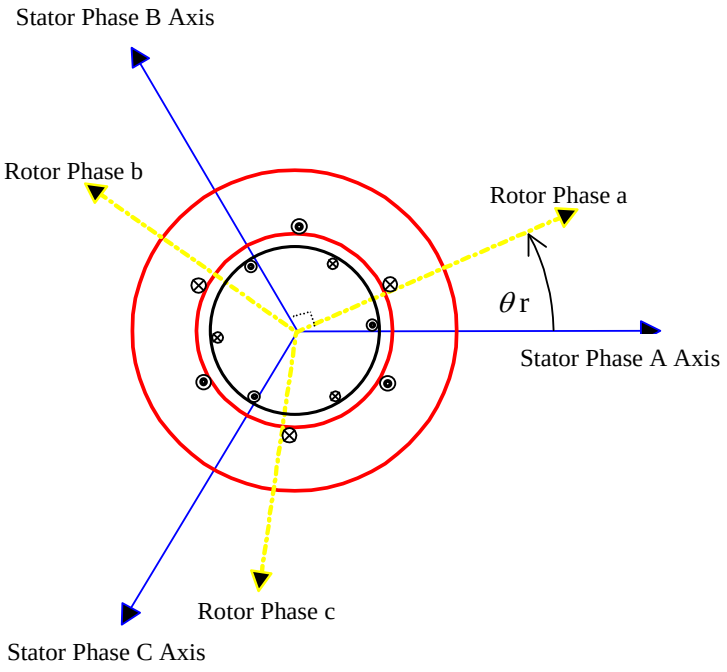

Figure 3.1 Induction motor schematic [61]

The three phase induction motor has three phase symmetrical windings in the stator, displaced by 120^o with N_s equivalent turns. The rotor also contains three phase windings, displaced by 120^o with N_r equivalent turns. Fig.3.1 shows a 3-phase stator and rotor winding, where subscripts ***A***, ***B***, ***C*** and ***a***, ***b***, ***c*** correspond to the stator and rotor three-phase supplies respectively. In the text the subscript ***s*** relates to the stator, and subscript ***r*** to the rotor.

The three phase axis of the stator and the rotor are separated by $\boldsymbol{\theta_r}$ the angle of the rotor [62]. The rotational speed of rotor w.r.t. stator is $\boldsymbol{\omega}$ [61]. Power to the motor creates an electromagnetic field in the stator windings which cuts through the air gap into the rotor windings. This way, the electromagnetic field induces a voltage in the

rotor bars, as described by Lenz's law and stimulates a current that circulates through them. Hence, another electromagnetic field is created that interacts with the electromagnetic field from the stator. The interaction between the two electromagnet fields generates a force, a rotating torque, that pushes the rotor in the direction of the resultant torque [17, 63-65]. As shown in Fig.3.2 when AC current passes through the stator windings each of the three phases will induce a magnetic field, these fields will have a phase difference of 120^{o} relative to each other.

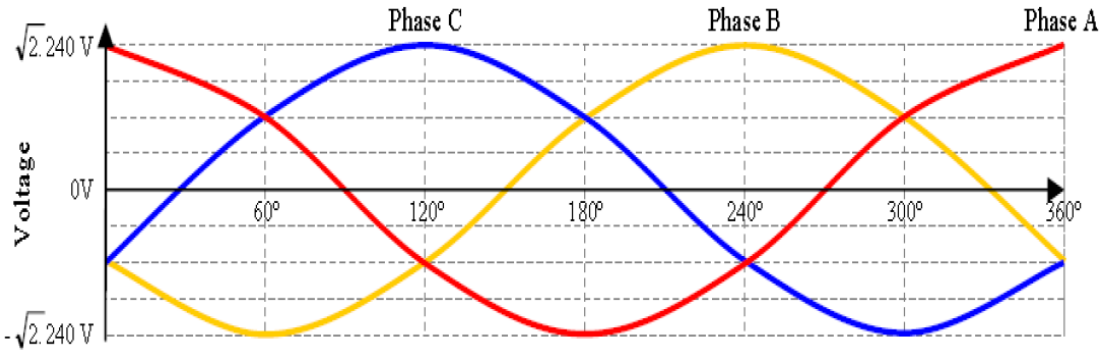

Figure 3.2 Three phase supply waveform [2]

3.1.1 Slip and Speed

The speed of the magnetic rotating field is the synchronous speed n_s (rpm), this is determined by the number of stator poles p, and the supply frequency f_s (Hz) as shown in Equation (3.1) [66]. The number of poles in a motor determines how fast the revolving field will move around the internal periphery of the motor at a given frequency. A motor with a higher number of poles will take longer to energize all the poles and will slower the revolve of the motor field at any given frequency (say at 50 Hz). The synchronous speed is the speed, usually in rpm, of the air-gap magnetic flux as it rotates in the air gap around the inner surface of the motor. In a four-pole stator, the phase groups span at angle of 90°.This is determined by the line frequency and by the number of poles of the stator winding.

$$n_S = \frac{120\, f_S}{p} \tag{3.1}$$

where, n_s is the synchronous speed (rpm), f_s is the supply frequency and p is the number of poles.

The slip, s, is defined as the ratio of the slip speed to the synchronous speed. This parameter plays an important role in the behaviour of the induction motor. The slip relates mostly to the rotor parameters on the stator side, hence it appears as a constant of proportionality in most relationships between the stator and rotor. The produced electromagnetic force tends to rotate the rotor in the same direction as the rotating stator field. The rotor accelerates until it reaches a speed near the synchronous speed but will never actually reach it. The difference between the rotor and synchronous speed is called the slip speed, see Fig.3.3. If the rotor speed is n_r, the slip speed, s_n, is given by Equation (3.2) [67]:

$$s_n = n_s - n_r \tag{3.2}$$

And $s_n = s.n_s$

It follows that the slip can be expressed as percentage [67]:

$$s = \frac{n_s - n_r}{n_s} \times 100\% \text{ or } s = \frac{N_s - N_r}{N_s} \times 100\% \text{ or } s = \frac{\omega_s - \omega_r}{\omega_s} \times 100\% \tag{3.3}$$

where ω_r, ω_s = the field and rotor angular speeds, respectively (rad s^{-1})

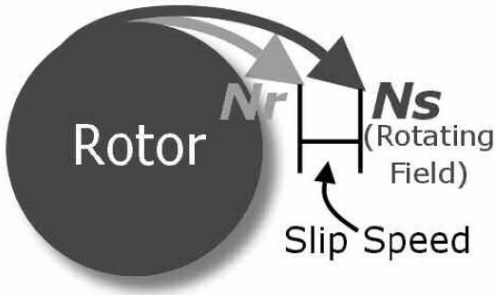

Figure 3.3 Illustration of slip speed [9]

The rotor speed is often expressed in terms of the slip and the synchronous speed, either in rpm or rad s^{-1} as [67]:

$$n_r = n_s(1-s) \tag{3.4}$$

The relative motion between the stator magnetic field and the rotor conductors induces voltages and currents in the rotor. If the rotor is locked, then the rotor will have the same frequency as the stator. On the other hand, if the rotor has reached the synchronous speed, the rotor frequency, voltages and currents will all be zero [68].

3.1.2 Motor Torque and Load Characteristics

Torque is the rotational equivalent of linear force, and is known as the turning force for rotating machinery. The unit of torque is Nm [22]. The torque developed by the induction motors varies with the motor speed as it accelerates from standstill (zero speed), to maximum operating speed. Typical torque-speed-current curves for a squirrel cage IM are shown in Fig.3.4 [14, 69, 70].

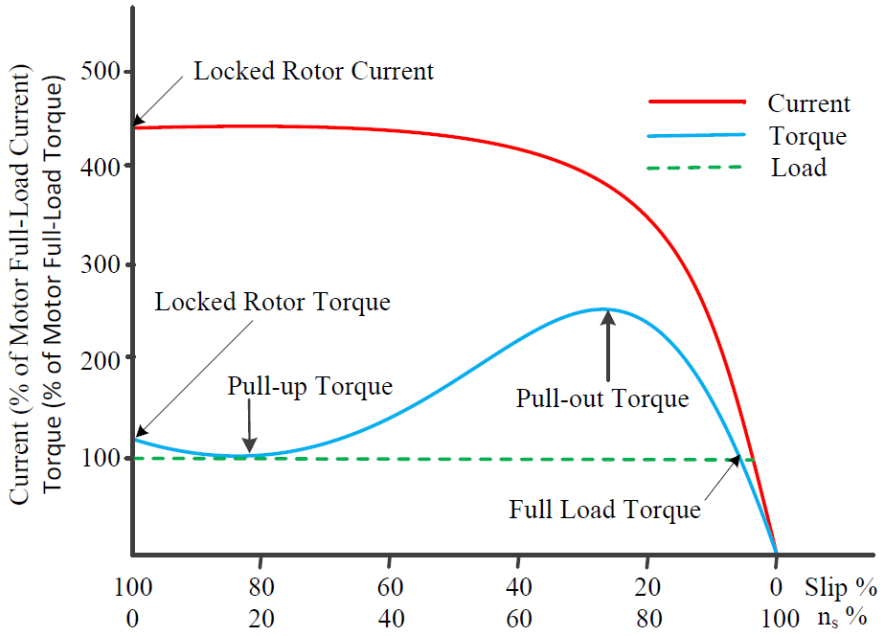

Figure 3.4 Torque-speed curve of the typical three-phase induction motor [70]

Starting of an induction motor with rated supply voltage, induce a high starting current in the rotor. This is commonly expressed as 'Locked Rotor Current'. This current induces a large amount of emf in the rotor and generates the Starting or

Locked Rotor Torque. As the rotor accelerates both the current and torque changes depending on the rotor speed, and if the supply voltage remains constant the torque reaches to its minimum value and this referred as 'Pull-up torque'. As the rotor speed increases further, at about 70% of synchronous speed, the torque reaches its maximum value, known as the pull-out, or breakdown, torque. Between synchronous speeds zero and 70% there is a gradual decrease in the current. As the rotor's speed increases further and accelerates up to the rated motor speed, with no load, both current and torque fall rapidly [17, 64].

3.2 Basic Concepts of ACIM Control Systems

An inverter-driven motor system controls the rotational speed of an AC electric motor by controlling the frequency and voltage of the electrical power supplied to the motor. The speed of an AC motor depends on three principle variables [14, 71]:

- ✓ The pole number which determines the motor's base speed.
- ✓ The frequency of the AC line voltage. Variable speed drives (VSD) change this frequency to adjust the speed of the motor.
- ✓ The amount of torque loading on the motor, which causes rotor slip relative to the synchronous speed.

For a given motor, when a continuously adjustable speed over a wide range is desired, the best method is to provide a variable frequency supply [14]. This is achieved by means of a variable frequency drive (VFD). This system is also called an inverter, an adjustable-frequency drive (AFD), an adjustable speed drives (ASD) and a variable speed drive (VSD). VSDs are widely used in all areas of industry. These include transport systems such as ships, railways, elevators, ventilation systems, conveyors; material handling plants, and mechanical equipment e.g. machine tools, extruders, fans, pumps and compressors [72].

Various types of AC induction motors are available for different applications and many methods have been investigated for monitoring their condition. This research focuses on sensorless flux vector control which is a common control scheme widely used for AC motor speed control. An introduction and a brief background are given to open-loop (Volts/Hz) control and closed-loop operation modes, which paves ways for analysis additional current and voltage signatures induced by various motor faults.

3.2.1 Influence of the open- loop (V/Hz) drive

The V/Hz induction motor drive maintains the air-gap flux constant by keeping the ratio *V/fs* constant. This aims to maintain the torque at a value given by the slip frequency, f_s-f_r , for a supply frequency of f_s. Induction motor drives normally employ pulse width modulation inverters that vary the magnitude and frequency of the output voltages. The drive continually feeds the motor with a constant V/Hz ratio, with the inverter output keeping the motor air-gap flux constant [16, 64]. Fig. 3.5 shows a simplified structure of an open-loop induction motor speed drive [64]. The air gap flux is held constant based on the following formula [16]:

$$\varphi_m = L_m \left| i_S + i_r \right| = \frac{vs}{\omega s} \tag{3.5}$$

where: φ_m is the air gap flux, L_m is the mutual inductance, i_s and i_r are the stator and rotor currents respectively, v_s is the stator voltage and $\omega_s=2\pi f_s$ is the supply angular speed.

By holding the air gap flux constant, as in Equation (3.5), the developed electromagnetic torque remains constant for a given slip value. That is, the electromagnetic torque depends mainly on slip frequency and stator flux. However, it is worth mentioning that the required terminal voltage is a function of both frequency and the load [16].

When a fault occurs in the stator and/or rotor, the air gap flux distribution is no longer balanced. This unbalanced flux causes the induced rotor current to have additional components that oscillates around the fault frequency component [73].

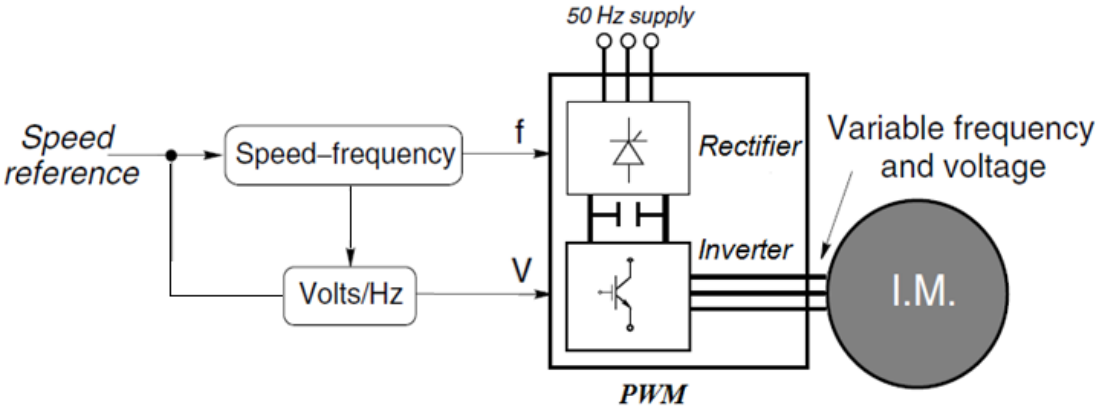

Figure 3.5 Simplified structure of the V/Hz drive [73]

However, this oscillation will also be modulated by the electromagnetic torque [16]. When the drive is in the open-loop operation, there is no feedback to the drive and torque oscillations will modulate the motor current only. The drive keeps the *V/Hz* ratio constant based on the reference speed.

To conclude, in the case of the open-loop mode, the drive keeps the voltage fixed based on the frequency requirements. The air flux will oscillate due to the presence of a fault and hence the torque will also oscillate causing changes in the slip frequency. The slip frequency will be influenced as it is sensitive to changes in electromagnetic torque, and the changes in the slip can be more dominant as the load increases.

3.2.2 Influence of the closed-loop drive

Many different schemes are used for this drive mode [64]. In this drive mode a feedback loop is used to provide better speed regulation and enhanced dynamic response. The drive used is a sensorless variable speed drive based on the Model Reference Adaptive System (MRAS). The output voltage is regulated separately using knowledge of the phase angle, while the frequency is controlled by timing the

switching of the inverter [16]. In the case of stator or rotor faults, the resistance of the stator winding is increased depending on the nature of the fault. Increasing the stator resistance further, increases the magnitude of the distortion in the corresponding output signals. Thus, the drive can use on-line stator resistance estimation for stable and effective operation of the induction motor, which includes estimators where value of stator resistance is updated.

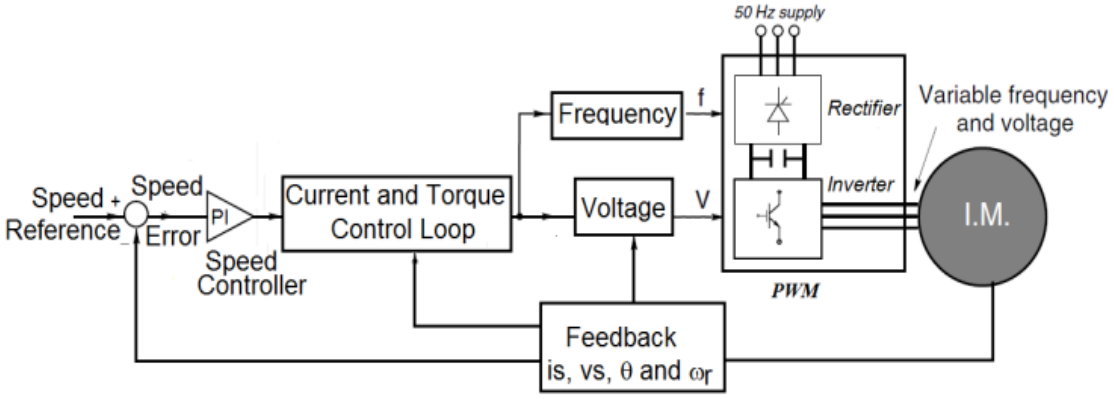

Figure 3.6 General structure of a closed-loop variable speed drive [73]

3.3 Principles of AC Variable Speed Drive System

The speed of an ACIM, generally, can be controlled by adjusting both voltage and frequency [17, 64]. The synchronous speed and slip are described by Equations (3.1) and (3.2) respectively. When the IM is supplied by a three phase sinusoidal voltage and neglecting the voltage drop across the stator windings, the magnitude of the voltage (u) can be approximated during the steady state as [74]:

$$u \approx \omega_s \psi_s \tag{3.6}$$

$$\psi_s \approx \frac{u}{\omega_s} = \frac{u}{2\pi f_s} \tag{3.7}$$

Equation (3.1) illustrates how motor speed is determined by the supply frequency, while Equation (3.7) shows that the stator flux remains constant when the voltage per frequency ratio is maintained constant [63, 74]. However, at low frequency and hence low *V/Hz* values, the voltage drop across the stator windings is considerable and needs

to be compensated. On the other hand, at elevated speeds the frequency needed is high and hence high voltage is also required to keep the *V/Hz* ratio constant. This high voltage may exceed the rated voltage values and may burn the winding insulation. In this case there is a need to break the *V/Hz* ratio rule and adjust the voltage to prevent damage. The rated voltage value must not be exceeded [74].

Principally, the AC drive changes a fixed supply voltage (V) and frequency (Hz) into a variable voltage and frequency. The output frequency determines the speed of the motor, while the *V/Hz* ratio regulates the electromagnetic torque the motor generates [17]. Fig. 3.7 illustrates the electromagnetic torque and speed of an induction motor fed with different voltage and frequency values. For a fixed current value, the electromagnetic torque of the motor is constant as long as the motor speed is less than the rated speed. This is called the constant torque region. However, in this regin the voltage, and hence the power, increases linearly with speed and the breakdown torque is constant for the entire region. When the motor speed reaches the rated value, both current and voltage level off and the electrical supply enters the constant power region. Once the voltage reaches the rated value, the breakdwon torque value is reached and torque will decrease as the speed increases [14, 65, 75, 76].

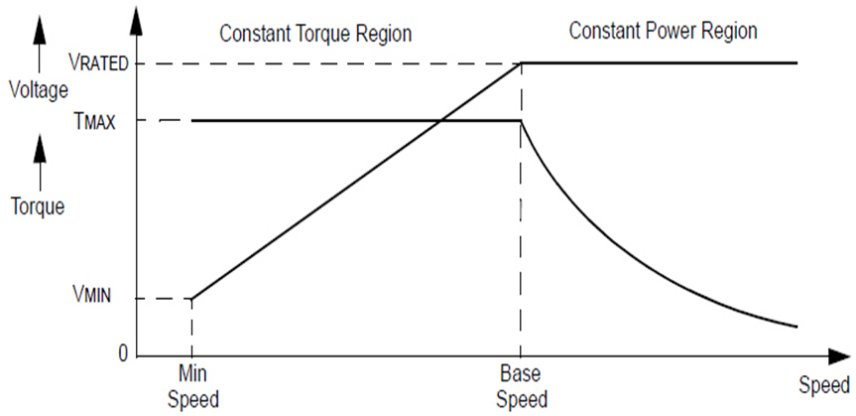

Figure 3.7 Motor torque-power characteristics [76]

Nevertheless, for every value of the frequency there will be a torque-speed curve. However, all these torque speed curves have the same breakdown torque value in the

constant torque region, see Fig. 3.8. Therefore different operating points can be found on the torque-speed curves when they cross the 100% torque level, indicating the rated torque. Fig 3.8 illustrates the motor torque curves at different supply frequencies [14, 17, 64, 77].

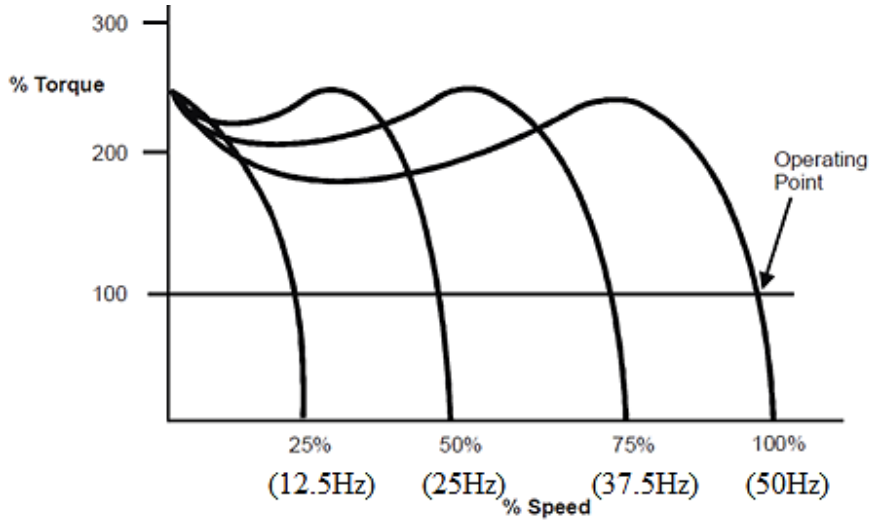

Figure 3.8 Motor torque vs. supply frequency [14]

3.4 AC Drive Technologies

3.4.1 Voltage Source Inverter

A voltage source inverter (VSI) also known as variable voltage inverter uses a silicon controlled rectifier (SCR) converter section to regulate the DC bus voltage. VVI_S have the following advantages: wide speed range, operation is independent of load, multiple motor control and simple design. The main disadvantages are: additional output harmonics are applied to the AC motor, poor input power factor, cogging below 6 Hz due to square wave output, which may cause equipment problems. The block diagram of a VSI is shown in Fig. 3.9 [14, 71, 78].

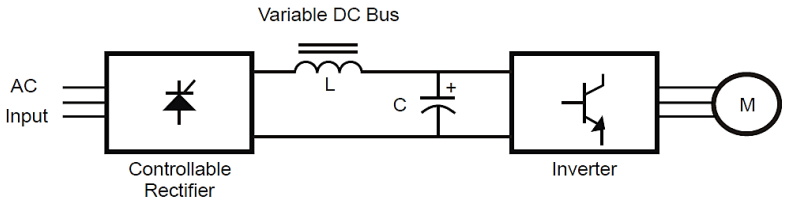

Figure 3.9 Block diagram of a typical VVI drive [14]

3.4.2 Current Source Inverter

A current source inverter (CSI), the current applied to the motor has six steps and similar to the VVI. The advantages of CSI are; higher efficiency and high power factor; simple circuit and the ability to continuously operate with a faulty device [14, 71]. The main shortcomings are; low input power factor at low speeds; limited speed range; motor cogging at low speed and generation of line spikes by the drive due to the use of silicon-controlled rectifiers (SCR) technology in the front end. Fig 3.10 below shows a typical CSI structure [14, 78].

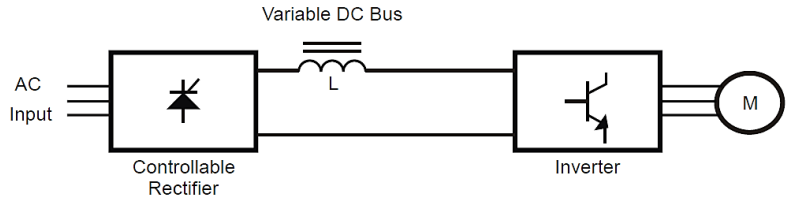

Figure 3.10 Block diagram of a typical CSI [14]

3.4.3 PWM Inverter

The pulse-width modulator (PWM) drive is an example of a VSD and consists of three main components as shown in Fig. 3.11.

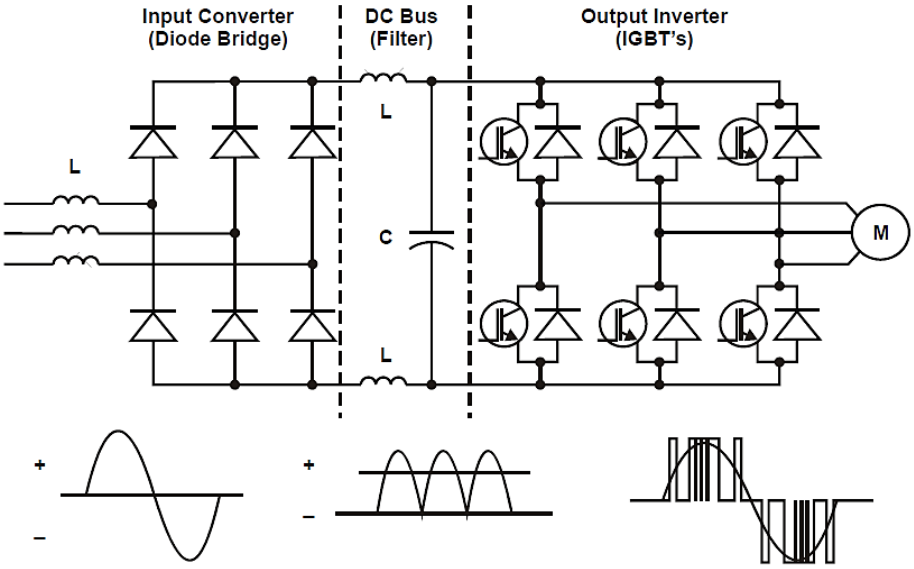

Figure 3.11 A block diagram of a PWM drive as an example of VSDs [64]

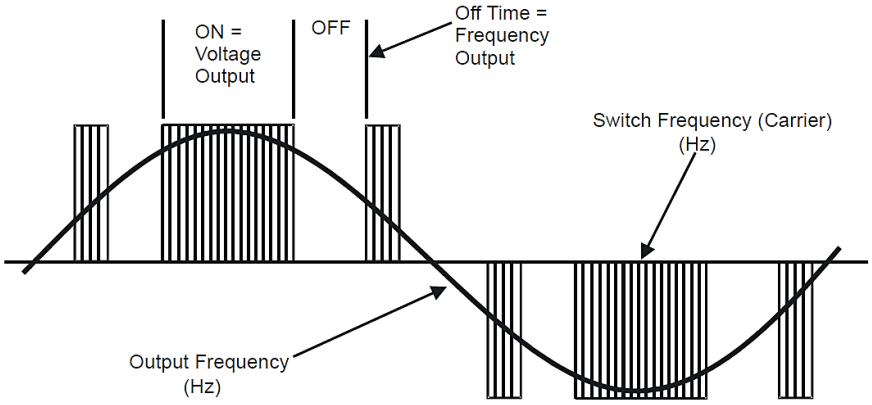

Figure 3.12 PWM inverter output switching waveform [18]

3.4.3.1 The Rectifier

The first component of all VSD's is a rectifier, or converter, shown on the left in Fig. 3.11. The three phase full wave rectifier converts the three phase voltage of the power supply into DC voltage. Although VSDs are usually supplied by a three-phase power supply, there are also AC drives supplied by single phase AC power supplies to control three-phase induction motors. Rectifiers may utilize diodes, SCRs, or transistors to rectify power [15]. One rectifier will allow power to pass through only when the voltage is positive. A second rectifier will allow power to pass through only

when the voltage is negative. Two rectifiers are required for each phase of the power. Since most large power supplies are three phase, there will be a minimum of six rectifiers used. Appropriately, the term “six pulses” is used to describe a drive with six rectifiers [79].

3.4.3.2 The DC Bus

Although the output voltage of a rectifier is notionally DC, it contains ripples. Thus, a DC bus filter uses a second stage to reduce the ripple, shown as the centre of the Fig. 3.11. The DC bus filter reduces the AC ripple voltage from the converted DC before it inters the inverter section. The DC bus filter can also include elements which impede harmful harmonic distortion that can feed back into the power source supplying the VFD [15].

3.4.3.3 The Inverter

The inverter uses three sets of high speed switching transistors to create DC “pulses” that emulate all three phases of the AC sine wave. These pulses not only dictate the voltage of the wave but also its frequency. The modern VSD inverter uses a technique known as “Pulse Width Modulation” (PWM) to regulate voltage and frequency as shown in the right of Fig. 3.11 which converts the DC voltage from the DC bus filter into a three phase balanced AC voltage [80]. The operating frequency and magnitude of this three phase AC voltage applied to the motor terminals can be controlled in order to maintain the developed torque of the motor constant from zero to the rated frequency so that the AC motor can operate in a wide range. The electronic power devices that constitute the switches in a PWM inverter for AC drives are in most cases IGBTs (insulated gate bipolar transistors) [15, 81], The IGBT can switch on and off several thousand times per second and precisely controls the power delivered to the motor. The control board in the drive activates the drive gates’ circuits turning the supply waveform positive or negative, creating the three-phase output. The amplitude of the output voltage is defined by the length of time the IGBT remains on, while the

signal frequency is controlled by the length of time the IGBT is off, as shown in Fig. 3.12 [17].

Advantages of the PWM VSDs [82]:

- ✓ Excellent input power factor due to fixed DC bus voltage.
- ✓ Highest efficiencies: between 92% and 96%.
- ✓ No motor cogging normally found with six-step inverters.
- ✓ Compatibility with multi motor applications.
- ✓ Ability to ride through a 3 to 5 Hz power loss.
- ✓ Lower initial cost.

The disadvantages of PWMs [82]:

- ✓ Motor heating and insulation breakdown in some applications due to high frequency switching of transistors.
- ✓ Line-side power harmonics (depending on the application and size of the drive).
- ✓ Non-regenerative operation.

3.5 Sensorless Field Oriented Control

Sensorless Field Oriented Control (SFOC) drives are very commonly used in industry. However, closed-loop and field oriented control, either with speed feedback sensors or sensorless, are all based on feedback regulation and electrical faults can give much the same effect [16].

A Sensorless FOC drives controls the IM's speed without any speed feedback devices. Motor model and parameters together with supply measurements are utilised to control the d-q axis electrical supply quantities. Sensorless FOC drives provide [14, 64, 71].

- ➢ Automatic slip compensation,

- High motor torque at low output frequencies,
- Improved dynamic response to demand and load variations,
- Compactness with less maintenance,
- Simpler application with no need for wires,
- Avoidance of the cost of encoders, and
- Suitability for different environments, including temperature.

In this drive mode, a feedback loop is used for providing better speed regulation and enhanced dynamic response. The drive used is sensorless VSD based on a Model Reference Adaptive System (MRAS). The output voltage is separately regulated utilising knowledge concerning the phase angle, while the frequency is controlled by switching the time of the inverter [16, 73]. MRAS is one of the most frequently used schemes in industrial applications [14]. It is presented here as it is used in the test rig drive upon which this study is based. MRAS utilises two independent machine models, namely reference and adaptive models, for estimating the same state variable [83]. The error between the two models estimates the induction motor speed. The model that does not involve the quantity to be estimated is considered as the reference model. The model that contains the quantity to be estimated is considered as the adaptive model. Comparison between the two model's outputs generates an error signal that is treated by an adaptation mechanism [83]. MRAS speed estimator based on voltage (reference model) and current (adjustable or adaptive) model is represented in Fig. 3.13.

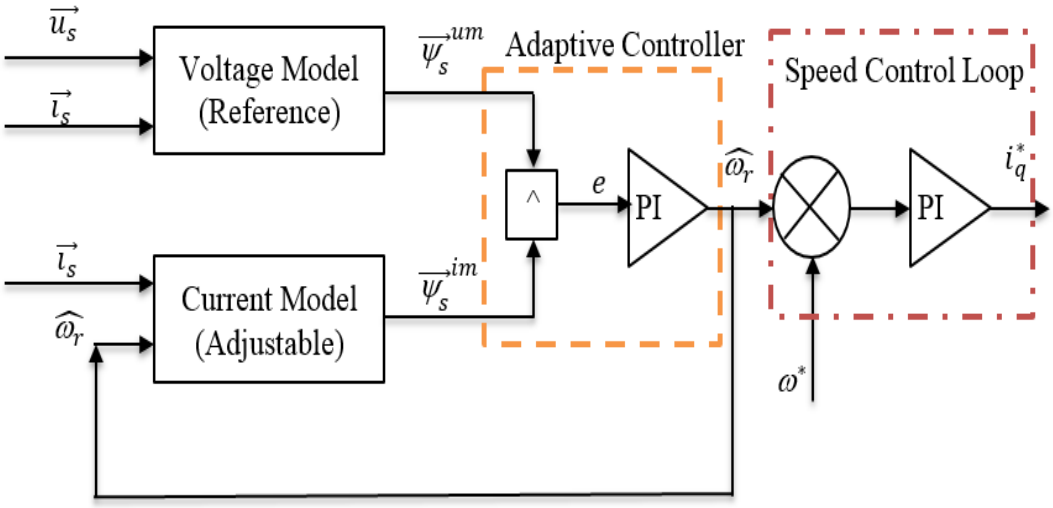

Figure 3.13 Schematic of MRAS and speed loop in a sensorless drive [14]

The reference model is composed of the stator voltage equations as follows [14, 84]:

$$\frac{d\psi^u \alpha r}{dt} = \frac{L_r}{L_m}(u_{\alpha s} - R_s i_{\alpha s} - \sigma L_s \frac{di_{\alpha s}}{dt}) \tag{3.8}$$

$$\frac{d\psi^u \beta r}{dt} = \frac{L_r}{L_m}(u_{\beta s} - R_s i_{\beta s} - \sigma L_s \frac{di_{\beta s}}{dt}) \tag{3.9}$$

The adjustable (adaptive) model is represented as follows [14, 84]:

$$\frac{d\psi^i \alpha r}{dt} = \frac{1}{T_r}(L_m i_{\alpha s} - \psi^i \alpha r - T_r \hat{\omega}_r \psi^i \beta r) \tag{3.10}$$

$$\frac{d\psi^i \beta r}{dt} = \frac{1}{T_r}(L_m i_{\beta s} - \psi^i \beta r + T_r \hat{\omega}_r \psi^i \alpha r) \tag{3.11}$$

$$\sigma = 1 - \frac{L^2 m}{L_r L_S} \tag{3.12}$$

where, L_{ls}, L_{lr} are the per phase winding leakage inductances in the stator and rotor, respectively, L_m is the motor mutual inductance, L_s, L_r are stator and rotor inductances, ψ_r, ψ_s are rotor and stator flux, σ is motor leakage coefficient, T_r is rotor time constant and subscripts α and β represent the stationary reference frame coordinates. The error between the two models is calculated in the following way [14]:

$$e = \psi^{u}{}_{\beta r}\psi^{i}{}_{\alpha r} - \psi^{u}{}_{\alpha r}\psi^{i}{}_{\beta r} \tag{3.13}$$

The most common method used for the adaptation mechanism is the PI controller, although certain other techniques are used such as fuzzy and neural network control systems [85]. The output from the PI controller replaces the estimated value in the adjustable model. The MRAS continually modifies the estimated variable quantity maintaining the error between the two models [14, 86]. The estimated speed is then used to calculate the rotor flux angle θ_e as follows:

$$\theta_e = \int \omega_e dt \tag{3.14}$$

The estimated speed from MRAS is fed into the speed loop for speed control as illustrated in Fig. 3.13. The outer is a speed PI control loop which compares the reference speed with the feedback speed and generates the speed error. The speed error sets the reference value of the inner control loops. The inner control loops are two PI control loops in series, i.e. the current control loop that sets the reference torque signal based on the difference between the actual current and the reference from the speed loop; and the torque control loop that sets the reference value for the voltage output based on the difference between the feedback torque and reference from the current loop. The fourth is the voltage control loop that activates the PWM to feed the motor with the required voltages and frequencies.

A block diagram of a general sensorless flux vector control drive is shown in Fig.3.14. The torque reference will include frequency components which will be directed to the voltage regulators as an output voltage to the motor supply.

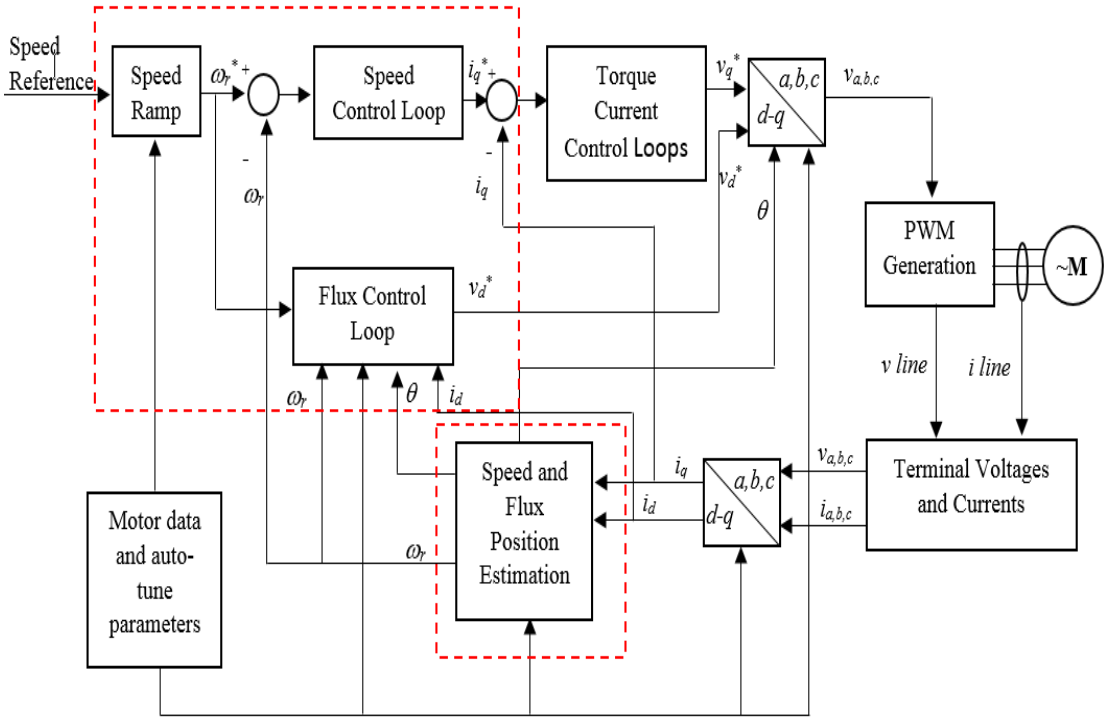

Figure 3.14 A block diagram of a general FOC drive [14]

The drive changes the terminal voltage more than the current due to its attempt to maintain the speed close to the desired level. Thus, more information about the health of the motor can be obtained from the voltage signals. On the other hand, the noise from the drive and the controlling activities of the closed-loop impose noise on the signal and hinder extraction of clear data [59, 60]. It is also worth mentioning that when a small fault occurs in the motor, the drive regulator actions, together with the noise from the PWM switches mask the presence of the fault features in the current signal and make detection difficult [70, 87]. The regulatory actions also propagate the fault characteristics into the voltages, in closed-loop systems. The voltage signals are likely to be more sensitive to stator and rotor faults than the current signals.

3.6 Summary

This chapter introduces details of the principles of induction motor AC drives. An inverter-driven motor system controls the rotational speed of an AC electric motor by controlling the frequency and voltage of the electrical power supplied to the motor. This system is also called a variable frequency drive (VFD), an adjustable-frequency drive (AFD), and a variable speed drive (VSD). VSDs are widely used in all areas of industry; including transport systems such as ships, railways, elevators, ventilation systems, conveyors, material handling plants and utility companies for mechanical equipment e.g. machine tools, extruders, fans, pumps and compressors.

Induction motor can only run efficiently at close to the synchronous speed of the rotating field. Thus, the best method for speed control is required to provide continuous smooth variation in synchronous speed, which in turn calls for variation in the supply frequency. This can be achieved by using an inverter to supply the motor. The majority of inverters used in motor drives are Voltage Source Inverters (VSI), in which the output voltage to the motor is controlled to suit the operating conditions of the motor. Pulse Width Modulated (PWM) inverter is the most commonly used. It receives DC power from a fixed voltage source and adjusts the frequency and voltage depending on the requirement. PWM types inverter cause the least harmonic noise.

The sensorless drive is considered in this thesis as it is very commonly used in industries. However, closed loop and field oriented control, either with speed feedback sensors or sensorless are all based on feedback regulation, and electrical faults can have nearly the same effect on them. It is worth mentioning that when the fault is not big enough, the drive regulator actions and the noise from the PWM switches masks the fault features in the current signal making it difficult to detect them. In the meantime, in closed-loop systems the voltage signals are likely to be more sensitive to stator and rotor faults than the current signals.

Chapter 4

Common Induction Motor Faults and Effective Diagnostic Techniques

This chapter begins by charactersing common faults in three phase induction motors. Then it investigates how such faults can show themselves in electrical signals: current and voltage waveforms. Finally based on an critical assesment of the performances of both the conventional methods used in MCSA and emerging methods for modulation signal processing, it proposes more effective methods to process the measured signals that can be more noisy due to the effect of VSD in order to extract the fault signatures accuratly.

4.1 Three Phase Induction Motor Faults

Induction motors are commonly considered rugged, robust and reliable. However, they are prone to a number of faults, and efficient and effective CM techniques are required to detect these faults at an early stage in order to prevent any motor failures causing serious disruption [10, 11]. To date, most work on the use of electrical signals for fault detection and diagnosis has been with open-loop systems.

In recent years, with the increasing demands for improved motor efficiency VSDs have been widely used. VSD based supply has been observed to be have various noises including increased supply harmonics and sudden waveform ripples. These less ideal supplies can influence not only the motor system in that higher temperature can be resulted, but also create difficulties in discriminate the fault signatures from the noise measurements.

To develop efficient and effective approaches for detecting and diagnosing faults from VSD system, the fundamentals of various faults are studied in this chapter, which mainly focuses on the fault frequency features and their interactions with that of main supply. This then allows for developing effective methods to process the signals with effective noise reduction and fault signature enhancement.

Particularly, as stator and rotor faults are very common in motors, the following sections review these particular faults and their influences on the power supply parameters i.e. both the current and voltage signals. In detail, stator faults can be the stator winding breakages and winding connection looseness. The rotor faults can be in the form of rotor bar breakages and rotor eccentricity. Especially, the rotor faults can also show as air-gap eccentricity, which results from not only the rotor eccentricity but also from the supporting bearings with various faults such as over-worn races and localised dents.

4.1.1 Stator Faults

Research has shown that 35–40% of induction motor breakdowns are because of stator winding breakages [5, 88, 89]. The Electric Power Research Institute sponsored

a survey, in which, 7500 induction motors were monitored and the outcomes showed stator faults to be liable for 37 % of motor failures [5]. Implementing predictive CM of motors to identify stator faults requires investigative tests dedicated to determining the stator winding condition [90].

Shorting of the insulation between turns can be damaging, with burning of the insulation, even melting of the copper conductors and motor failure. The location of the fault is usually at, or near, the main exit, normally located at the first or second coil from the line end of the winding [45, 91, 92].

Sharifi and Ebrahimi [45] developed a method for the diagnosis of inter-turn short circuit faults in the stator windings of induction motors. The technique is based on MCSA and utilizes three phase current spectra to overcome the problem of supply voltage unbalance. Alwodi, et al., [51] provided details of the application of MSB analysis to current signals to enhance feature components for the detection and diagnosis of faults in stator using the open loop control mode. Results presented by [51] demonstrate that MSB analysis has the potential to accurately and efficiently evaluate the degree of modulation and overpower from random and non-modulation components.

4.1.1.1 Stator Fault Features and Effects

While stator windings may have many different types of faults, there are four main stator faults: turn-to-turn fault, phase-to-phase short fault, phase-to-earth short fault and open circuit coil fault [93]. These are asymmetric faults, which are typically associated with insulation failures caused by various factors such as; poor connection, overloading and overheating, Fig. 4.1 shows these main four faults. An open circuit in the stator winding will affect the distribution of the stator MMF in the air gap. Early detection and mitigation of such faults can be of great value for the maintenance of induction motor CM [94].

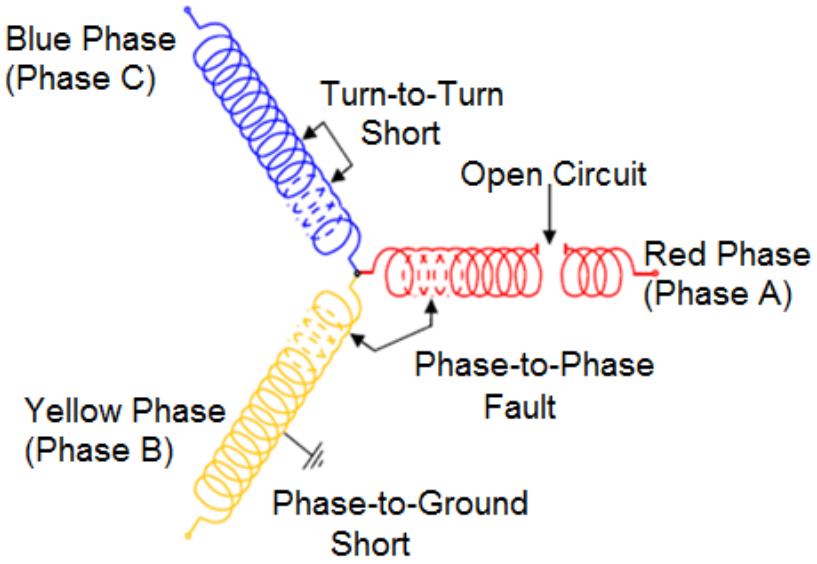

Figure 4.1 Common three-phase stator-winding faults [73]

Studies [95, 96] showed that stator faults generate unbalanced flux waveforms that cause the motor to draw asymmetric phase currents with unbalanced air gap flux. Additionally, distortion caused by the fault can be attributed to the changes in the air gap flux caused by resistive and inductive changes across the stator windings. Due to the fact that the rotor's magnetic field includes harmonics related to the rotor slots, this field induces frequency components in the current in the stator windings which change with supply frequency. Hence when a fault occurs, harmonics are generated around the base frequency and modulated by rotor slots harmonics. The feature frequency f_{sf} for the stator fault according to [51, 97] is:

$$f_{sf} = f_s\left[1 \pm mN_b\left[\frac{1-s}{p}\right]\right] \tag{4.1}$$

The rotor frequency f_r is calculated as:

$$f_r = \frac{1-s}{p} f_s \tag{4.2}$$

where f_s denotes the frequency of supply, f_r is the speed of rotor, N_b is the number of rotor bars, p the number of pole-pairs, s is the motor per unit slip, and m = 1, 2, 3… is the harmonic order.

Equation (4.1) can be rewritten as:

$$f_{sf} = f_s \pm mN_b f_r \tag{4.3}$$

The per unit slip s is calculated as follows:

$$s = \frac{f_{slip}}{f_{sync}} = \frac{f_s / p - f_r}{f_s / p} \tag{4.4}$$

Equations (4.1- 4.3) show that stator fault frequency components are a function of slip and number of rotor slots. Since the slip varies with load, the feature frequency will be different under different motor loads.

4.1.2 Rotor Faults

The squirrel cage rotor contains bars that are welded to end-rings, see Fig.2.1. The required torque is produced by the electric current that is induced by the stator field and then flows through these bars to produce an electro-magnetic force. Broken rotor bar (BRB) problems arise when these bars break or get separated from the end-rings. This malfunction prevents the flow of current and detracts from the performance of the motor [98]. The absence of current means there is no magnetic field, resulting in less or no attractive force. MCSA based on MSB analysis has been presented in [52] with new improved method of diagnosis and an explanation of the difference in current signals obtained from a healthy machine and one with a BRB. The electromagnetic relationships for the healthy driving motor and a motor with a BRB show an additional current with sinusoidal wave of frequency $2sf_s$ is present in the case of the BRB.

4.1.2.1 Rotor Fault Features and Effects

BRBs and broken end-ring are the most common causes of asymmetrical rotor and/or stator winding connections in induction machines. This asymmetry results in an unbalanced air gap voltage with resulting unbalanced line currents, increased losses, increased torque pulsations and decreased average torque. In the case of severe faults, it will result in significantly reduced efficiency and excessive heating which eventually leads to the failure of the machine. Fig. 4.2 (a) and (b) shows the equivalent circuits of the BRB detailing the rotor loop current and end ring current. Detailed calculations are shown in [70].

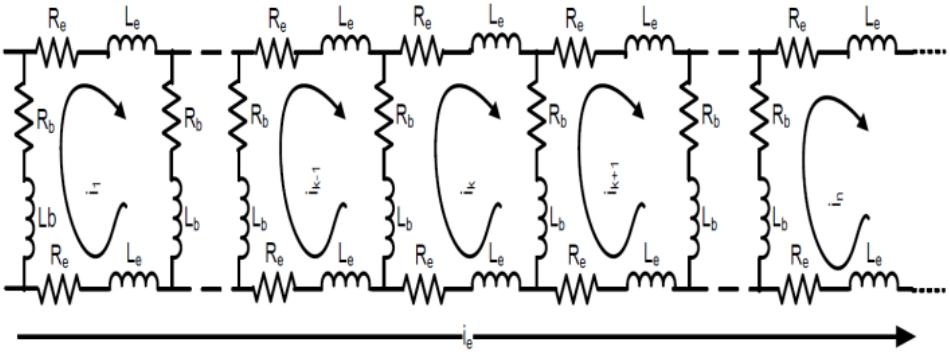

(a)

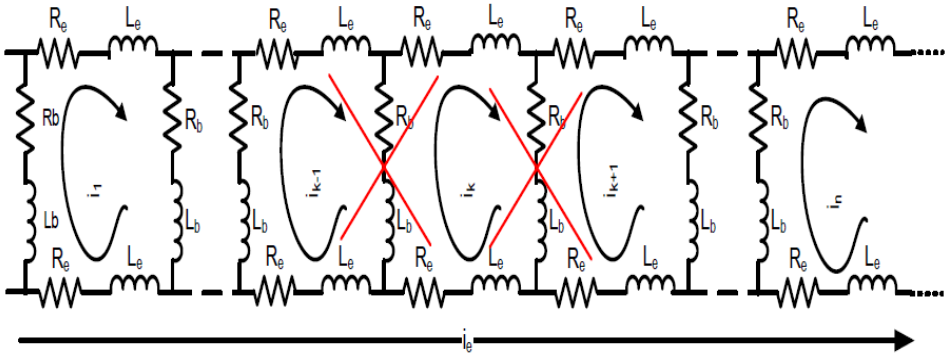

(b)

Figure 4.2 (a) Equivalent circuit of healthy rotor (b) Equivalent circuit of a rotor with two broken bars [70]

The sidebands found on either side of the supply frequency, see Equation (4.5) are likely to be present in the phase current power spectrum. There are unique characteristic frequencies of a BRB fault (f_{brb}) [11]:

$$f_{brb} = f_s(1 \pm 2ks), \quad k = 1, 2, 3, ... \tag{4.5}$$

The per unit slip, ***s***, is calculated as:

$$s = \frac{f_s / p - f_r}{f_s / p} \tag{4.6}$$

Broken bars it can result in particularly noticeable first-order sidebands *(k=1*) which can be used to diagnosis the existence of a BRB fault. The right sideband $f_s(1+2ks)$ is caused by the speed variation or ripple; and the left sideband $f_s(1-2ks)$ is due to magnetic or electrical rotor asymmetry caused by the BRB. The presence and amplitudes of the sidebands are reliant on the physical position of the BRB, as well as motor load and speed.

4.1.3 Asymmetric Stator Supply Voltage

Increases in stator resistance of a three phase induction motor can lead to voltage imbalances, causing a reduction in motor efficiency, increase in motor temperature and oscillatory running conditions. These, in turn, can generate subsequent electrical or mechanical failures. There are many reasons for stator winding asymmetry, such as generator terminal voltages, load currents, faults, power factor correction, equipment and voltage regulators in the utility distribution lines [99]. However, this fault will remain undetected by the drive system because despite these imbalances the motor is still functioning, albeit operating less efficiently. Even if there is only a small imbalance in motor resistance, large unbalanced motor current can flow which create difficulties in induction motor applications, heat generation, vibrations and acoustic noise, and shortening of working life [100]. The maximum amplitude of the current and torque are significantly increased by increasing the stator winding asymmetry factor.

4.1.3.1 Asymmetric Stator Supply Voltage Features and Effects

A small imbalance in motor resistance will cause a big increase in the winding temperature. As a general rule, the temperature rises by 25% (in ºC) for every 3.5% voltage imbalance [2].

A resistance fault simulated in one winding inside the AC motor will affect one motor phase in a star-connected motor as shown in Fig. 4.3. National Electric Motors Association (NEMA) has defined voltage imbalance as [3]:

$$\text{Voltage imbalance} = \left(1 - \frac{3U_{\min}}{\Sigma U_i}\right) \times 100 \tag{4.7}$$

where U_{min} is the lowest phase voltage among the three phases, and ΣU_i is sum of the voltages across the three phases.

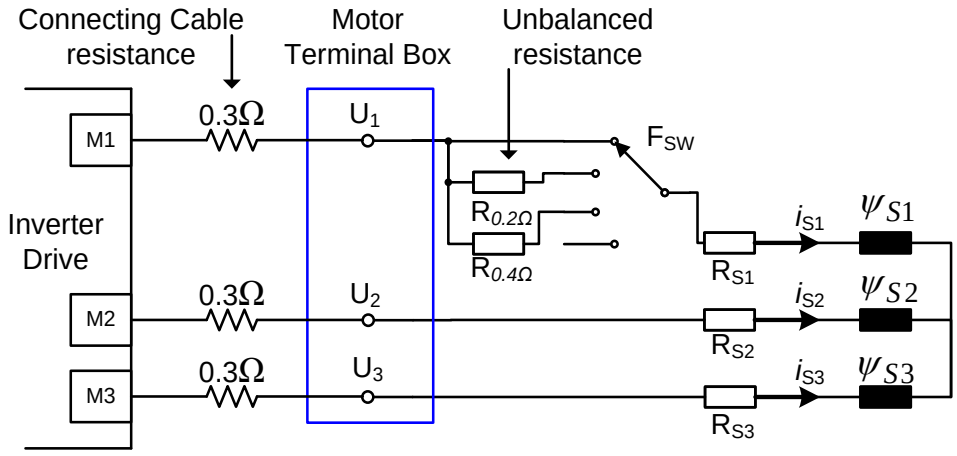

Figure 4.3 Asymmetric stator winding faults due to loose electric connection or winding shortages

An imbalance in the supply voltage induces sidebands in the stator current spectrum of an induction motor at the following frequencies [48].

$$f_{usv} = (1 + 2.k)\, f_s \tag{4.8}$$

where the order of harmonics: $k = 1, 2, 3\ldots$

4.1.4 Bearing Faults

Bearings are a part of a machine, designed to allow other parts to move more freely by, amongst other things, reducing friction between the moving parts. Studies have shown, see literature review (Chapter 2), that common faults in induction motors (about 40%–50% of the total) take place in the rolling bearings, depending on the type of installation, the motor size, and the supply voltage [101, 102]. In general, such faults are due to lack of lubrication, installation errors, wear and tear and even manufacturing faults. According to the elements affected, see Fig. 4.4, bearing faults can be classified as inner race, outer race, ball element and cage faults.

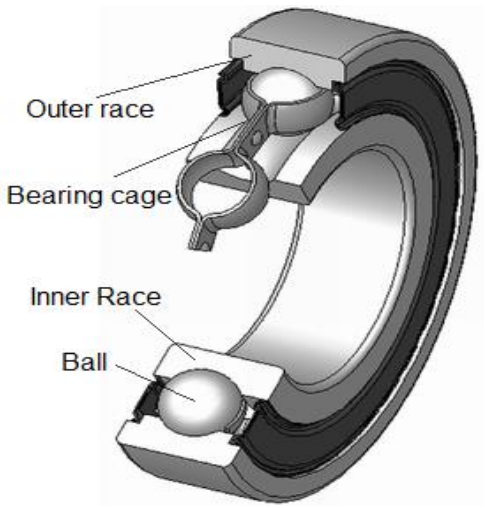

Figure 4.4 Components of the rolling bearing [102]

4.1.4.1 Bearing Fault Features and Effects

The bearing consists essentially of the outer and inner raceways, the balls, and the cage, which keeps the distance between the balls equal. The number of balls is N_b, their diameter is D_b, and the pitch diameter is D_p. Fig. 4.5 illustrates the geometry of a rolling- element bearings, note the contact between a ball and the raceway is characterised by the contact angle β [101].

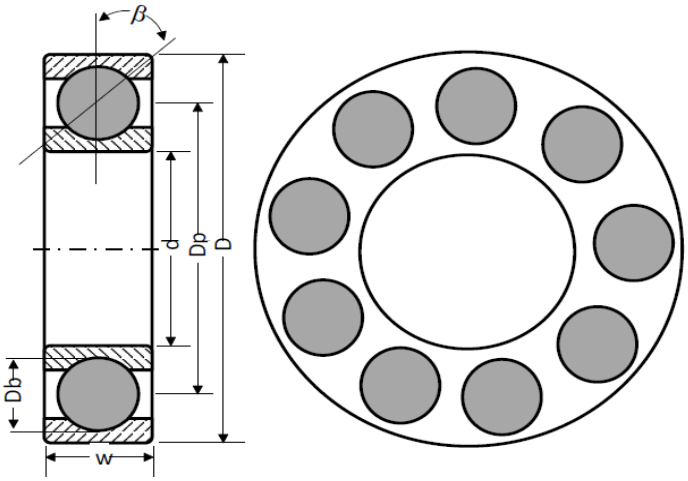

Figure 4.5 Geometry of a Rolling-Element Bearing [101]

Bearing faults can be classified into distributed and localised defects [103]. Distributed defects affect a whole region and are difficult to characterise by distinct frequencies. On the other hand, single-point defects are localised and can be classified according to the following affected element [103]:

- *Outer raceway defect,*
- *Inner raceway defect,*
- *Ball defect, and*
- *Cage defect*

There will be a periodicity corresponding to each fault which will be a function of bearing geometry and mechanical rotational frequency, and each periodicity will have its associated frequency. Thus, each of the above bearing faults has its associated characteristics frequency. For the four fault types listed, the characteristic frequency are [104-106]:

Outer race fault frequency:

$$f_O = \frac{N_b}{2} f_r \left(1 - \frac{D_b}{D_p} \cos\beta\right) \tag{4.9}$$

Inner race fault frequency:

$$f_i = \frac{N_b}{2} f_r \left(1 + \frac{D_b}{D_p} \cos\beta \right) \tag{4.10}$$

Ball fault frequency:

$$f_b = \frac{D_p}{D_b} f_r \left(1 - \frac{D_b^2}{D_p^2} \cos^2 \beta \right) \tag{4.11}$$

Cage fault frequency:

$$f_c = \frac{1}{2} f_r \left(1 - \frac{D_b}{D_p} \cos\beta \right) \tag{4.12}$$

where N_b is the number of balls, D_b is ball diameter, and D_p is the pitch diameter. β is the contact angle.

Schoen, et al., [107] have presented the most often referred to model of the influence of bearing damage on induction machine stator current. These authors considered the generation of rotating eccentricities at the characteristic bearing fault frequencies, f_V, which leads to periodical changes in machine inductances. This produces additional frequencies, f_{bf}, in the stator current, which can be predicted by [101, 108, 109]:

$$f_{bf} = \left| f_S \pm k f_V \right| \tag{4.13}$$

where f_s is the supply frequency, f_v is one of the four characteristic fault frequencies defined by Equations 4.9 to 4.12 with k = 1, 2, 3...

4.1.5 Air-gap Eccentricity

Induction motors might fail because of air-gap eccentricity. Air-gap eccentricity happens due to shaft deflection, inaccurate positioning of the rotor with respect to stator, bearing wear, stator core movement, etc. The eccentricity occurs when the

rotor is not centred within the stator. This fault produces problems of vibration and noise. The main types of air gap eccentricity as illustrated in Fig. 4.6 [70, 93, 110, 111] are:

- Static eccentricity,
- Dynamic eccentricity, and
- Mixed eccentricity

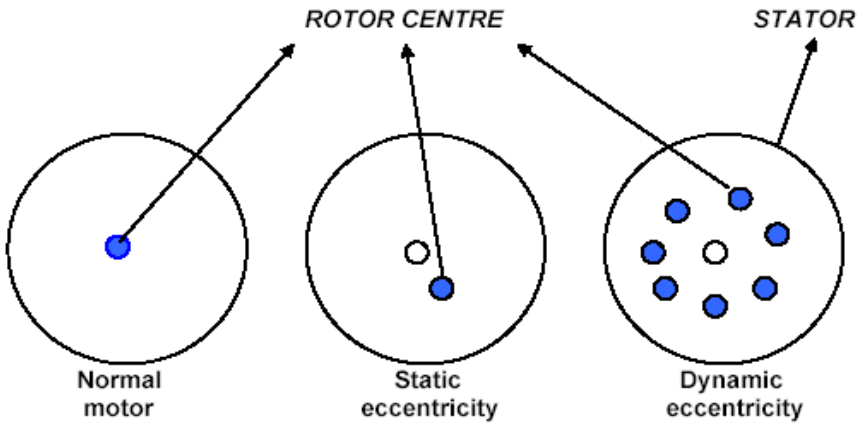

Figure 4.6 Air-gap Eccentricity

4.1.5.1 Air-gap Eccentricity Fault Features and Effects

The frequency components in the stator current due to air-gap eccentricity can be written as [70, 105, 112-114]:

$$f_{ecc} = \left[(kN_b \pm n_d) \frac{1-S}{P} \pm m \right] f_s \qquad (4.14)$$

where: f_s is the fundamental supply frequency, k =1, 2, 3..., N_b is the number of rotor bars, n_d = 1, 2, 3 ... (dynamic eccentricity), n_d = 0 (Static eccentricity), s is the slip, p is the number of pole pairs and m is the order of stator time harmonics that are present in the power supply driving the motor, given by ±1, ±3, ±5, etc.

If both static and dynamic eccentricities exist together, spectral components can be observed around the fundamental, which are given by [70, 115-119]:

$$f_{mix} = f_S \pm m f_r \quad (4.15)$$

where: f_{mix} is the current components, f_s is the supply frequency, m is the harmonic number, f_r is the rotational speed frequency of the rotor in Hz, ($f_r = (1\text{-}s)\, fs\, /p)$ and p is the number of pole pairs

4.2 Fault Induced Modulations in the Motor Electric Signals

4.2.1 Baseline Signal

When a motor drive is operating under healthy conditions, the electromagnetic relationships of the driven motor can be investigated using any one of the three phases. The instantaneous current and voltage signals for a healthy motor drive are [52, 70, 120, 121]:

$$i_A = \sqrt{2} I \cos(2\pi f_s t - \alpha_I) \quad (4.16)$$

$$u_A = \sqrt{2} U \cos(2\pi f_s t) \quad (4.17)$$

Correspondingly, the magnetic flux in the motor stator is:

$$\psi_A = \sqrt{2} \psi \cos(2\pi f_s t - \alpha_\psi) \quad (4.18)$$

The electromagnetic torque is calculated as:

$$T = 3 p \psi I \sin(\alpha_I - \alpha_\psi) \quad (4.19)$$

where I, V and Ψ are the RMS values of the phase current, voltage and stator flux respectively, α_I and α_Ψ are the phases of the current and flux, f_s is the supply frequency and p is the number of pole pairs [14, 60, 70].

4.2.2 Fault Signals

If there is a fault on the rotor such as a BRB, there will be an additional current component, denoted as, i_f, in the stator winding due to interaction between the main magnetic fields between stator and rotor [52, 120, 122]. Supposing that the additional current is a sinusoidal wave with a frequency $f_F = 2sf_s$ for the case of BRB, an

associated current wave with a BRB amplitude I_F, and phase angle α_F, referring to the supply voltage, that current can be expressed as:

$$i_f = \sqrt{2} I_F \cos(2\pi f_F t - \alpha_F) \tag{4.20}$$

There will be an additional torque component oscillating around the electric torque. Supposing that the additional torque ΔT is a sinusoidal wave with a frequency f_F, current amplitude I_F and phase α_F, the oscillatory torque can be obtained using Eq (4.19) [14, 19]:

$$\Delta T = 3p\psi I_F \sin(2\pi f_F t - (\alpha_I - \alpha_\psi) - \alpha_F) \tag{4.21}$$

The angular speed of the induction motor is represented as [14, 60]:

$$\frac{d\omega(t)}{dt} = \frac{1}{J}(T(t) - T_{load}(t)) \tag{4.22}$$

When a fault occurs, the speed of the motor (ω) will also oscillate by an amount ($\Delta\omega$) as presented in the following equation:

$$\Delta\omega = \frac{p}{J}\int \Delta T \, dt = -\frac{3p^2\psi I_F}{2\pi f_F J}\cos(2\pi f_F t - (\alpha_I - \alpha_\psi) - \alpha_F) \tag{4.23}$$

The angular variation in the rotor is:

$$\Delta\alpha_F = \Delta\theta = \frac{p}{J}\int \Delta\omega dt = \frac{3p^2\psi I_F}{4\pi^2 f_F^2 J}\sin(2\pi f_F t - (\alpha_I - \alpha_\psi) - \alpha_F) \tag{4.24}$$

where J is the inertia of the rotor system. This angular variation produces phase modulation in the linkage flux and Eq.(4.18) becomes:

$$\psi_A^F = \sqrt{2}\psi \cos[2\pi f_s t - \alpha_\psi - \Delta\psi \sin(2\pi f_F t - (\alpha_I - \alpha_\psi) - \alpha_F)] \tag{4.25}$$

where $\Delta\psi = \frac{3p^2\psi I_F}{4\pi^2 f_F^2 J}$. This shows that the flux wave will contain nonlinear effects because of the fault in the rotor system. This nonlinear interaction of linkage flux will produce a corresponding electromagnetic force (EMF) and hence induce a nonlinear current signal in the stator.

Considering $\Delta\alpha_F$ as very small, resulting in $\cos(\Delta\alpha_F) \approx 1$ and $\sin(\Delta\alpha_F) \approx \Delta\alpha_F$, the linkage flux now can be simplified and examined in three components explicitly:

$$\psi_A^F = \sqrt{2}\psi\cos(2\pi f_s t - \alpha_\psi) + \sqrt{2}\psi\Delta\alpha_F \sin(2\pi f_F t - \alpha_\psi) \tag{4.26}$$

$$\begin{aligned}\psi_A^F = {} & \sqrt{2}\psi\cos(2\pi f_s t - \alpha_\psi) + \sqrt{2}\psi\Delta\psi\cos[2\pi(f_s - f_F)t - \alpha_I - \alpha_F] - \\ & \sqrt{2}\psi\Delta\psi\cos[2\pi(f_s + f_F)t - 2\alpha_\psi + \alpha_I - \alpha_F]\end{aligned} \tag{4.27}$$

It is noticeable that the flux in equation (4.27) contains the fundamental frequency and the sidebands around it [19]. Based on the analysis given in [52, 60], the interaction between the stator flux and the equivalent circuit impedance generates sideband components either side of around the main supply frequency in current signals as follows [14, 60]:

$$\begin{aligned}& i_A^F(t) = \sqrt{2}I\cos(2\pi f_s t - \alpha_I) \\ & +\sqrt{2}I_l\cos[2\pi(f_s - f_F)t - \alpha_I - \alpha_F - \phi] \\ & +\sqrt{2}I_r\cos[2\pi(f_s + f_F)t - 2\alpha_\psi + \alpha_I - \alpha_F - \phi]\end{aligned} \tag{4.28}$$

where, ∅ is the angular displacement of motor equivalent circuit impedance at the supply frequency, I_l, and I_r are the RMS values of the lower and upper sideband components of the current oscillations, respectively, at frequencies of f_s - f_F and f_s + f_F . It shows that by checking the amplitude of the sidebands through spectrum calculation, various faults such as BRB and eccentricity can be diagnosed with a high degree of accuracy. However, conventional spectrums use amplitude information only and overlooks the phase effect which also contains fault information, as shown in Eqs.(4.28) and (4.29). The phases of sidebands are not only related to the same factors

as their amplitudes, but also the phase variation of the fault current. However, it will be shown in Section (4.3.3) that an appropriate phase combination between sidebands and the carrier of the fundamental supply can eliminate the phase variation in order to achieve reliable and accurate sideband estimation.

4.2.3 Modulation in Voltage Signals

As shown in Chapter 3, in the closed-loop control the oscillations in current signals due to fault effects can pass to the voltage signals because of the feedback regulations for maintaining desired motor speed and load characteristics. Therefore, the voltage signals will also exhibit sidebands similar to current signals:

$$\begin{aligned} u^F(t) &= \sqrt{2}U\cos(2\pi f_s t) \\ &+U_l\cos[2\pi(f_s - f_F)t - \alpha_F - \phi) \\ &+U_r\cos[2\pi(f_s + f_F)t - 2\alpha_\psi + \phi_F - \phi] \end{aligned} \tag{4.29}$$

where U_l and U_r are the RMS values of the lower and upper sideband components of the voltage oscillations

4.3 Data Processing

In order to monitor the condition of electrical drives effectively, the small modulations need to be extracted accurately. Different signal processing methods for fault identification have been developed based on different machine parameters, i.e. current, voltage, speed, efficiency, temperature and vibration, which allows vital diagnostic information to be obtained with certain degrees of accuracy and sensitivity before the system fails.

4.3.1 Time Domain Analysis

Recorded data is a collection of measured parameters consisting of individual values taken at different instances of time, each representing a particular characteristic. Time domain is the fundamental method of data collection.

Time domain analysis is used to describe, for example, electronical signals, biological systems and, market behaviours. With electrical signals, time domain analysis is usually based on current-time or voltage-time plots where the variable is measured as a function of time [123, 124]. The typical motor current waveform in each phase of a three-phase supply is illustrated in Fig. 4.7.

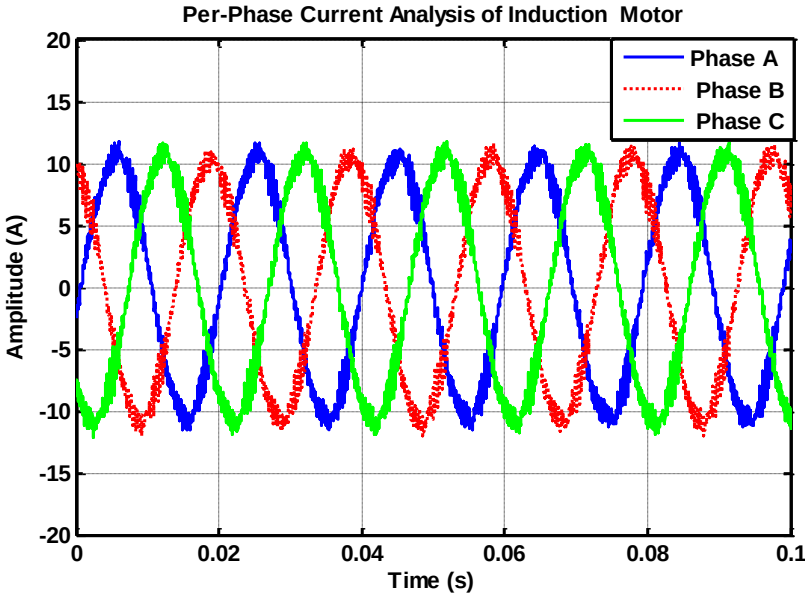

Figure 4.7 Three-phase motor current with healthy motor at 80% load

Voltage or currents in AC circuits are most commonly defined by their Root Mean Square (RMS) [125, 126]. A number of other statistical measures are used for particular purposes, these include peak value, crest factor and kurtosis [127, 128]. In this study, the RMS value of the stator current signal is used for investigation of induction motor health condition, due to its simplicity.

RMS values of the motor current signals against different load conditions (0%, 20%, 40%, 60% and 80% of full load) for a stator faulty and healthy motor are showed in Fig. 4.8. (See Chapter 6 and Appendix A and Appendix B for more details on motor current and voltage analysis under open loop and sensorless control in time domain).

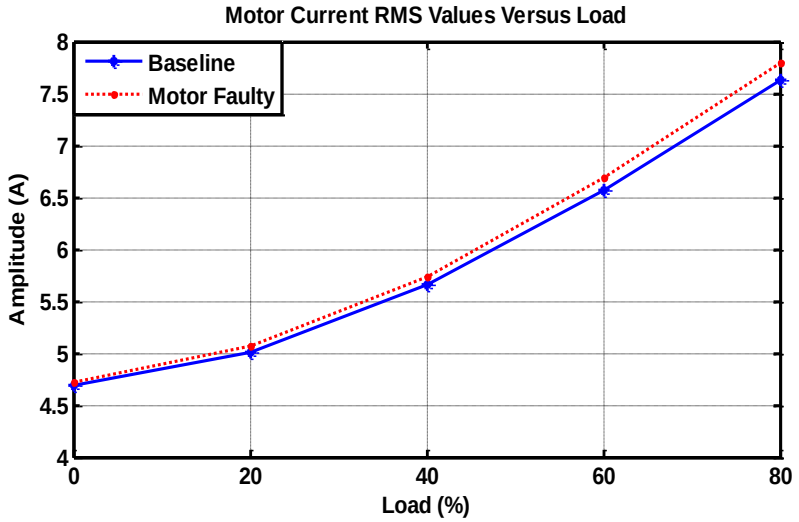

Figure 4.8 RMS value of motor current for healthy motor and motor with stator fault at different load

4.3.2 Frequency Domain Analysis

It has been found immensely useful to transform time domain data into the frequency domain. The most commonly used transformation is the Fourier Transformation. The Fast Fourier Transform (FFT) is the most extensively used method currently. This method is very productive because, the frequency-domain representation describes the energy contained in the signals as a function of frequency and has the enormous advantage that, often, the signals generated by the individual components can be seen directly in a spectrum [123, 129, 130].

This approach is particularly useful when electrical and mechanical faults generate distinct harmonics, which can be clearly differentiated in a frequency spectrum of the current signatures to show the difference between healthy and faulty motors [131, 132]. The FFT can also be utilized for the detection of on-line failure of motors that are asynchronous. The literature contains descriptions of this method being used for detection and diagnosis of common faults that occur in induction motors, including BRBs, short-circuits and stator winding asymmetry [4, 9, 43, 133-135]. Mehala and Dahiya have presented fault frequency equations using FFT analysis of the measured current signals [136].

Fig. 4.9 shows phase current spectra for healthy motor and motor with a broken rotor bar at 75% full motor speed and loads 0% and 80% of full load. It can be seen that the amplitude of sidebands for BRB is clearly higher when compared with the spectrum of the healthy motor at higher load. The amplitude of sidebands changes with the load and fault.

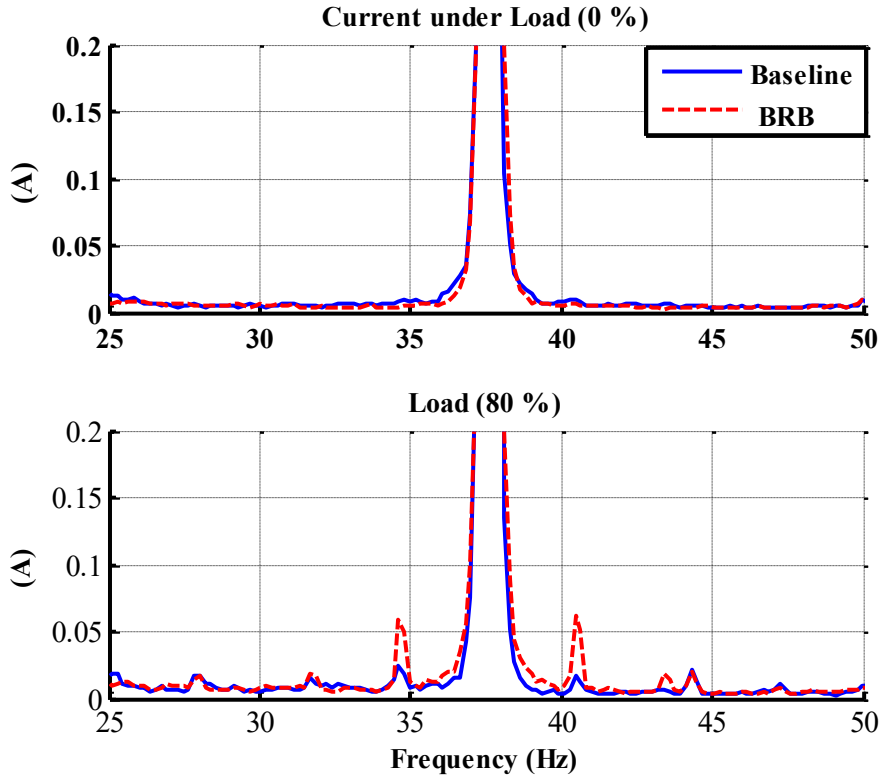

Figure 4.9 Phase current spectra for healthy motor and motor with BRB at 75% motor speed and different loads

4.3.3 Sideband Extraction Using Modulation Signal Bispectrum (MSB)

The sideband components can be estimated using spectrum analysis. However, the amplitudes from conventional power spectrum includes not only the sidebands of interest but also the additive random noise which is inevitable in measurement systems and VSD motor operating processes. [49] and [50] have shown the adverse consequence of ignoring phase information by using only the power spectrum for detection and diagnosis of faults. When the sidebands are small, as in the case of

incipient faults, their presence can be masked by random noises and this may degrade diagnosis performance.

For a discrete time current or voltage signal $x(t)$ its power spectrum (PS) can be calculated using:

$$P(f) = E[X(f)X^*(f)] \tag{4.30}$$

where $X(f)$ is the discrete Fourier transform:

$$X(f) = \sum_{t=-\infty}^{\infty} x(t)e^{-2j\pi t} \tag{4.31}$$

$X^*(f)$ is the complex conjugate of $X(f)$, and $E[\,]$ denotes the statistical expectation. The power spectrum is a linear transform and a function of the frequency f. Extending this definition and increasing the order of the spectrum to three gives rise to the conventional bispectrum:

$$B(f_1, f_2) = E[X(f_1)X(f_2)X^*(f_1 + f_2)] \tag{4.32}$$

where, f_1, f_2 and $f_1 + f_2$ indicate the individual frequency components achieved from the Fourier series integral.

Comparing with the power spectrum of Equation (4.30), the bispectrum has a number of unique properties such as nonlinear system identification, phase information retention and Gaussian noise elimination. The bispectrum is especially effective for detecting quadratic phase coupling (QPC) which occurs when two waves interact non-linearly and generate a third wave with a frequency and phase equal to the sum or difference of the first two waves. It is thus particularly useful for characterizing harmonic components which are commonly present in vibro-acoustic signals.

The conventional bispectrum shown in Equation (4.32) characterises the presence of QPC from the harmonically related frequency components of f_1, f_2 and $f_1 + f_2$. However, it neglects the occurrence of $f_1 - f_2$, the lower sideband in PS which may be also due to a nonlinear relationship between the two components of f_1 and f_2.

Therefore, the conventional bispectrum it is not sufficient to describe amplitude modulated (both AM and FM) signals such as motor current signals [101].

To improve the performance of the conventional bispectrum in characterising the motor current signals, a new variant of the conventional bispectrum, the modulation signal bispectrum (MSB) is introduced [19, 51, 52, 101] as in Equation (4.33):

$$B_{MS}(f_1, f_2) = E[X(f_2 + f_1)X(f_2 - f_1)X^*(f_2)X^*(f_2)] \tag{4.33}$$

The total phase of the MSB is:

$$\varphi_{MS}(f_1, f_2) = \varphi(f_2 + f_1) + \varphi(f_2 - f_1) - \varphi(f_2) - \varphi(f_2) \tag{4.34}$$

When two components f_1 and f_2 are coupled, their phases are related by:

$$\begin{aligned} \varphi(f_2 + f_1) &= \varphi(f_2) + \varphi(f_1) \\ \varphi(f_2 - f_1) &= \varphi(f_2) - \varphi(f_1) \end{aligned} \tag{4.35}$$

By substituting (4.35) into (4.34) it is seen that the total phase of MSB will be zero and MSB amplitude will be the product of four magnitudes, which is the maximum of the complex product. Therefore, a bispectral peak will appear at (f_1, f_2). Equation (4.33) now takes into account both $(f_1 + f_2)$ and $(f_1 - f_2)$ for systematically measuring the nonlinearity of modulation signals. If $(f_1 + f_2)$ and $(f_1 - f_2)$ are both due to nonlinear effect between f_1 and f_2, a bispectral peak will appear at bifrequency $B_{MS}(f_1, f_2)$. This is a more accurate and efficient representing the sideband characteristics of modulation signals.

A motor current signal with features of electrical and mechanical faults will contain a series of sideband components which are concentrated around the supply frequency. A bispectrum slice at the supply frequency will be sufficient to characterize these sidebands for fault detection and diagnosis. By setting f_2 in Equation (4.33) to a constant value such as the fundamental, $f_2 = f_s = 50Hz$, an MSB slice at the supply frequency can be expressed as:

$$B_{MS}(f_1, f_s) = E[X(f_s + f_1)X(f_s - f_1)X^*(f_s)X^*(f_s)] \quad (4.36)$$

The amplitude of the supply frequency is predominant in the spectra of the current signals and can be identified easily. This allows the spectral peaks such as those due to induction motor faults in the higher frequency range to be estimated more accurately and hence to obtain more accurate and better diagnostic results.

An MSB slice based sideband estimator, abbreviated as MSB-SE, is introduced as:

$$B_{MS}^{SE}(f_1, f_s) = E\left[X(f_s + f_1)X(f_s - f_1)X^*(f_s)X^*(f_s)\right] / E\left[\left|X(f_s)\right|\left|X(f_s)\right|\right] \quad (4.37)$$

MSB-SE also has its coherence function. According to [19] and Equation (4.37), MSB-SE coherence can be expressed as:

$$b^2{}_{MSB-SE}(f_1, f_s) = \frac{\left|B_{MS}^{SE}(f_1, f_s)^2\right|}{E[|X(f_s + f_1)X(f_s - f_1)|^2]} \quad (4.38)$$

Equation (4.38) can be used to confirm the coupling effects between sidebands and carrier, and to check the degree of random noise influence, which allows confirmation of the existence of MSB-SE peaks for the detection of modulation process in noise measurements.

Fig. 4.10 shows a direct comparison between a MSB slice at the supply frequency and PS for the voltage signals under 40% load at full speed for the healthy motor. MSB shows very good noise reduction compared with PS, see Fig.4.10 (a) The 50 Hz supply component present in the PS is largely eliminated in the MSB. This makes for easier and more reliable observation of components that relate to motor health conditions. The sideband components $(f_s - f_r)$ and $(f_s + f_r)$ around f_s shown by the power spectra of Fig. 4.10 (b) is represented by a single component at 24.88 Hz in the plot of the MSB. This makes spectral peaks such as those due to eccentricity faults in the high frequency range to be estimated more accurate with better diagnostic results.

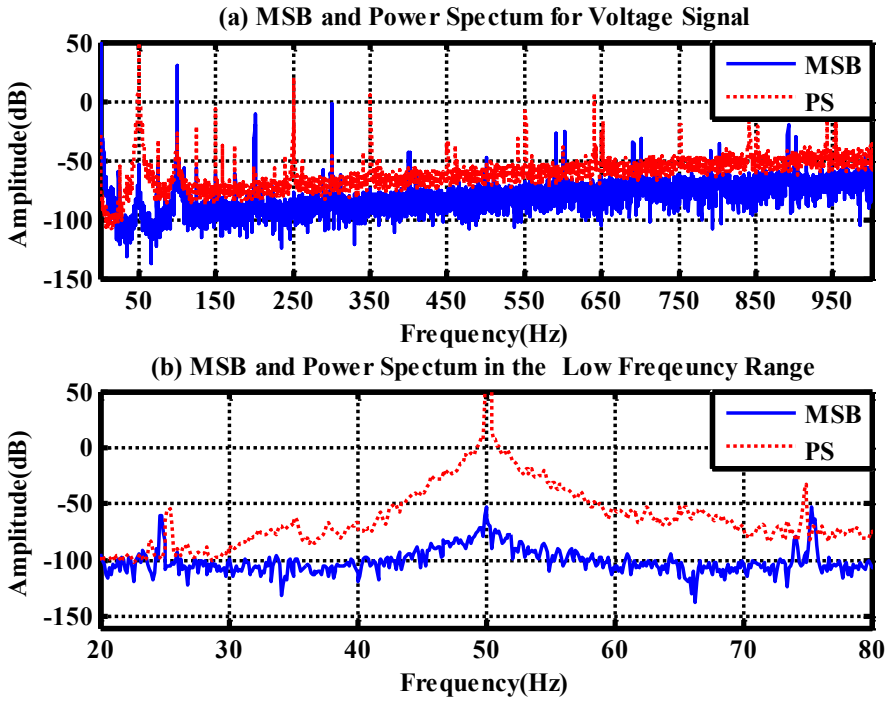

Figure 4.10 MSB and power spectrum characteristics for voltage signals

Figure 4.10 is in good agreement with previous work in the literature as detailed in Table 1.

Table1. Summary table of the application of MSB for fault detection

Reference	Major Contribution
Zhang, R., et al.,(2017) [49]	Gear wear monitoring by MSB based on MCSA.
Haba, U., et al., (2017) [137]	Detection and diagnosis of reciprocating compressor faults based on MSB analysis.
Rehab, I., et al., (2016) [38]	Diagnostic amplitude of rolling bearing under increasing radial clearance using MSB analysis.
Hassin,O., et al., (2016) [138]	Journal bearing condition monitoring based on MSB analysis of vibrations.
Tian, X., et al., (2015) [139]	Diagnosis of Combination Faults in a Planetary Gearbox using MSB based Sideband Estimator.
Alwodai A et al., (2012) [51]	MSB analysis of motor current signals for stator fault diagnosis is studied.

4.4 Summary

The most prevalent faults in induction motor have been described in this chapter, these included stator faults, broken rotor bars, asymmetric stator supply voltage, bearing faults and air-gap eccentricity faults. Each of them show addition ossicallation at its chracterstic frequency which modulates the main supply components. As a results, the measured signals are of nonlinear modulation signals. Especially the modulating components are very weak and often masked by various noises including the VSD induced ones.

Modulation signal bispectrum (MSB) and MSB based sideband estimation (MSB-SE) has been examined based on its theritical basis. As it has the capbablity of noise suppression and nonlinear modulation chracterstic, it will be take as the main signal processing tools in this research to chracterise the motor current and voltage signals from sensorless control mode and thereby to develop effective methods for detecting and diagnosing various faults from induction motors with VSD under different loads and different speeds.

Chapter 5

Development of an Induction Motor Test Rig

This chapter presents the specifications of the test facility used in this study. The details of control systems, measuring equipment and sensors, data acquisition system and application software are presented. Finally, the chapter describes the faults seeded into the motor.

5.1 Introduction

Experimental tests play an important role in condition monitoring research. It is difficult to study fault detection and failure progression without practical tests. There are a number of parameters that may be monitored to detect the onset of a failure condition (current, voltage, speed, vibration, etc.). The test rig employed here, was designed to perform a series of deterministic, repeatable tests and to obtain data from tests carried out at different speeds, loads, faults, and different severities of each fault. This chapter gives a detailed description of the experimental facilities required and also describes the test rig. The details of measured parameters, data acquisition system and application software is provided.

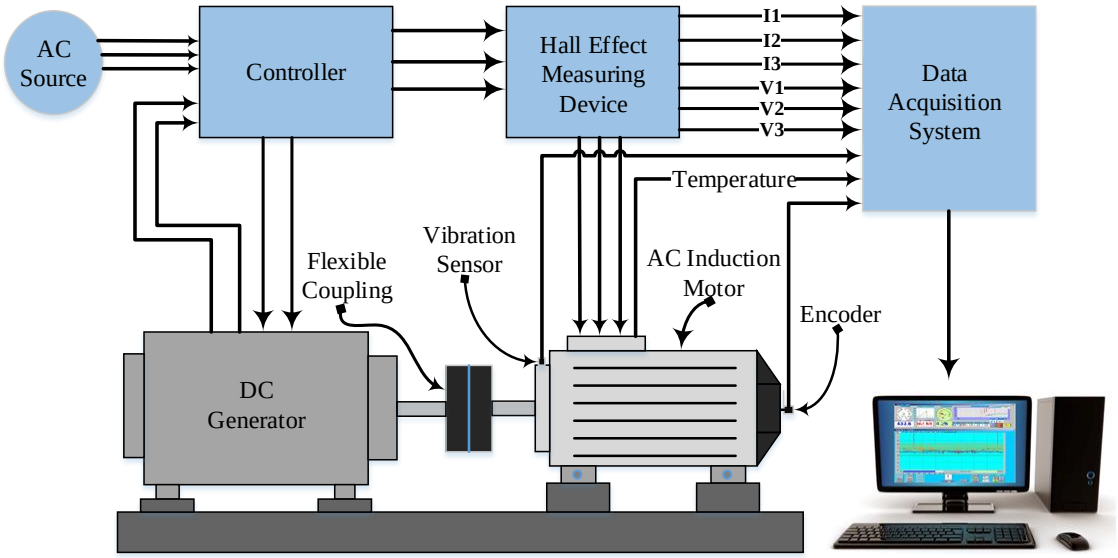

Figure 5.1 Schematic diagram of the induction motor test facility

Fig. 5.1 shows a schematic diagram of the test rig which was used to conduct the experimental investigations, and Fig. 5.2 shows photographs of the individual items comprising the rig. The system consists of a three phase, 4 Kw, AC induction motor (IM) with speed 1420 rpm (two-pole pairs). To change the speed of the motor, a digital variable speed controller is attached to the test rig between the power line source and the motor. The controller can be programmed to any specific shaft rotation speed. The IM is coupled to a DC generator as load using a flexible spider coupling.

The DC generator is controlled by a DC variable drive that varies the armature current to provide the required load to the AC motor. The field of the generator is connected to the DC source through the controller while the generated power is fed back to the mains electrical grid. The load in the IM can be adjusted by changing the field resistance of the DC generator. The operating speeds and loads are set by the operator via a touch screen on the control panel.

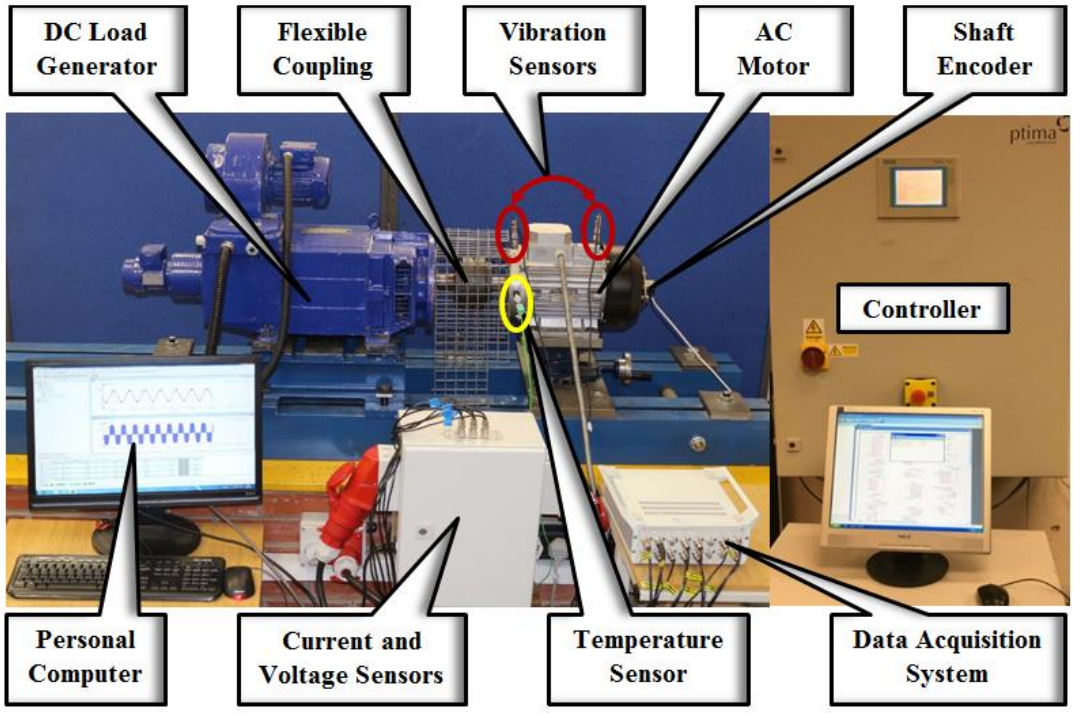

Figure 5.2 Photographs of the test rig facility

Five identical motors were purchased and labelled sequentially so that the source of any data collected could later be identified. The AC IM is shown in Fig.5.3 and the details of the IM placed into the test facility are presented in Table 2.

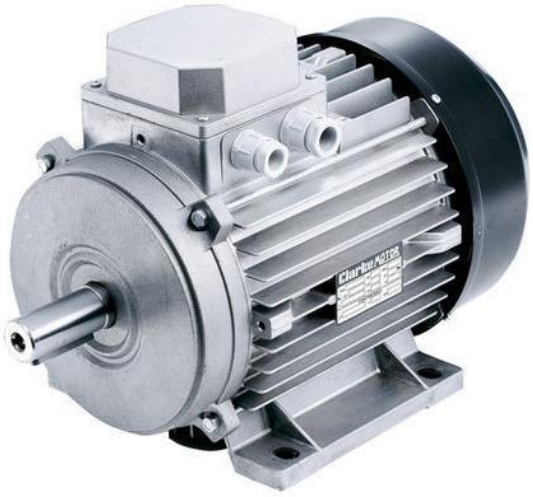

Figure 5.3 AC induction motor (Clarke type)

Table.2 Induction motor specification

parameters	value
Number of phases	3
Motor power	4 (kW)
Rated voltage (Δ/Y)	230/400 (V)
Motor speed	1420 (rpm)
Number of poles	4 poles/phase
Supply frequency	50 (Hz)
Number of stator slots	36
Number of rotor slots	28
Rated current (Δ/Y)	15.9/9.2 (A)

5.2 DC Generator

The test rig uses a Siemens DC generator as a torsion loader, where the load is adjusted through the Siemens micro master controller. The magnitude of the load is expressed as a percentage of the maximum power which is 10 kw at speed of 1720 rpm, Armature voltage 350 V and current of 35 A. A DC generator was used to provide the torque loads to make it easier to control the loading.

5.3 Spider Flexible Coupling

The spider flexible coupling, also known as a hard rubber coupling, is illustrated in Fig. 5.4, and provided a flexible connection between the drive shaft of the AC motor and DC generator. This type of compensation is essential, since a perfect alignment between two rotating shafts is incredibly difficult to achieve. Coupled rotating machines often shift from their primary position, leading to potential shaft misalignment, so a flexible coupling is used in order to compensate for shaft misalignment. Such misalignment would inevitably cause wear that would, in turn, lead to early failure and require renewal of machine components [140]. The specification of the flexible coupling used in this test rig is given in Table 3.

Figure 5.4 Hard rubber coupling

Table.3 Flexible coupling specifications

Manufacture	Sinocera
Type	Fenner
Size	130
Outer diameter	130 mm
Border diameter	14-42 mm
Hub diameter	105 mm
Hub length	18 mm
Rubber width	36 mm
Taper lock bush size code	1610

5.4 Speed and Torque Controller

The test rig should be able to be operated at different speeds and different torque loads, so a speed and torque controller was required. Fig. 5.5 shows the Siemens Micro Master Controller that was installed so that the motor could be run at different speeds and different torque loads. The Siemens controller proved easy to use and was able to deliver torque and speeds accurately. The control panel is equipped with a LCD touch screen to enter the required test profile and to monitor the key variables when the rig is running. The block diagram in Fig. 5.6 illustrates the main features of the speed control system.

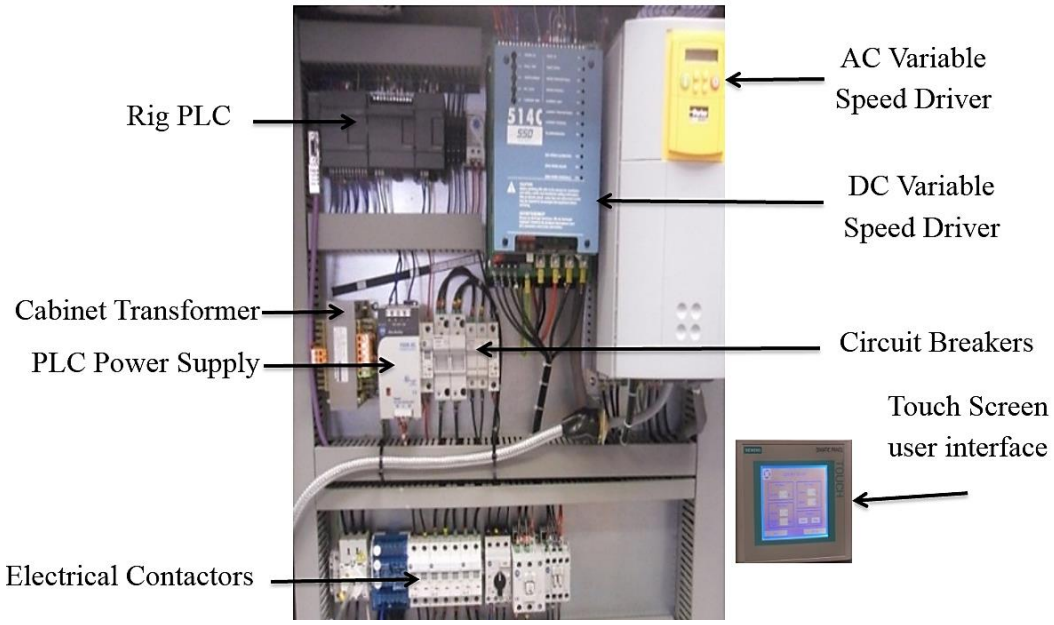

Figure 5.5 Photograph of Siemens Micro Master Controller

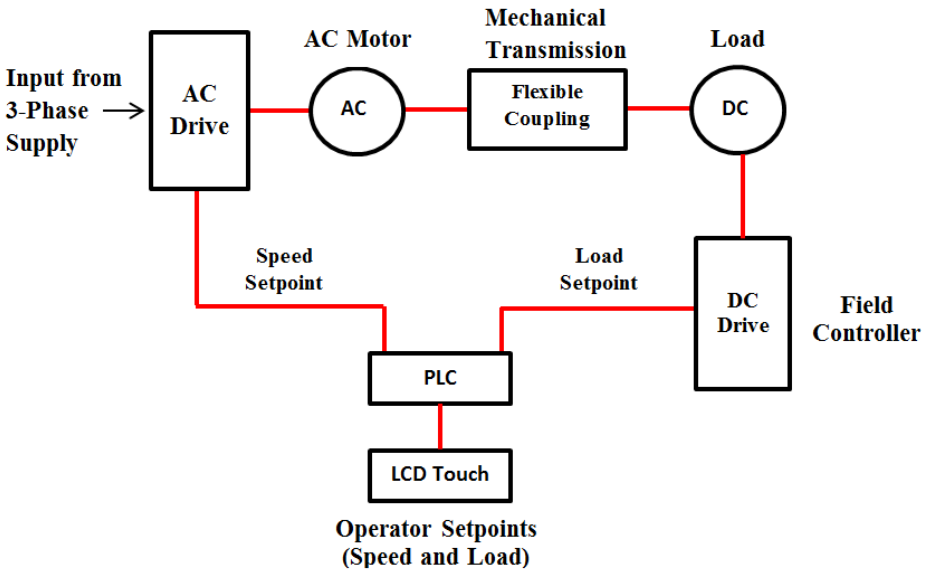

Figure 5.6 Block diagram of experimental test rig control system

5.4.1 AC Variable Speed Drive

The AC variable speed drive (VSD) is a Parker 650V which is made for industrial applications. It can be set either to open loop control mode (V/Hz) or sensorless control mode for adjusting the speed of the system. The technical specifications of the drive are illustrated in Table 4.

Table.4 The parker 650 V drive technical specifications

Product Description	AC variable speed drive
Model	650 V
Frequency Output	0-240 Hz
Current Output	0-33 A
Voltage Output	0-460 v ±10%
Rated motor power	15 kW
Frequency Switching	3 kHz nominal
Voltage Boost	0-25%
Flux Control	1. V/F control with linear or fan law profile 2. Sensorless flux vector
V/Hz Profile	-Constant torque - Fan Law
Inputs Analogue	2 inputs – one is configurable; voltage or current
Outputs Analogue	1 configurable voltage or current
Digital Inputs	6 configurable 24V DC inputs (2 suitable for encoder)
Basic error	± 0.5% of full range

5.4.2 DC Variable Speed Drive

This drive regulates the torque of the DC motor with a linear closed-loop and without the need for a feedback from an encoder or a tachometer. The drive utilises the armature voltage to calculate the speed. A summary of the DC drive specifications is shown in Table 5.

Table.5 The 514C DC drive technical specifications

Product Description	DC speed drive
Model	514C
Control Action	Closed Loop with Proportional Integral Control
Speed Feedback	Selectable: Armature Voltage or Tacho-generator
100% Load Regulation	2% when Armature Voltage mode used; 0.1% when Tacho-generator mode selected
Maximum Torque/Speed Range	20:1 when Armature Voltage mode used; 100:1 when Tacho-generator mode selected
inputs Analogue	7 non-configurable inputs
outputs Analogue	7 outputs: Setpoint Ramp, Total Setpoint, Speed, Current Demand, Current Meter (Bipolar or Modulus), +10V reference and -10Vreference.
S Ramp and Linear Ramp	Symmetric or asymmetric ramp up and down rates
Current Limit	Adjustable 110% or150%
Supply Voltage	110 – 480 Vac ± 10%
Nominal Armature Voltage	90 Vdc at 110/120 Vac 180 Vdc at 220/240 Vac 320 Vdc at 380/415 Vac
Overload	150% for 60 seconds
Field Current	3 A DC

5.5 Data Acquisition System

During the experimental work all the data were recorded using a Sinocera YE6232B high speed data acquisition system (DAS). This system has 16 channels as shown in Fig. 5.7; each channel is equipped with a 24 bit analogue/digital converter at a sampling frequency of 96 kHz. The DAS is supported by general purpose YE76000 software which allows users to set up parameters for data acquisition, data

conditioning, data formatting, real time analysis and signal sources. It also processes efficient data storage and fast data conversion to Matlab format. It has the capability of real time domain analysis, frequency domain, statistical analysis and time-frequency domain and its main specifications are contained in Table 6.

Figure 5.7 Photograph of DAS, Sinocera YE6232B

Table.6 Data acquisition system specification

Parameter	Performance
Manufacturer	Sinocera YE6232B
Number of Channels	16 channels
A/D resolution	24 bit
IEPE power supply	4 mA/+24 VDC
Input range	±10V
Gain	Selectable either 1, 10 or 100
Filter	Anti-aliasing
Sampling rate (maximum)	96kHz per channel, Parallel sampling
Interface	USB 2.0

Eleven parameters (two encoder speeds ,one temperature signal, three current signals, two vibration signals and three voltage signals) were measured and recorded regularly on the induction motor test facility, so that their relative usefulness in effective CM could be investigated. In each test the raw data was acquired and displayed on a computer monitor in the form of plots. This allows the data to be examined before

being stored. The data for each operation was recorded for 30 seconds. For such settings the length of data collected for each set is 30*96000 = 2 880 000 data points. This data acquisition system is equipped with an anti-aliasing filter which guarantees that the aliased frequencies are not captured. Additionally, the anti-aliasing filter is used to automatically adjust the cut-off frequency of another built in low pass filter based on the pre-selected sampling rate.

5.6 Power Supply Measurement Unit

To investigate the characteristics of the current and voltage signals, the AC voltages, currents and power were measured using Hall Effect voltage and current transducers, and a universal power cell which is independent of the controller to avoid any interruptions to the control process. The voltage transducer is the LEM LV 25-P and the current transducer is the ABB EL55P2. A photograph of the three phase measuring device is shown in Fig. 5.8 and the specifications of the voltage and current transducers are presented in Tables 7 and 8, respectively.

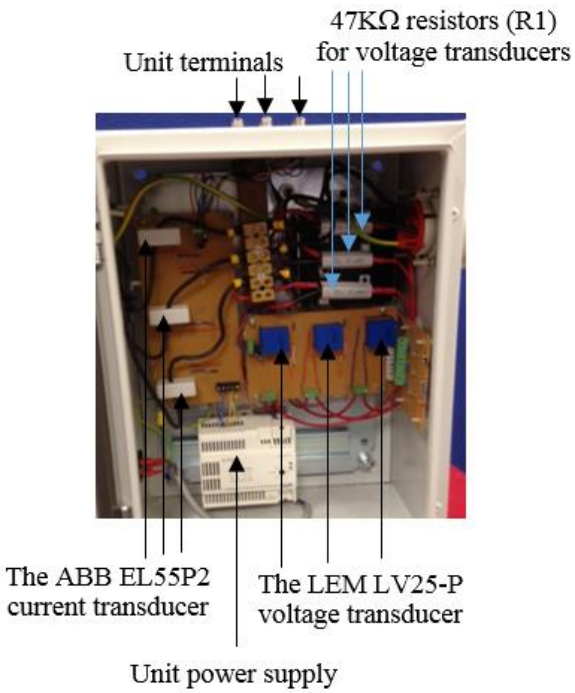

Figure 5.8 Three phase electrical signals measurement device

Table.7 Specifications of the voltage transducer

Brand and Type	*LEM* Voltage Transducer LV 25-Pt
Primary nominal voltage (V_{pn})rms	10:500 V
Primary nominal current (I_{pn})rms	10 mA
Primary current, measuring range	0 : ±14 mA
Secondary nominal current (I_{sn})rms	25 mA
Supply voltage (±5%)	± (12:15) V
Current consumption	10(@±15V) + I_s mA
Overall accuracy	±0.9% @ (I_{pn} , 25^{o}C and ±15V)
Linearity error	<0.2%
Response time to 90% of I_{pn} step	40μs

Table.8 Specifications of the current transducer

Technology	Hall Effect
Primary nominal current (I_{pn}) rms	50 A
Supply voltage (Va)	±(11:15.7) V
Measuring range @ Va	0:±80 A
Secondary nominal current (I_{sn}) rms	25 mA
Thermal drift/ I_{sn}	$2*10^{-4}$ /^{o}C
Bandwidth (-1 dB)	0:200 kHz
Accuracy	±0.5% @ (I_{pn} , 0:70^{o}C and ±15V)
Linearity	Better than 10^{-3}
Response time	<0.1 μs

5.7 Vibration Measurement (Accelerometer)

The vibration transducer used to measure machinery or structural vibration converts vibration energy into a measurable voltage. Velocity pickups, accelerometers and eddy current or proximity probes can be used for vibration measurement [141, 142]. Here accelerometers were used because of their relative sensitivity, wider frequency range and robustness. The accelerometers attached to the test rig were Sinocera model CA-YD-185TNC. They were placed horizontally and vertically on the motor and

were each connected to the DAS. The results obtained by vibration analysis are shown in Appendixs A and B. The specification of the accelerometer is given in Table 9.

Table.9 Specification of the Sinocera accelerometer

Manufacture	Sinocera
Type	Accelerometer
Model No	CA-YD-185
Sensitivity	4.887 mV/ms^{-2}
Temperature Range	-40^{o}C to 120^{o}C
Frequency Range	0.5~5000 Hz
Weight	25 g
Mounting Method	M5
Power Supply	12~24VDC
Output Connector	TNT

5.8 Shaft Encoder

Encoders or speed transducers are widely used for measuring the speed of rotating machines such as electrical motors, turbines and internal combustion engines. Here the Hestler RI 32 shaft encoder was used, this produces a signal due to the rotational movement of the shaft of the IM. The encoder was coupled to the end of the IM shaft by a torsional rigid rubber coupling, see Fig. 5.9. The outputs of the encoder were connected to the DAS via channels 1 and 2. The specification of the encoder is shown in Table 10.

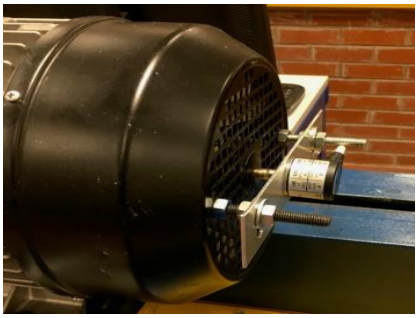

Figure 5.9 Hengstler Shaft Encoder

Table.10 Encoder specification

Manufacturer	HENGSLER
Type	RI 32
Mounting	Round flange
Number of pulses	100
Shaft diameter	5 mm
Maximum speed	6000 rpm
Operating temperature	-10 – 60 C
Supply voltage	DC 5V 10%

5.9 Induction Motor Fault Seeding

5.9.1 Rotor Fault Seeding

Failures in the rotors in squirrel cage IMs are due to a combination of different stresses, including: mechanical stresses due to fatigued parts or bearing faults; Dynamic stresses and centrifugal forces arising from shaft torque and unbalance; thermal stress due to thermal overload; magnetic stress caused by unbalanced magnetic forces, varying electromagnetic forces, and vibration [70, 93, 143]. When a rotor bar cracks, it overheats around the crack due to losses. The broken bar will also affect the adjacent bars, and this will be most noticeable during the start-up operation with any given load, because during start-up the bars carry higher current and so higher thermal stresses will occur [70].

The failures in the rotor in three phase IMs are represent about 10% of reported faults, see Fig. 2.3 [5, 70]. In this research, two faulty motors were used, with one broken rotor bar (1BRB) and with two broken rotor bars (2BRB), see Fig.5.10. These faults were introduced by drilling carefully into the bars along their length in such a way that the hole cut the bar simulated completely broken rotor bar.

Figure 5.10 Rotor with one and two broken bars

The results obtained with the healthy motor under different speeds and different torque loads were compared with those obtained with 1 BRB and 2 BRBs. Fig. 5.11 shows a healthy motor and motor with BRB at full speed with different loads. More details for different speeds and different loads are given in Appendix A and B.

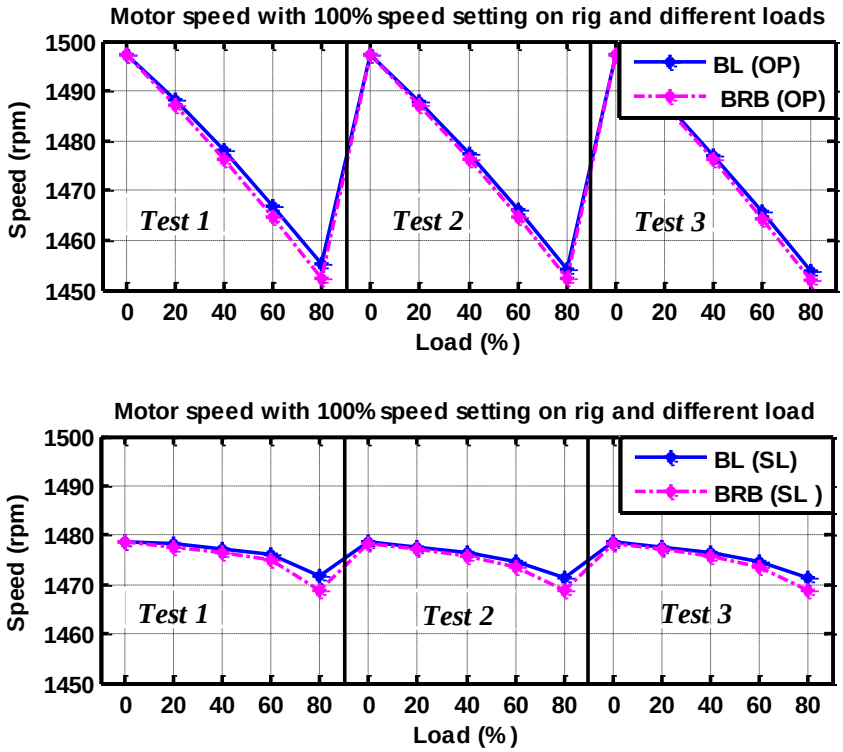

Figure 5.11 A healthy motor and motor with BRB at full speed with different loads using OP and SL control modes

5.9.2 Stator Fault Seeding

Stator windings may have different types of faults [5, 70]. However, the four most common and typical stator faults are: turn-to-turn fault, phase-to-phase short fault, phase-to-earth short fault, and open circuit coil fault [93]. These are asymmetric faults, which are typically associated with insulation failures, caused by such factors as; poor connection, overloading and overheating. An open circuit in the stator winding will affect the distribution of the stator MMF in the air gap. Early detection and mitigation of such faults can bring a great value to IM condition monitoring [94]. Studies have showed that stator faults generate unbalanced flux waveforms that cause the motor to draw asymmetrical phase currents resulting in unbalanced air gap flux [95, 96]. The distortion caused in the air gap flux by the fault can be attributed to resistive and inductive changes across the stator windings.

5.9.2.1 Open Circuit Fault Seeding

In this work, current and voltage signals were collected for three different conditions of the winding; healthy motor, one coil removed, and two coils removed, for equal increments in the load: 0%, 20%, 40%, 60%, and 80% of full load. This approach allows IM performance to be inspected at different loads and avoids possible damage of the test system if the faults were simulated only at the full load. As illustrated in Fig. 5.12, there are three concurrent coils, each with its individual phase.

Rearranging the connections to terminals B1, B2 and B3 permits rewiring the coils in phase B in three ways, supply to B1-B2-B3 is the healthy case, supply B1-B2 is the case of one coil removed (the smaller fault), and supply to only B1 removes two coils (the larger fault). Clearly, removal of these coils simulates an asymmetric stator that will enhance the motor's equivalent impedance and therefore damage its overall performance.

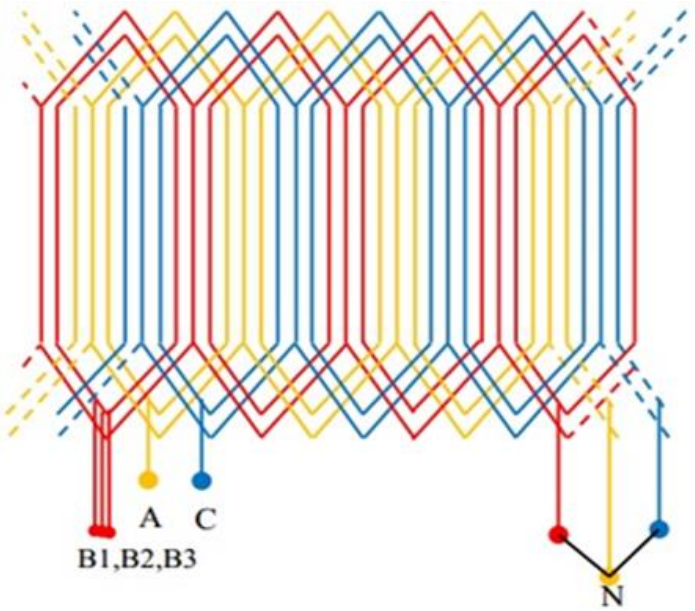

Figure 5.12 Schematic of stator fault simulation in phase B

To seed this fault, insulation surrounding the copper wire of three conductors was scraped off at the end of the same phase of an end stator winding and then a length of wire was soldered to each of these points, and these joints were subsequently reinsulated as can be seen in Fig. 5.13. The three wires were sent to the other terminal box, this box was fixed on the motor as shown in Fig. 5.14.

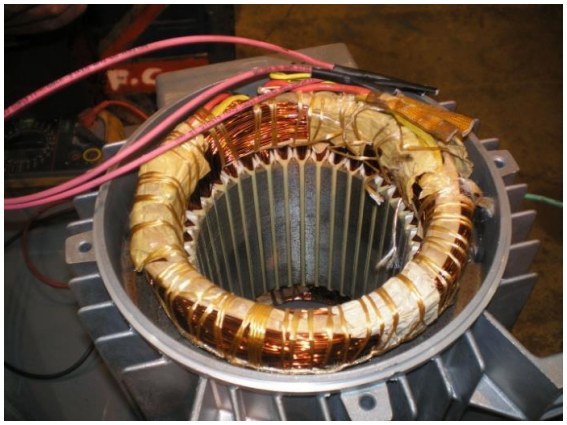

Figure 5.13 Soldered tappings into one phase

The terminal box contains a main phase supply. The three conductors of the phase were marked by points 4, 5 and 6, as shown in Fig. 5.14. The phase supply came from main box of the motor. This work was made by Lawton Electrical Services LTD

(LESL). Fig. 5.15 shows a healthy motor and motor with stator fault at full speed with different loads. More details for different speeds and different loads for healthy motor and motor with stator fault are given in Appendix A and B.

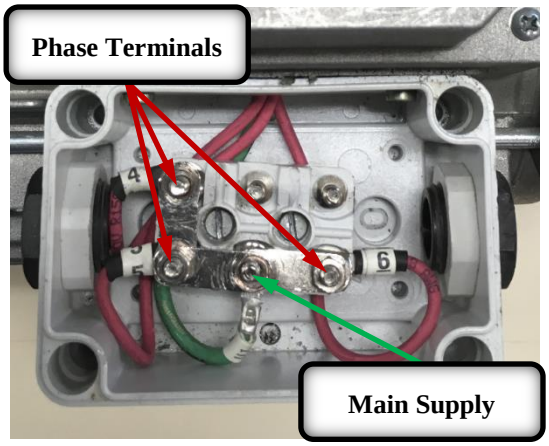

Figure 5.14 Terminal connection box

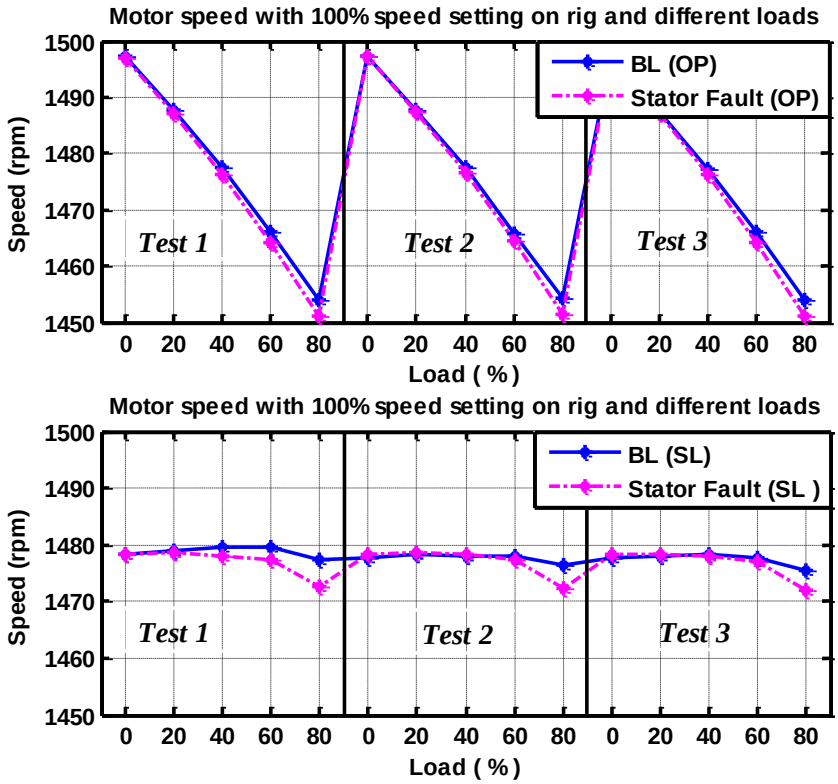

Figure 5.15 A healthy motor and motor with stator fault at full speed and different loads using OP and SL control modes

5.9.2.2 Short Circuit Fault Seeding

To evaluate the performance of the MSB analysis, current and voltage signals were collected for three different stator winding configurations, firstly a healthy motor, then with two inter turn short circuits and finally with four inter turn short circuits in the first coil in one phase. In each case there were two successive load conditions: 0% and 80% of full load. The simulated faults are as shown in Fig. 5.16. Each of the phases has 168 turns situated in 12 slots and distributed in four coils, each coil is further divided into two parts; the internal part includes 28 turns, whereas, the external part includes 14 turns. The wires for turns shorted were sent to the other terminal box, this box was fixed on the motor as shown in Fig. 5.17. This work was made by Westin Drives Ltd.

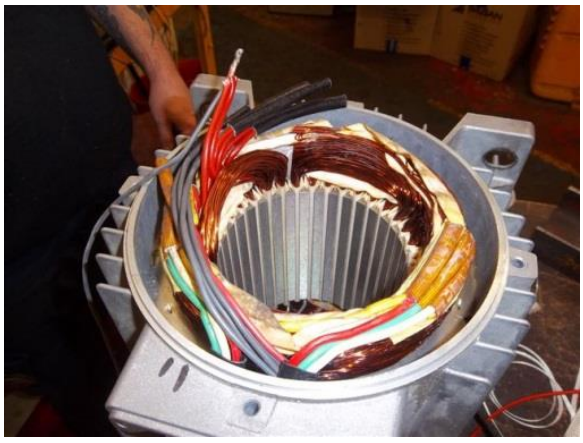

Figure 5.16 A-phase stator winding tapped at different numbers of turns

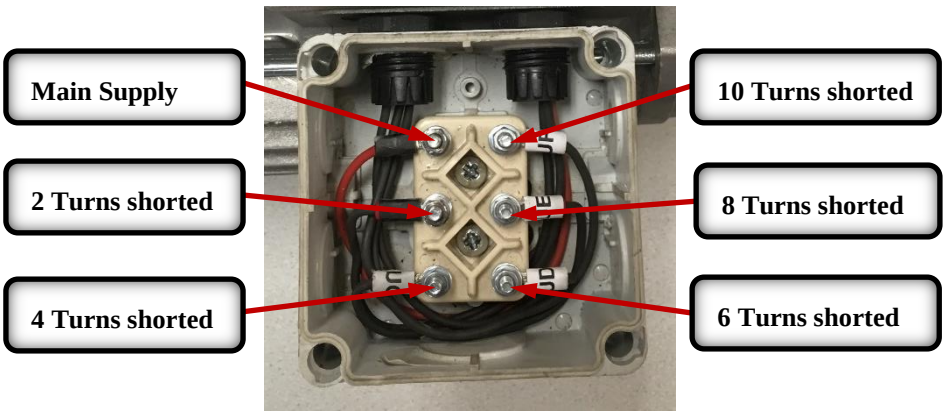

Figure 5.17 Terminal connection box

5.9.3 Combination Faults Seeding

The exposure of the motor to stator winding asymmetry, combined with a broken rotor bar fault reduces the efficiency and significantly increases the temperature and, consequently, the damage to the IM. Even if there is only a small imbalance in the motor resistance, a large unbalanced motor current can flow. A large unbalanced current creates difficulties for IM applications, due to heat generation, vibrations and acoustic noise, and shortening of the working life [100, 144-146].

The resistance fault simulated in one winding inside the AC motor affected one phase in a star connected motor. This is indicated in Fig. 5.18. The connecting cable resistance from drive to motor was measured at 0.3 Ω for each phase. The maximum fault resistance introduced a resistance of 0.4 Ω so that the total resistance between the drive and motor is increased from 0.3 Ω to 0.7 Ω in the faulty phase leg. In order to evaluate the performance of MSB analysis, current and voltage signals were collected for five diverse motor formations: healthy motor (BL), one broken rotor bar (1BRB), two broken rotor bar (2BRB), then further tests were carried out with 1 BRB compounded with a phase winding resistance increment ($R_{fs} = 0.4\Omega$) and 2 BRB fault also compounded with the phase winding resistance increment ($R_{fs} = 0.4\Omega$). The resistance increments were realised by an external resistor bank connected into one of the three winding phases, as shown in Fig. 5.19.

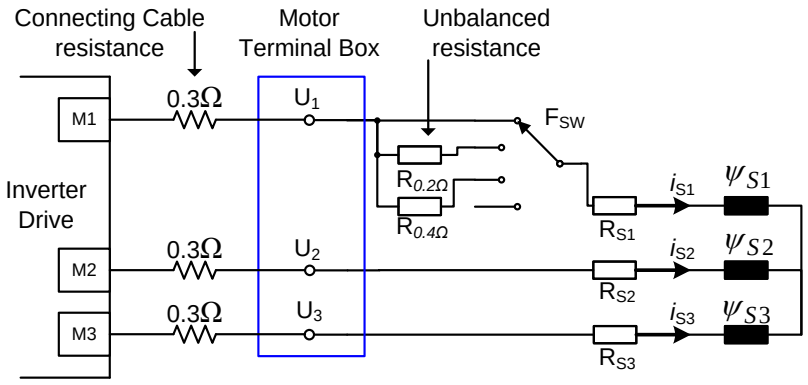

Figure 5.18 Asymmetry stator winding faults due to loose electric connection or winding shortages

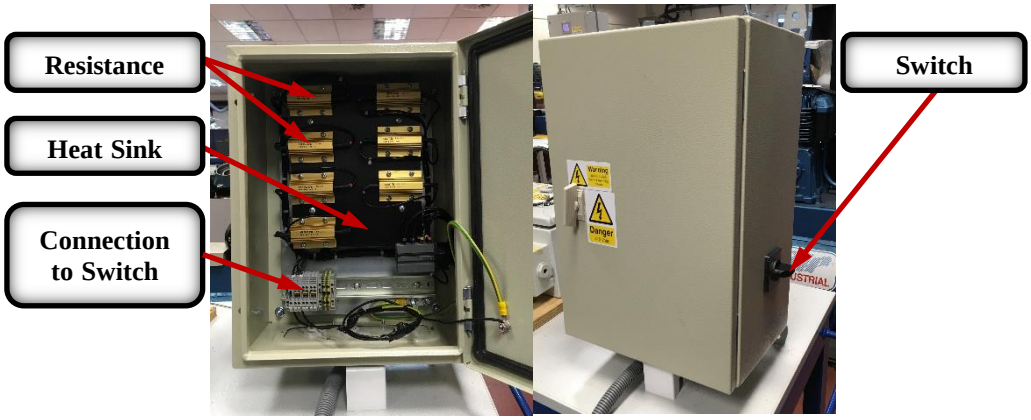

Figure 5.19 Photograph of external resistor bank

5.10 Summary

The test facility is located at the Centre for Efficiency and Performance Engineering, the University of Huddersfield. It has been used to carry out the experimental tests necessary for this thesis. This chapter has explained in detail the development of the test rig, including all the mechanical and electrical components: control systems, measuring equipment and sensors, and data acquisition system. The fault simulations and test procedure used to carry out in this research have also been explained.

In order to achieve the best results, every care was taken during the preparation and testing processes. For the safety of staff and visitors, all moving parts were covered with a safety grid and eye protection glasses and gloves were used. For the security of data and to obtain as accurate recordings as possible all cables were insulated and kept away from each other to eliminate any unwanted signal pick up.

All the data files and folders containing data from the experiments, sampling rate, fault types, and the name of all channels used by DAS, were given unique labels. From the results obtained, it could be said that the test facility is well equipped and it could be run for accurate and sophisticated tests with confidence and assured good results.

Chapter 6

Detection and Diagnosis of Induction Motor Faults Using Electrical Signals from Variable Speed Drives

This chapter reports the use of MCSA and motor voltage signature analysis applied to open loop control and sensorless control. Experiments are performed and motor current and voltage data collected by implementing different loads, different speeds, and both open loop control and sensorless control. The data collected is analysed in both the time and frequency domains. The baseline data (healthy motor) is compared with the corresponding data sets from tests of the motor with stator and rotor faults. The results obtained using open loop and sensorless controls are compared. Both current and voltage signatures from the sensorless control mode can give more effective and powerful in identifying these faults.

6.1 Introduction

As described in Chapter 2, there are a number of techniques that may be employed for the CM of induction motors. Signal processing of data obtained from these techniques provides accurate and consistent results. The methods of data processing vary from time domain statistical analysis to joint time-frequency analysis and it has been demonstrated that the spectrum analysis of motor current and voltage signals can be used to detect various faults without disturbing motor operation [147]. This work applies MCSA and voltage spectra analysis for the CM of induction motors subject to OP and SL control, with different loads and different speeds. The results obtained for the OP and SL control modes are compared with each other to decide the best approach.

6.2 Detection and Diagnosis of Stator Faults in Induction Motors

6.2.1 Stator Faults Diagnosis Using Open Loop (OP) Control

The study commenced by using time domain analysis of the measured current signals, with the motor under open loop (OP) control. The most common time domain measures used for CM are RMS, Kurtosis (K) and Crest Factor (CF). Fig. 6.1 shows these values for the current signal for the healthy motor and motor with faults seeded into it (removal of 1 and 2 coils), at full speed and under different loads.

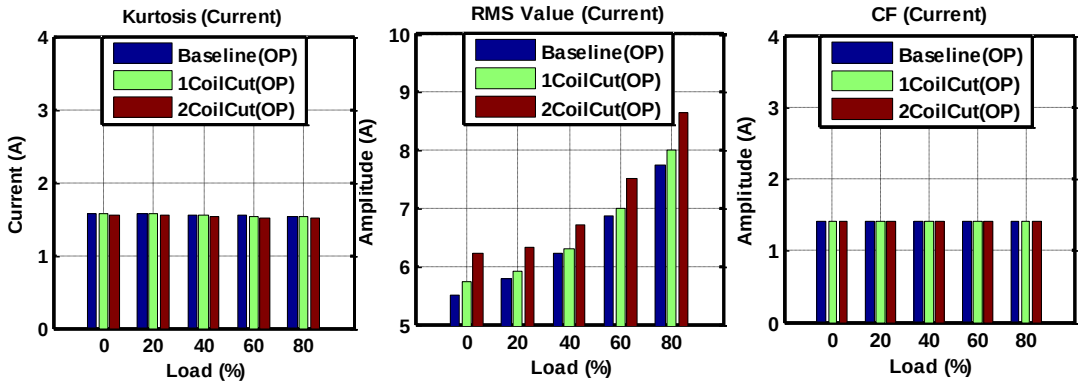

Figure 6.1 Statistical parameters Kurtosis, RMS and Crest Factor for the time-domain of the current signal under open loop control at full speed and different loads

It can be seen from Fig. 6.1 that the changes in CF and K were not significant with either load or fault. It was concluded that these features would not be effective indicators of the seeded faults. The changes in the RMS values for different faults and load are obvious and significant.

Fig. 6.2, 6.3 and 6.4 show the spectra of the stator current for healthy induction motor and motor with two coils removed, under 80% load and at three speeds, under OP control mode. These figures shows that the amplitude of the sideband at the frequency component is sensitive to the load, in other words slip frequency, and fault severity and the fault can be best detected under higher load.

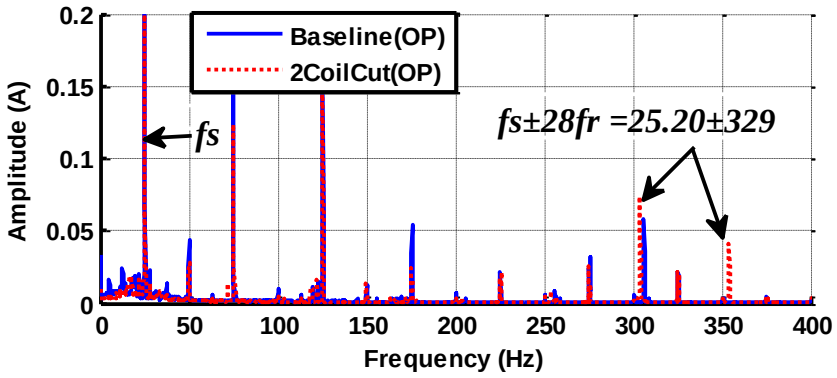

Figure 6.2 Phase current spectra under OP control with 80 % load and 50% speed

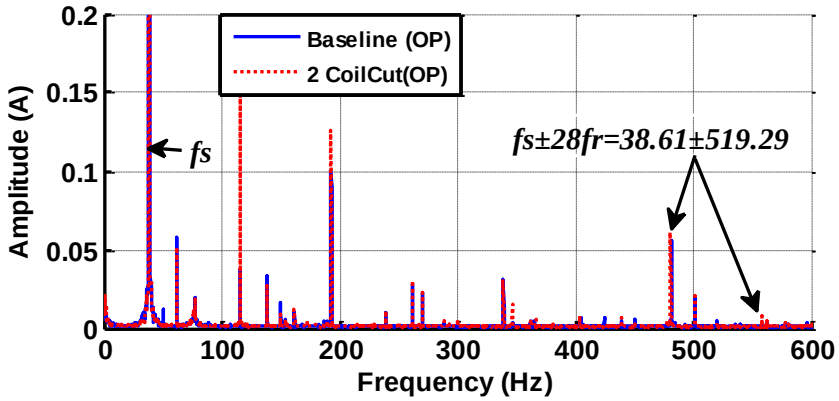

Figure 6.3 Phase current spectra under OP control with 80 % load and 75% speed

Fig 6.4 and bottom plot in Fig. 6.5 both refer to maximum speed and 80% full load and the apparent different between them is that Fig.6.5 shows the spectrum of stator

current which was obtained by applying the FFT to signals measured under the healthy condition and with the two seeded faults (one coil removed and two coils removed at full speed and under different loads with OP control mode.

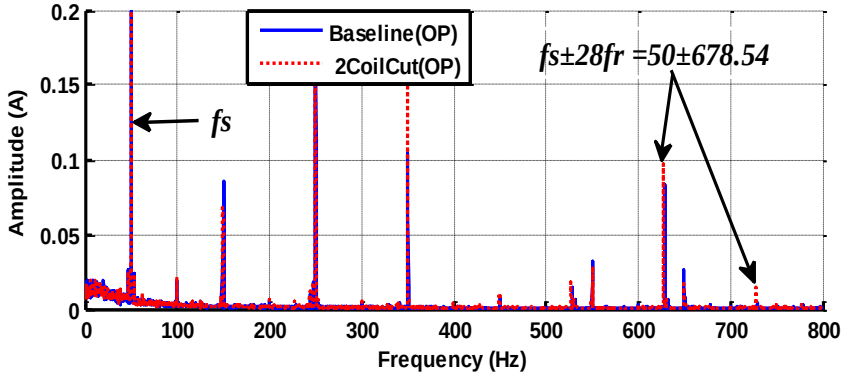

Figure 6.4 Phase current spectra under open loop control with 80 % load and full speed

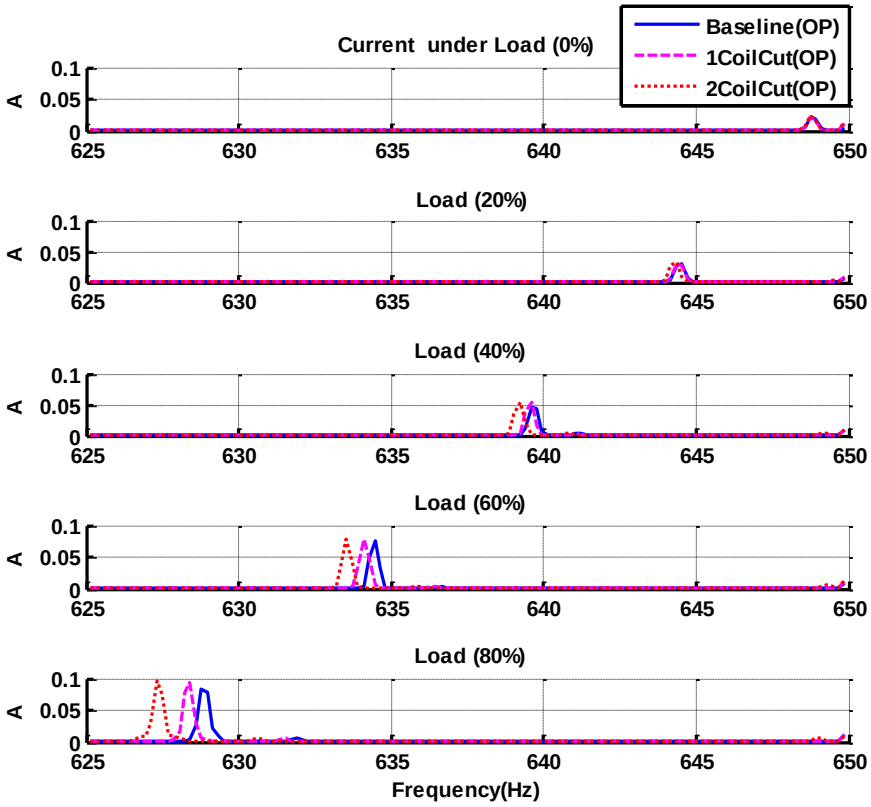

Figure 6.5 Phase current spectra under OP control with different loads and full speed for healthy motor and motor with one coil and two coils removed

It can be seen that there is a small visible sideband for stator faults under 0% motor load since the slip is small, as shown in the uppermost plot in Fig. 6.5. It can also be seen that the amplitude and frequency of the sideband changes as the load increases such that the fault can be best detected under higher loads. Additionally, Fig. 6.5 indicates that the presence of the fault increases the slip frequency. This is can be explained as the stator faults resulting in additional oscillations in the magnetic flux that transfer to the electromagnetic torque, which in turn has a direct effect on the slip frequency.

However, insufficient changes were found in the spectrum to be used to analyse the faults by using motor voltage signature analysis with respect to the OP control mode. This is due to the fact that in the OP mode the drive feeds the motor with a supply of a constant V/Hz ratio regardless the changes in the motor electromagnetic torque and current. Oscillations in the motor torque due to the fault are not seen by the drive as there is no feedback. The V/Hz ratio is kept constant even when the slip changes either due to the load or the fault. No compensation action is taken by the drive as long as the speed reference stays the same.

6.2.2 Stator Fault Diagnosis Using Sensorless (SL) Control

Fig 6.6 shows the RMS, CF and K values for the current signal for the healthy motor and motor with stator faults specified above, at full speed and under different loads with respect to the sensorless (SL) control mode. The changes in CF and K were not significant with either load or fault, and the changes seen in the RMS showed no significant differentiation between the seeded faults and the healthy case.

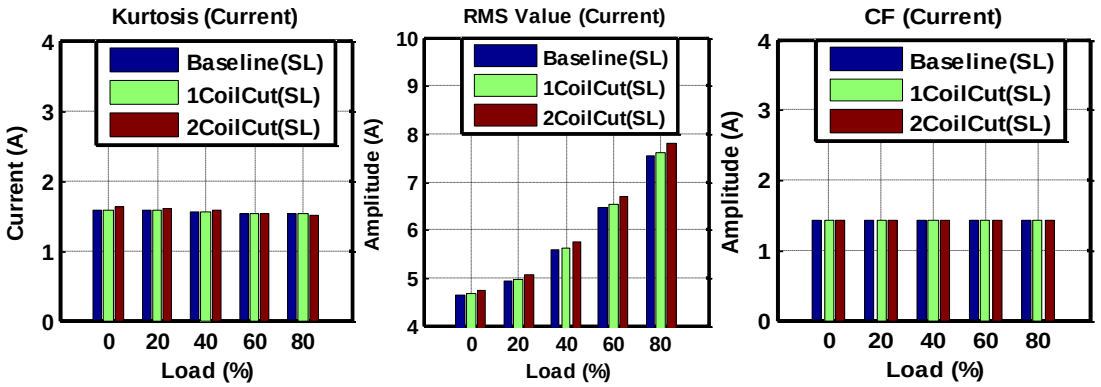

Figure 6.6 Statistical parameters Kurtosis, RMS and Crest Factor for the time-domain of the current signal under sensorless control mode

Fig 6.7 shows the RMS, CF and K values for the voltage signal for the heathy motor and motor with the two stator faults, at full speed and under different loads with respect to SL control mode. No significant differences were observed in CF or K with either load or fault. There were only small changes in the RMS for different faults at any given load.

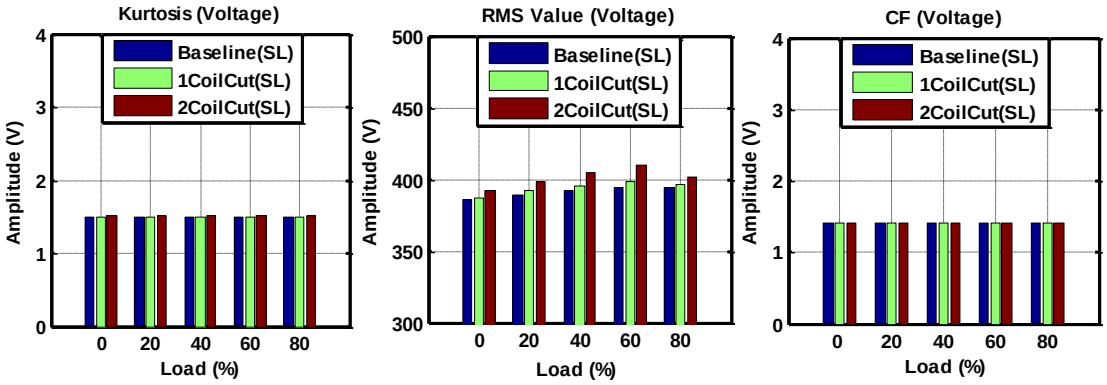

Figure 6.7 Statistical parameters Kurtosis, RMS and CF for the time-domain of the voltage signal under sensorless control mode

It was concluded that these statistical features extracted from the time domain will not be effective indicators of the given faults. More signal processing techniques are necessary to determine a robust feature able to diagnose induction motor stator faults.

Fig 6.8 shows the spectrum of the stator current, healthy and with the two stator faults, under different loads (0%, 20%, 40%, 60% and 80% of full load) and at full speed using SL control mode. It can be seen that there are visible sidebands in the stator current signal for both healthy and faulty condition. However, the sidebands cannot be discriminated one from another at low loads until the load reaches 60% and 80% full load can the peaks be separated and the fault identified. It is clear that the amplitude of the sideband increases as the severity of the fault and load increases and the fault can be best detected under high load.

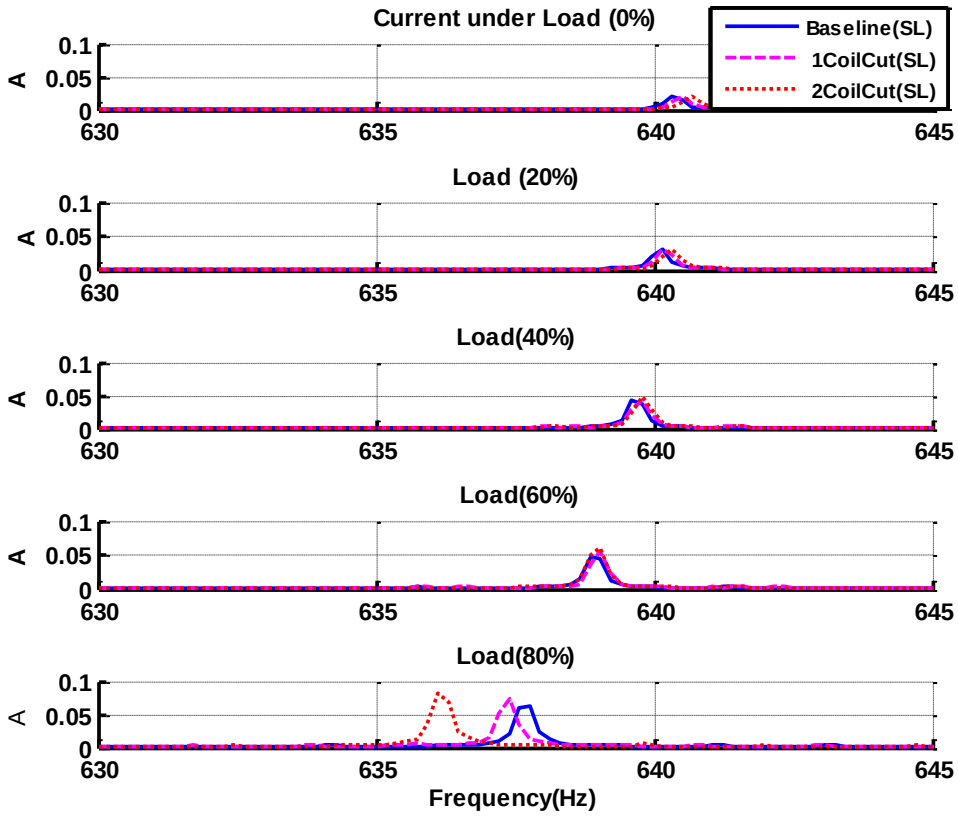

Figure 6.8 Phase current spectra under SL control with different loads and full speed for healthy motor and motor with one coil and two coils removed

These changes show more prominently when the load reaches 80% on the graph of results obtained for the SL mode, where the controller was less able to accurately in maintain the desired speed because of the fault effects. However not much of a difference can be seen in the OP graph when the load touches 80%.

Fig 6.9 depicts the spectra of the output voltage from the drive to the motor terminals. The sidebands contained in the voltage signal increase in amplitude with load and severity of the fault increases. The main concern is how well motor voltage signature analysis (MVSA) performs when it comes to detecting faults that occur in an induction motor. There have been some very strong arguments and references about the effectiveness of this technique with respect to SL but when it comes to the OP mode, there aren't any inevitable results that can be used in order to analyse the faults [73]. Experiments and results presented in this chapter demonstrate the same thing.

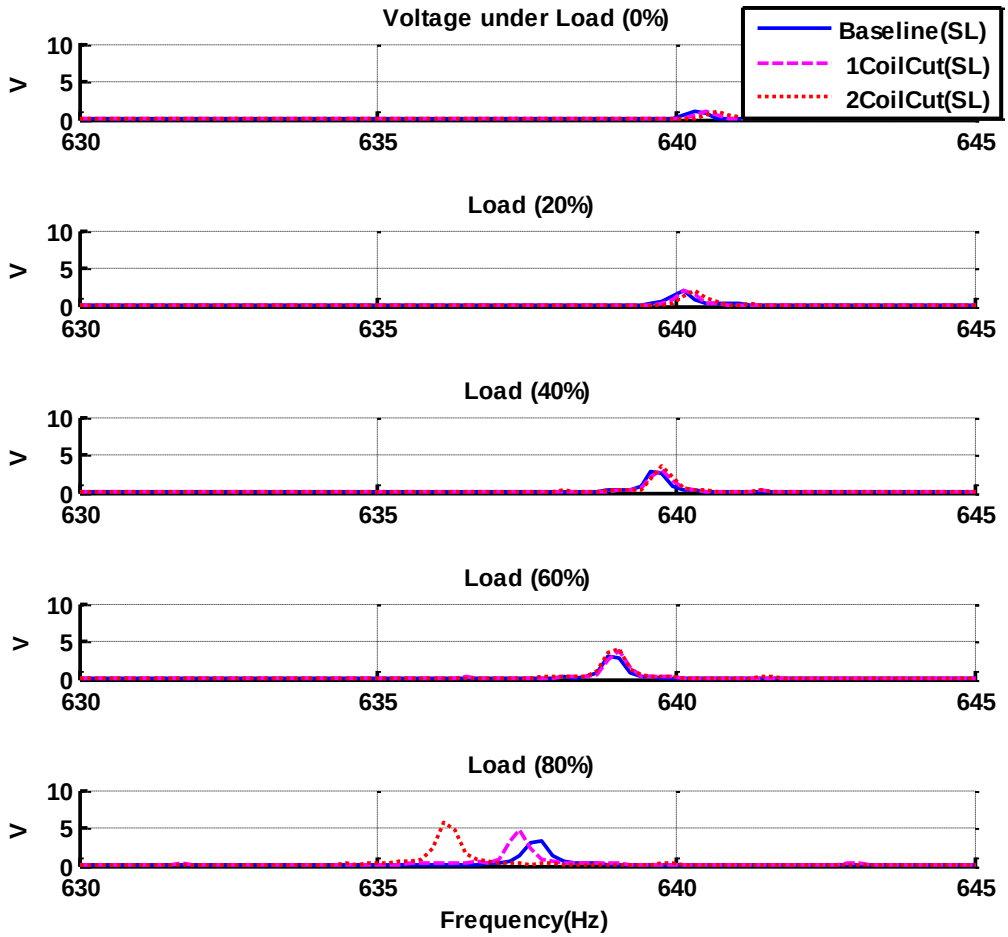

Figure 6.9 Voltage spectra for SL control with different loads and full speed for healthy motor and motor with one coil and two coils removed

Motor voltage signature analysis when used with the OP control mode doesn't provide a clear indication of the presence of a fault, even when the load is raised to 80%. On the other hand, in the SL the graph shows significant differences between the three sideband signals, mainly due to the differences in frequencies but also due to amplitude. This proves that readings taken with the SL mode allows more accurate and efficient analysis as compare to the OP mode.

6.3 Detection and Diagnosis of BRBs in Induction Motors

6.3.1 Broken Rotor Bars Diagnosis Using Open Loop (OP) Control Mode

Motor current signature analysis data sets were processed to achieve the current spectra which are then discussed. There are unique characteristic frequencies of a BRB fault that can be measured as described in Chapter 4. Fig. 6.10 and Fig 6.11 illustrate the current spectra for a healthy motor and a motor with broken rotor bars, at zero load and 80% of full load and at 75% of full speed and 100% full speed. For zero load the sidebands are weak, for the healthy and faulty motor. When the load is increased to 80% the amplitude of the sidebands increases substantially, with the signal for the two broken bars significantly larger than the signal for one broken rotor bar. It concludes that this fault (one or two bars) can be diagnosed under high loads using the phase current spectra for the OP control mode.

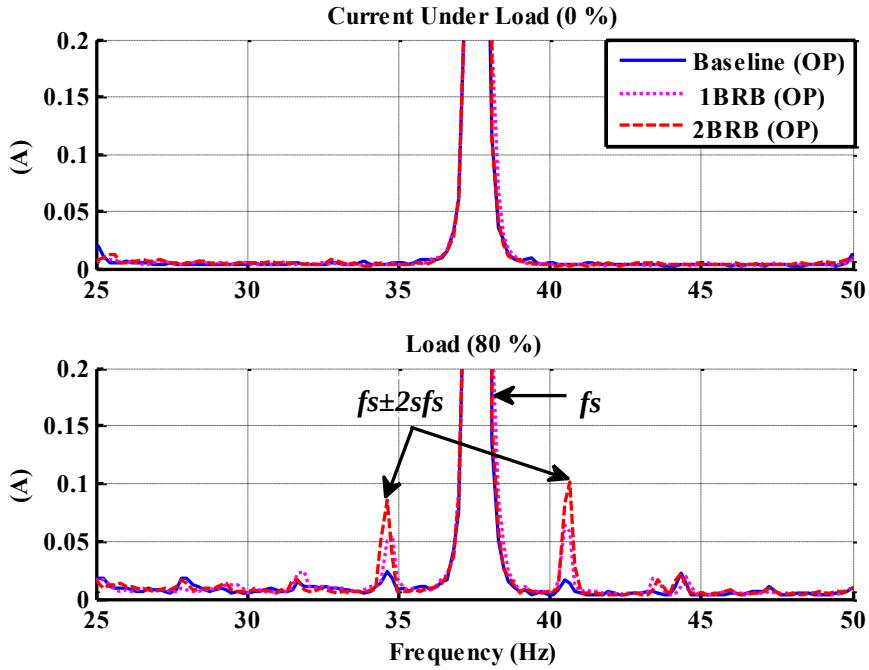

Figure 6.10 Phase current spectra for healthy motor and motor with one and two broken rotor bars under zero and 80% full load, at 75% full speed using OP control

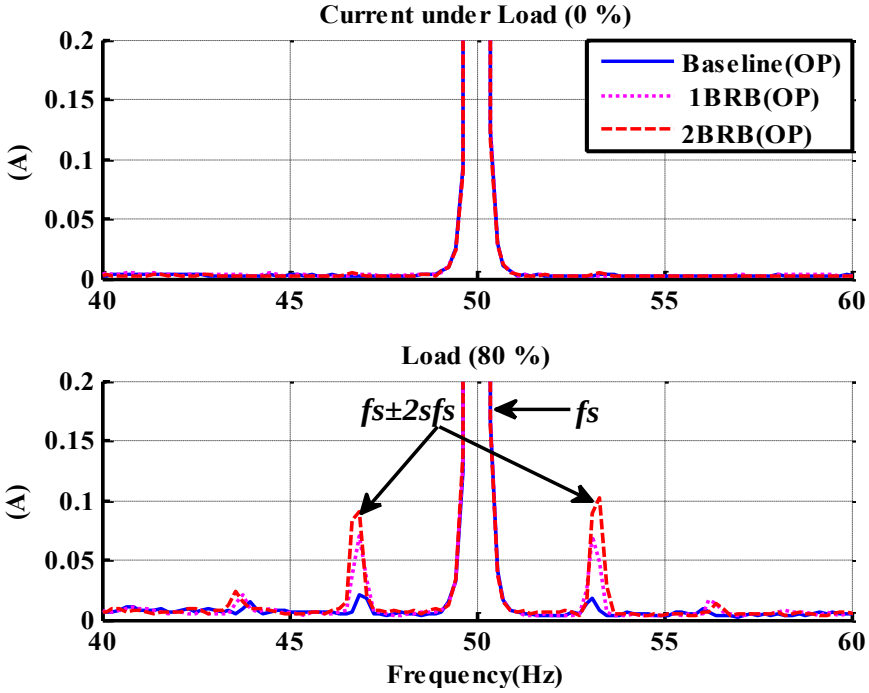

Figure 6.11 Phase current spectra for healthy motor and motor with one and two broken bars under zero and 80% full load, at full speed using OP control mode

As can be seen from Fig. 6.12, the detection of the slip frequency sidebands at low loads, certainly 20% of full load or less, is too difficult, since the peaks are too small to distinguish. However, for loads of 40% or more of full load the three peaks (for the healthy motor and the motor with broken rotor bar faults) are clearly seen and can be distinguished, the one from the others.

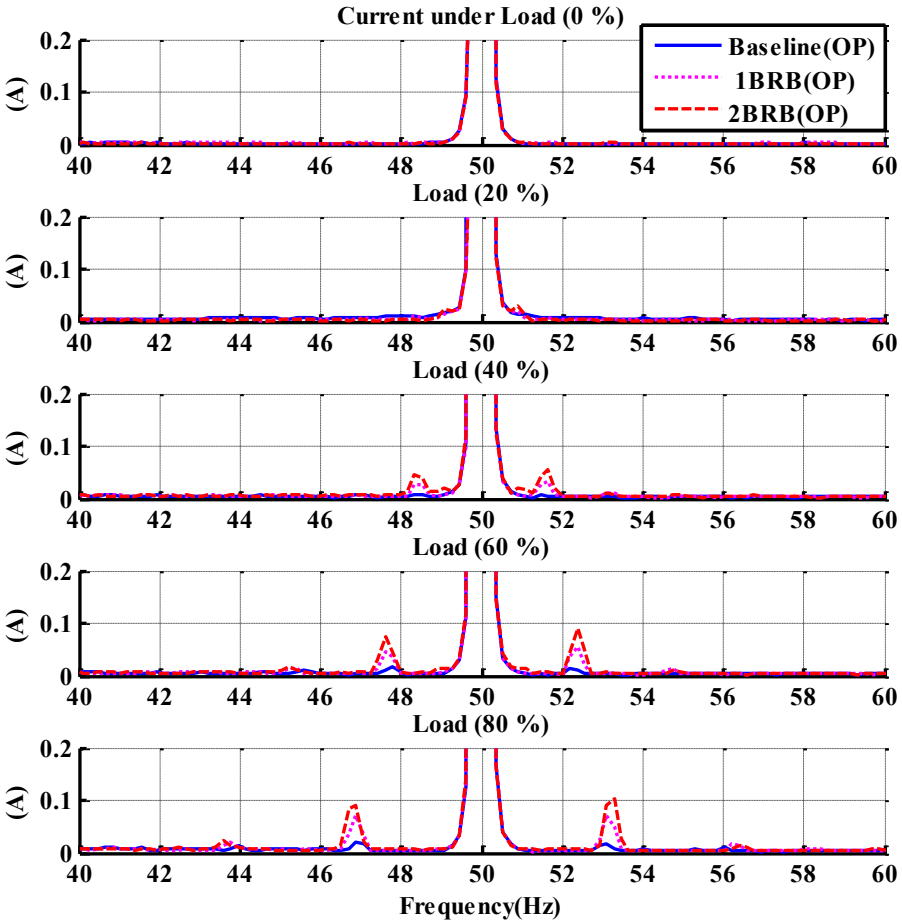

Figure 6.12 Phase current spectra for healthy motor and motor with one and two broken bars with different loads and full speed using OP control

The above discussion is clarified with the help of the Table 11, which presents the different quantities referred to in the plots. Each and every aspect of the experiment and present the result w.r.t load, speed, types of faults, and slip. From the details

presented in Table 11, it can be understood how differences in load affected the overall scenario and how easy it is to identify the fault if the load is increased.

Table.11 Tabulated results of MCSA for healthy motor and motor with two broken rotor bars under OP control at full speed

	Heathy Motor						Two Broken Bars					
Load	$f_{s(Hz)}$	$f_{r(Hz)}$	**Ls**	**Rs**	**Slip**	$2sf_s$	$f_{s(Hz)}$	$f_{r(Hz)}$	**Ls**	**Rs**	**Slip**	$2sf_s$
0%	50.014	24.954	49.803	50.224	0.002	0.210	50.014	24.954	49.799	50.228	0.002	0.214
20%	50.014	24.797	49.177	50.850	0.008	0.836	50.014	24.787	49.134	50.893	0.008	0.879
40%	50.014	24.625	48.487	51.540	0.015	1.526	50.014	24.603	48.403	51.626	0.016	1.612
60%	50.014	24.436	47.733	52.294	0.022	2.280	50.014	24.407	47.617	52.410	0.024	2.396
80%	50.014	24.238	46.939	53.088	0.030	3.074	50.014	24.199	46.781	53.246	0.032	3.232

6.3.2 Broken Rotor Bars Diagnosis Using Sensorless (SL) Control Mode

The analysis and measurement methodology for the SL mode is not much different from the OP control and the equations that were used in the previous sections are repeated here. The results are presented and discussed in the same way as in previous sections. Fig. 6.13 shows the spectrum of stator current for a healthy motor and motor seeded with broken rotor bars under different loads at full speed, using the SL mode. It can be seen that there are no visible sidebands with a broken rotor bar at 20% load since the slip is too small to be identified. It is clear that the amplitude of the sidebands increases as the severity of the fault and load increases and the fault can be best detected under high load. The sideband beaks rise and spread, most noticeable when the load reaches 60% and 80% of full load. These peaks are more noticeable than the sideband peaks seen in Fig. 6.12, the OP graph. This suggests that the SL mode approach is likely to be more effective and accurate than the OP mode approach.

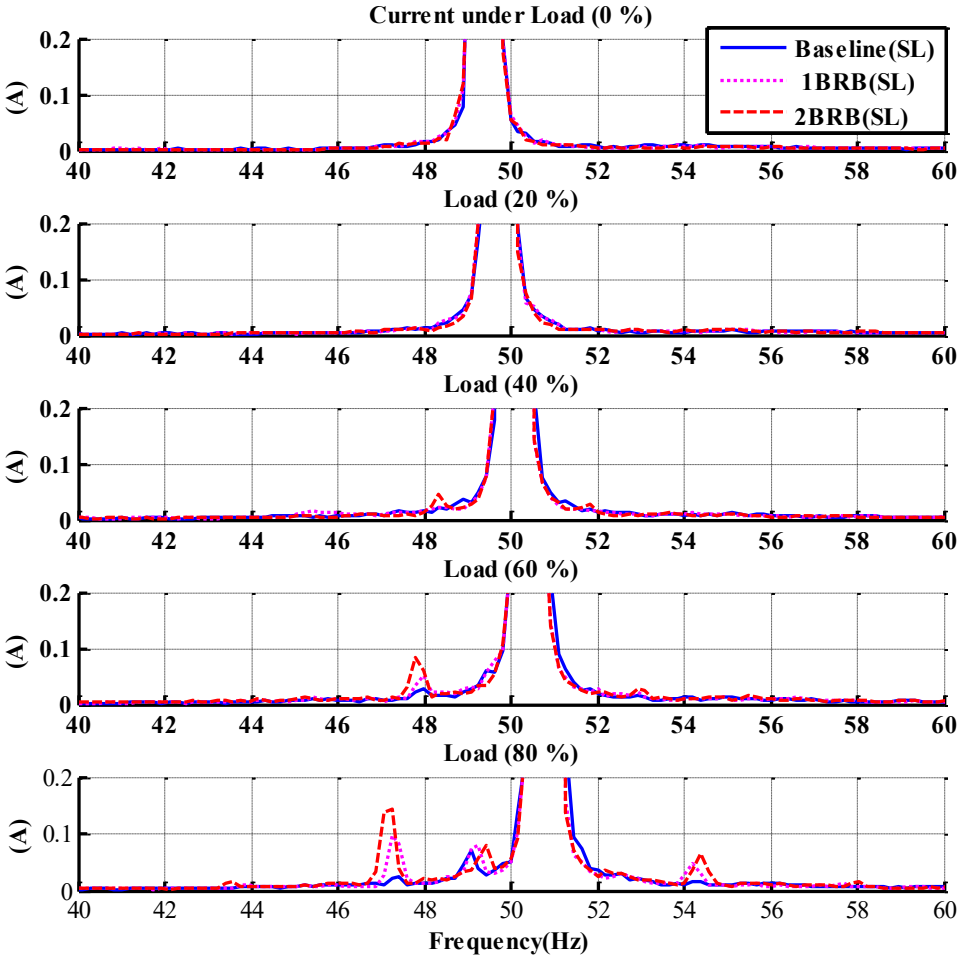

Figure 6.13 Phase current spectra for healthy motor and motor with one and two broken bars under different loads and full speed using SL control mode

Justification of this can be understood with the help of the factual values given in Table 12 below, which shows how the load is affecting the frequency and how it is significantly drawn in the Fig.6.13.

Table.12 Tabulated results of MCSA for healthy motor and motor with two broken rotor bars under SL control at full speed

	Heathy Motor						Two Broken Bars					
Load	$f_{s(Hz)}$	$f_{r(Hz)}$	**Ls**	**Rs**	**Slip**	$2sf_s$	$f_{s(Hz)}$	$f_{r(Hz)}$	**Ls**	**Rs**	**Slip**	$2sf_s$
0%	49.464	24.645	49.115	49.814	0.003	0.297	49.464	24.640	49.097	49.832	0.003	0.297
20%	49.830	24.631	48.696	50.964	0.011	1.134	49.647	24.619	48.829	50.466	0.008	0.818
40%	50.014	24.613	48.440	51.587	0.015	1.573	50.014	24.595	48.367	51.660	0.016	1.646
60%	50.380	24.589	47.976	52.784	0.023	2.404	50.380	24.560	47.863	52.897	0.025	2.517
80%	50.746	24.538	47.406	54.086	0.032	3.340	50.746	24.480	47.173	54.319	0.035	3.552

As introduced and discussed in the previous section, the voltage signal was analysed for a healthy motor and a motor with seeded broken bar faults, at different loads and full speed, using the SL control mode, in a similar manner to the current, see Fig. 6.14. The results showed some notable and inevitable differences.

Low loads of zero and 20% full load don't produce any notable change in the plot, but as the load in increased above 40% both right and left sidebands appear with more or less equal amplitudes, which drastically increased when the load reached 60% and 80%. This demonstrates that analysis of the voltage signal is useable as a means of determining the presence of a broken rotor bar, possibly at an early stage of development.

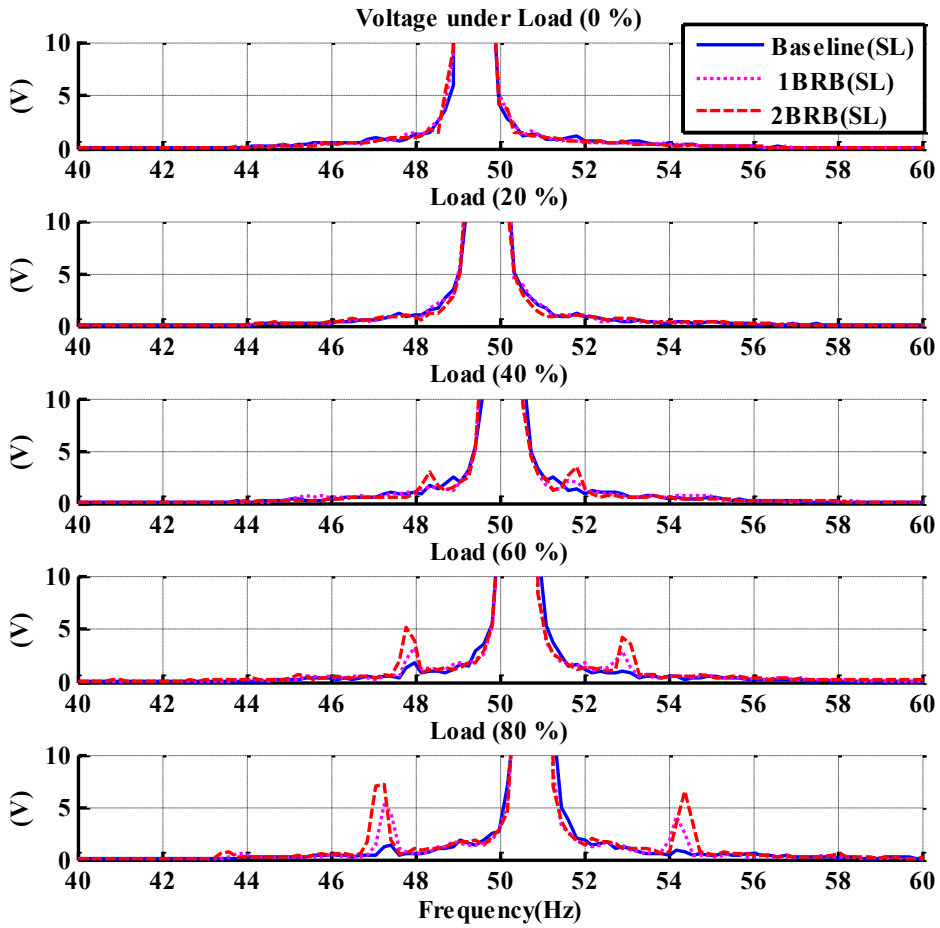

Figure 6.14 Phase voltage spectra for healthy motor and motor with one and two broken bars under different loads and full speed using SL control

6.4 Comparison between Techniques

A comparative study of different CM techniques which include analysis of motor current and voltage signatures using OP and SL control modes has been made for a healthy motor and a motor with seeded stator and rotor faults. Fig. 6.15 shows the diagnostic performance of the current signal with one and two coils removed from the stator under OP and SL control modes, under different loads. It is significant that during OP and SL operation using MCSA, the amplitude of sidebands increased as the severity of the fault and load increased.

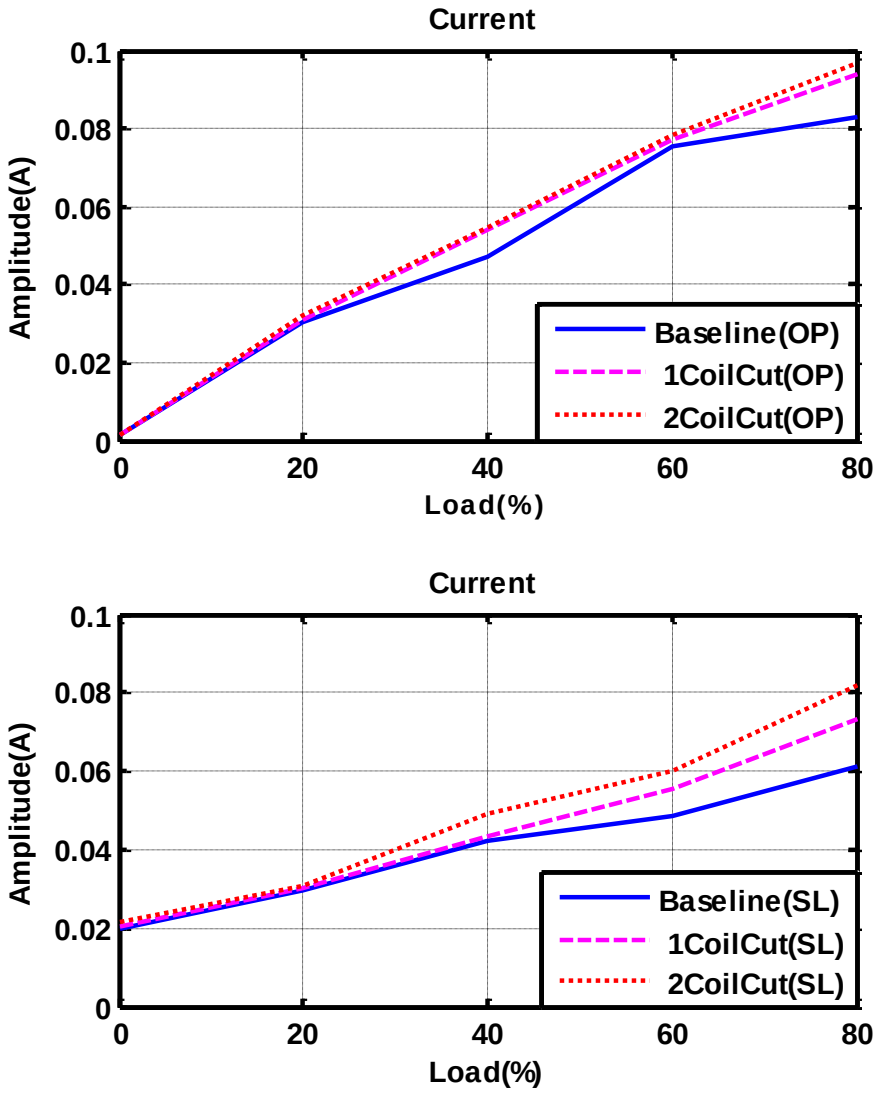

Figure 6.15 MCSA diagnostic performance under OP and SL control modes for health motor and motor with stator faults

However, motor voltage signature analysis provides effective diagnostic features under the SL control mode as shown in Fig.6.16. The voltage spectrum demonstrates slightly better performance in detecting the faults than the motor current spectrum because the VSD regulates the voltage to counteract changes in the electromagnetic torque caused by the fault.

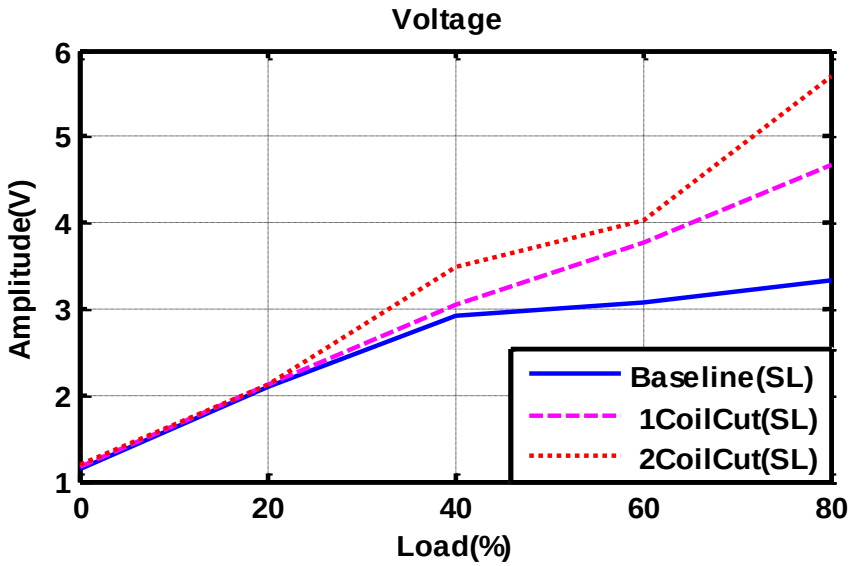

Figure 6.16 Voltage diagnostic performance under SL control mode for healthy motor and motor with stator faults

Fig 6.17 shows the diagnostic performance of current signals under different cases of broken rotor bars, and under different loads with respect to the OP and SL controls mode. It can be seen that at zero and 20% load the two controls modes give the same, minimal response. At the 60% and 80% of full load the SL mode is more sensitive to the presence of either fault.

It is significant that the amplitude of sidebands increases as the severity of the fault and load increase, and the presence of spectrum peaks enable the faults to be detected under high loads (60% and 80% of full load).

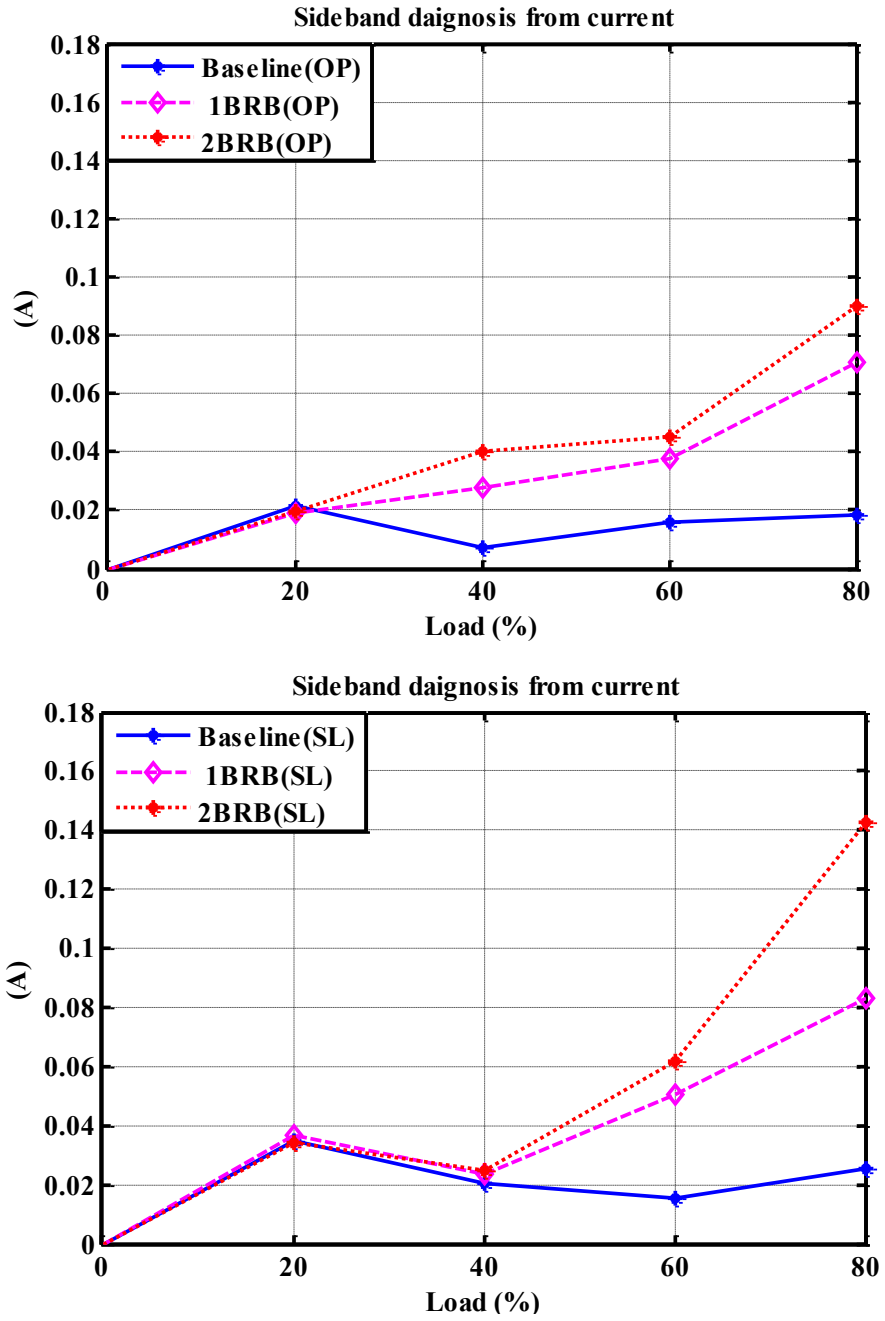

Figure 6.17 Current signal diagnostic performance under OP and SL control modes for a healthy motor and motor with broken bar faults

Compared to the MCSA based diagnosis shown in Fig. 6.17, the voltage based diagnosis shown in Fig.6.18 is able to provide more effective fault diagnosis when it comes to detecting faults that occur in an induction motor. The SL control mode gives

measurable indication of the rotor faults once the load is above 40%, and at 80% load the graph shows prominent increases in sidebands and the results show some notable and inevitable changes. Therefore, in closed-loop systems the spectrum based on voltage signals is more sensitive to these faults and hence produces more accurate results than current signals. This can be explained that the VSD regulates the voltage to adapt changes in the electromagnetic torque caused by these faults.

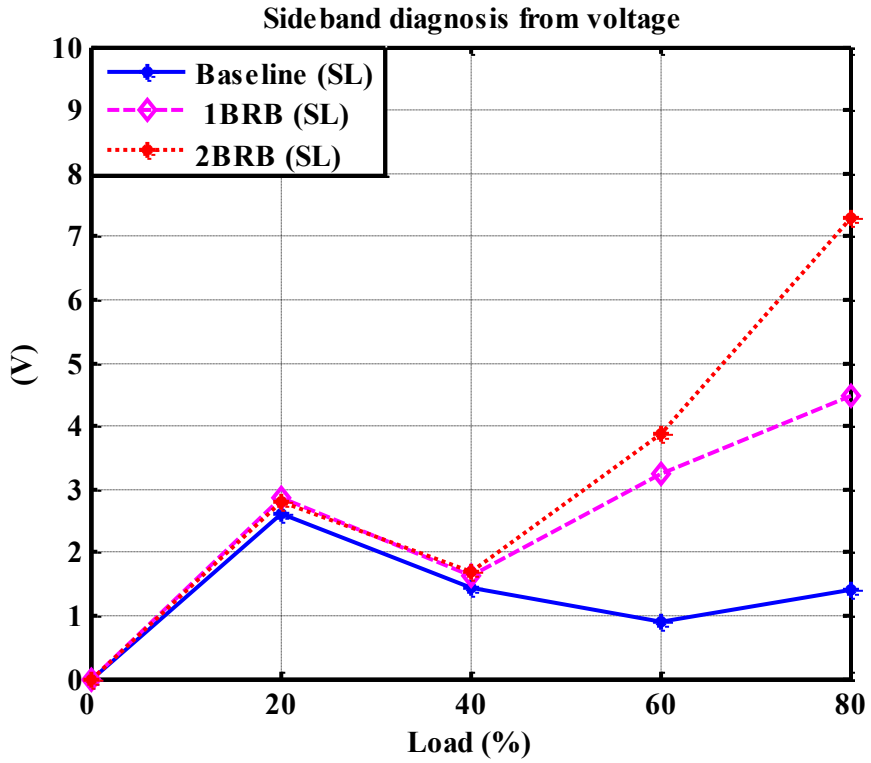

Figure 6.18 Voltage signal diagnostic performance under SL control mode for a healthy motor and motor with broken bar faults

6.5 Summary

This chapter gave an insight into different techniques used to monitor the condition of a three phase induction motor for early detection and prevention of a catastrophic incident that could occur if proper precautionary measures were not taken. The experimental results that are presented in this chapter provide a clear demonstration that the techniques can be used to monitor the condition of an induction motor. A

comparative study has been made of different CM techniques (motor current and voltage signal analysis) for detection of specific stator and rotor faults for both OP and SL control modes.

Fig. 6.15 and Fig. 6.17 show the comparative diagnostic performance of MCSA for the given fault cases under the two control modes, for loads equal to or less than 80% of full motor load. The spectrum of the stator current shows that the amplitude of the sidebands increases with fault severity and load for both open loop and sensorless operating modes.

Similarly, with voltage signature analysis the sidebands in the voltage spectrum increase in amplitude with increase in load and fault severity, but they appear only for the SL control mode, see Fig. 6.16 and Fig. 6.18. The voltage spectrum demonstrates slightly better performance than the motor current spectrum because the VSD regulates the voltage to adapt to changes in the electromagnetic torque caused by the fault. Additionally, a significant increase in slip frequency has been noted as fault severity and load increase in both SL and OP modes.

It is shown that sensorless control gives a more reliable and accurate diagnosis. However, it is difficult to detect the presence of the seeded faults under low load and low speed conditions because of a low signal to noise ratio. Therefore, this research will focus on developing advance signal processing techniques such as higher order statistics.

Chapter 7

Motor Stator Fault Detection Based on Modulation Signal Bispecrum Analysis Using Variable Speed Drives

This chapter proposes a method for the condition monitoring of a three phase induction motor using electrical signals obtained from variable speed drives and advanced signal processing techniques, for detection and diagnosis of stator winding faults. The electrical signals from the variable speed drive contain unique fault frequency components that can be used for stator winding fault detection. Evaluation results show that the stator faults cause an increase in the sideband amplitude and this increase is observed in both the current and voltage signals under the sensorless control mode. MSB analysis provides a good noise reduction and produces a more accurate and reliable diagnosis in that it gives a more correct indication of the fault severity and its location, for all operating conditions.

7.1 Introduction

A motor failure due to stator winding faults may result in the shutdown of a generating unit or production line. Stator windings may have different types of faults. However, there are four main typical stator faults: turn-to-turn fault, phase-to-phase short fault, phase-to-earth short fault and open circuit coil fault [2, 70, 93, 148, 149]. These are asymmetric faults, which are typically associated with insulation failures, caused by, for example, poor connections, overloading and overheating, Fig. 7.1 shows these four main faults. Early detection and mitigation of such faults would be of great value to induction motor condition monitoring. In addition, it would help eliminate costly lost production time and avoid expensive maintenance and repair [73, 94, 150, 151].

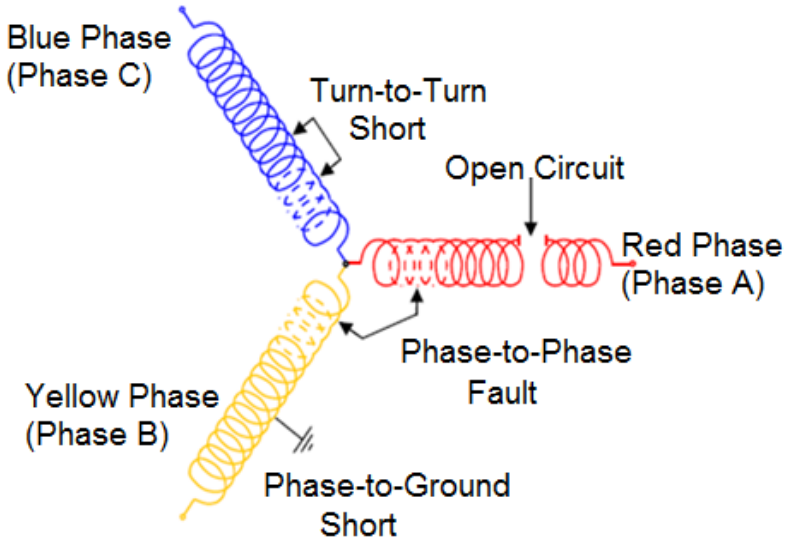

Figure 7.1 Different three-phase stator winding faults [73]

Electrical failures are common in the induction motor windings. Most of them are caused by over-voltage and current overload in the circuit during testing or operation. The inter-turn short circuit of the stator winding is influenced by the quality of the insulation between the turns and phases of the coils inside a motor [93, 152]. Mechanical stress is generated by stator coils moving during the operation of a motor.

When the motor starts, the current in the coils will reach its highest value and it will result in a large magnetic force. This magnetic force will cause the coils to vibrate at twice the line frequency. This vibration could damage the stator and other motor components. Another fault consequence is electrical stress [152, 153].

Thermal stress is another major reason for a stator short circuit and results from the insulation deterioration due to the motor working temperature being higher than the designed temperature. The insulation life will be reduced by half every 10^{o}c temperature increase above the design temperature [152]. Thermal stress can also reduce the life of a motor when the motor is overloaded and operating at higher than rated voltage. Environmental stress cannot be neglected, contamination, such as dust, oil and moisture, may enter into the motor and these contaminations influence the stator insulation lifetime and result in winding faults in the motor [153, 154].

In order to evaluate the performance of MSB analysis, current and voltage signals were collected under three different stator winding configurations: healthy motor (baseline - BL), a two inter-turn short circuit and a four inter-turn short circuit as shown in Fig. 7.2 for the coil designated phase A. The tests were performed under different loads 0% and 80% of full load. Table 13 shows the severity of short winding faults and load conditions for various experiments conducted to diagnose the short winding fault. A schematic diagram and a photograph of the test rig which was used to conduct the experimental investigations are shown in Fig. 5.1 and Fig.5.2 and the details of the AC induction motor used in this test are presented in the Table 2.

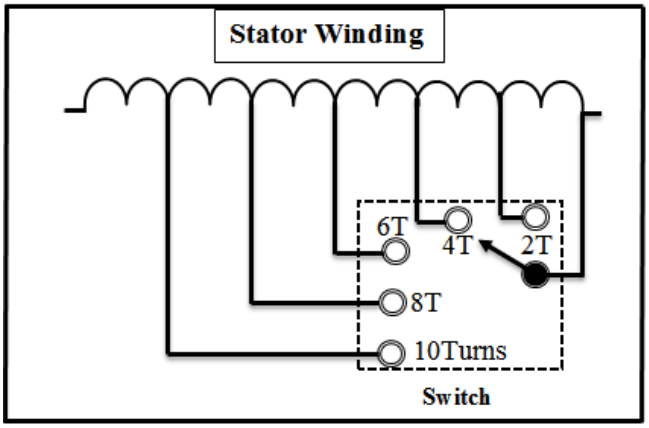

Figure 7.2 A-phase stator winding tapped at different number of turns

Table.13 Experimental conditions for short winding fault detection

Experiments	Severity of short winding fault	Load condition
1	Motor Healthy (BL)	0% and 80%
2	2 Turns Shortened (2T)	0% and 80%
3	4 Turns Shortened (4T)	0% and 80%

A power supply measurement box was used to measure the AC voltages, currents and power using Hall effect voltage, current transducers and a universal power. During the experimental work all the data was acquired using the Sinocera YE6232B high speed data acquisition system, as described in Section 5.5. The system, including encoder, sampling frequencies and anti-aliasing is fully described in section 5.5. In all the following measurements the motor was at full speed.

7.2 Baseline of Electrical Signals from Sensorless Control Mode

Fig. 7.3 and Fig. 7.4 show a direct comparison between a MSB slice at the supply frequency, and power spectrum for the current and voltage signals, both under 80% load at full speed with sensorless drives when the motor was healthy (baseline). MSB shows a very good noise reduction performance compared with the power spectrum, as shown in Fig. 7.3 (a) and Fig. 7.4 (a). The 50 Hz supply component in the power spectrum is eliminated completely in the MSB. This makes it easier and more reliable

to observe components that relate to motor health conditions. For example, the sideband components: (50.54-3.125) Hz and (50.54+3.125) Hz either side of the 50.54 Hz shown by the power spectrum in Fig. 7.3 (b) and Fig. 7.4 (b) due to rotor asymmetric errors, are combined into a signal bispectral peak at frequency 3.125 Hz, which is much easier to be identified and hence MSB allows a significant reduction of the effort needed for spectrum analysis.

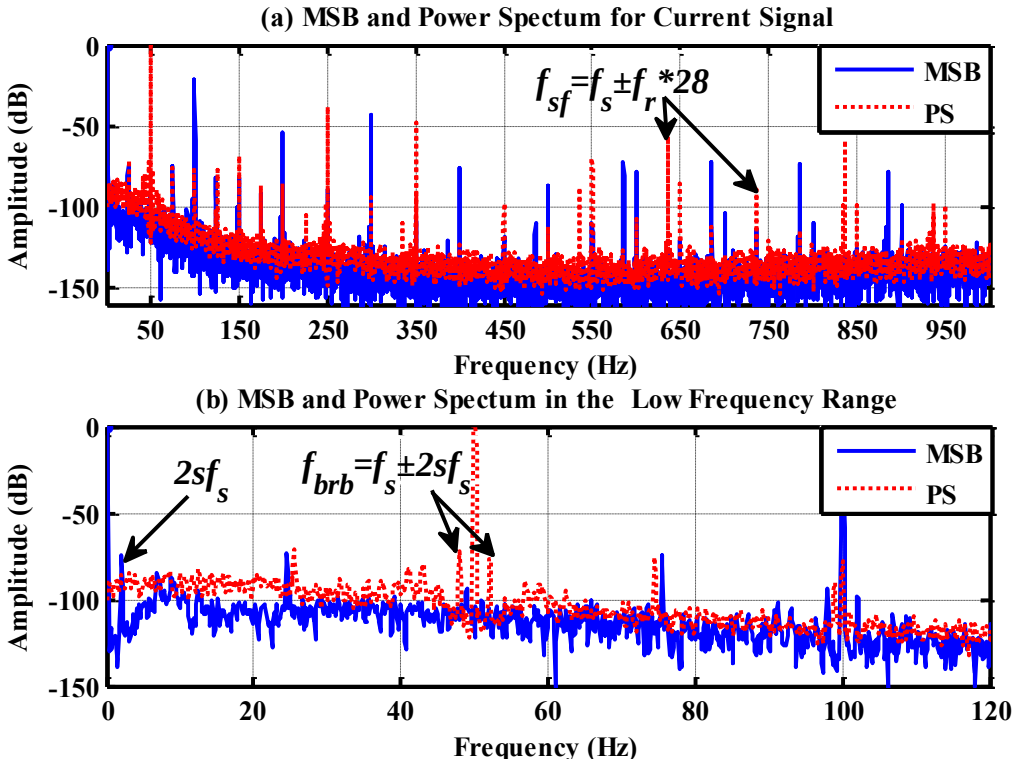

Figure 7.3 MSB and power spectrum characteristics for current signals at 80% of full load

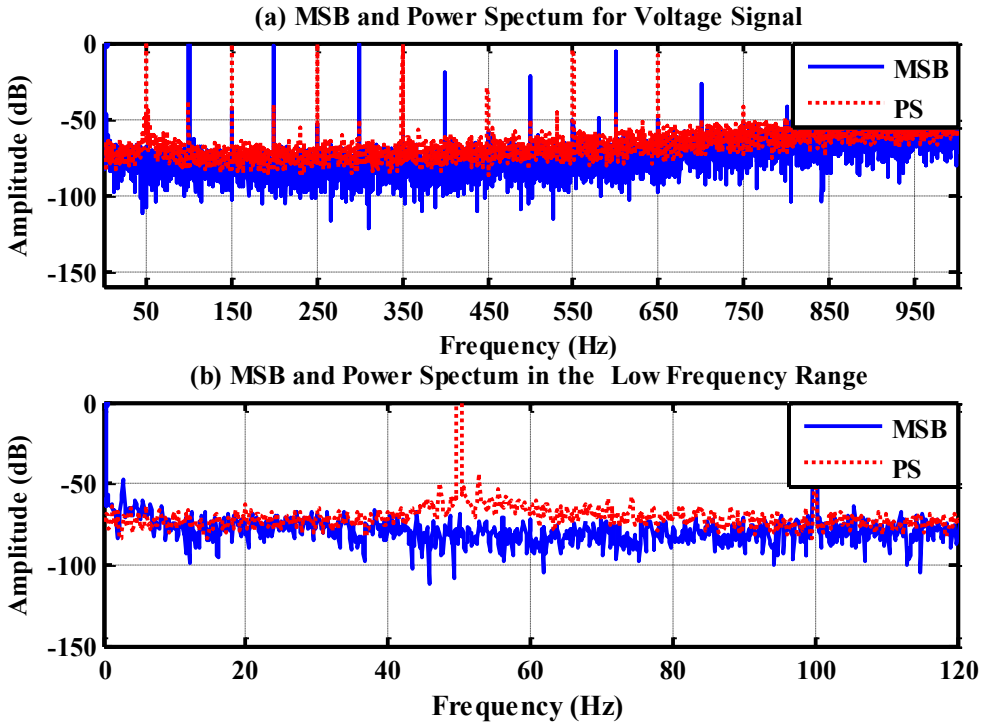

Figure 7.4 MSB and power spectrum characteristics for voltage signals at 80% of full load

Moreover, the MSB analysis shows better performance in noise reduction than the power spectrum. This allows the spectral peaks such as those due to inter-turn short circuits in the high frequency range to be estimated more accurately and hence to obtain more accurate and better diagnostic results.

7.3 Detection and Diagnosis of Stator Short Circuit Faults Using Electrical Signals from Sensorless Drives

Mehala [93] and Penman [148] derived the following formula to predict the components in the airgap flux waveform that is due to shorted-turns.

$$f_t = \left[\frac{n}{p}(1-s) \pm q\right] f_s \qquad (7.1)$$

where f_t are the frequency components due to the shorted turns, f_s is the supply frequency, p the number of pole-pairs, s is the motor per unit slip, and n = 1, 2, 3… is an integer and q = 1, 2, 3… is also an the integer.

Thomson and Gilmore [9] and Abdelhamid [3] used the above relationship to predict the frequency components generated by the presence of shorted turns and claimed that the diagnostic components are 125 Hz and 175 Hz (with *q* set to 1 and n set to 3, 5). Fig. 7.5 shows the A- phase stator current power spectra under healthy conditions and 4 shorted turns at 0% and 80% loads, with respect to the sensorless control mode. It can be seen that from Fig. 7.5 the two frequency components located at 125.5 Hz and 176.4 Hz are present in the faulty current spectrum and the amplitude of these sidebands increase as the load and fault increase. For the healthy motor, these components are small. The results presented in Fig. 7.5 agree with those obtained by Thomson and Gilmore [9] and Abdelhamid [3].

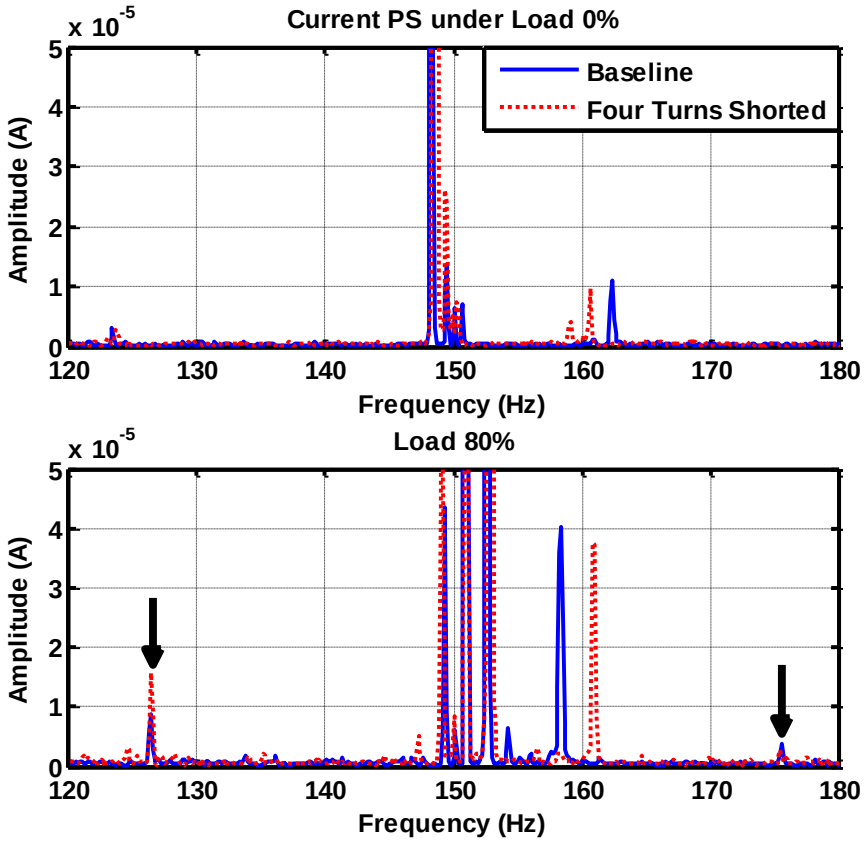

Figure 7.5 A-phase current power spectrum for healthy motor and motor with a four inter-turn short circuit fault at zero and 80% full load using SL control mode

Typical stator current MBS are shown in Fig. 7.6 for the current signals for 0% and 80% loads and motor healthy and motor with 4 shorted turns under sensorless control mode. Similar to the characteristics observed from power spectra in Fig. 7.5 MSB peak amplitudes at the characteristics frequencies increase with increase in load. However, the amplitude increases more significantly with introduction of the fault. MSB analysis shows very much better performance in noise reduction than power spectrum.

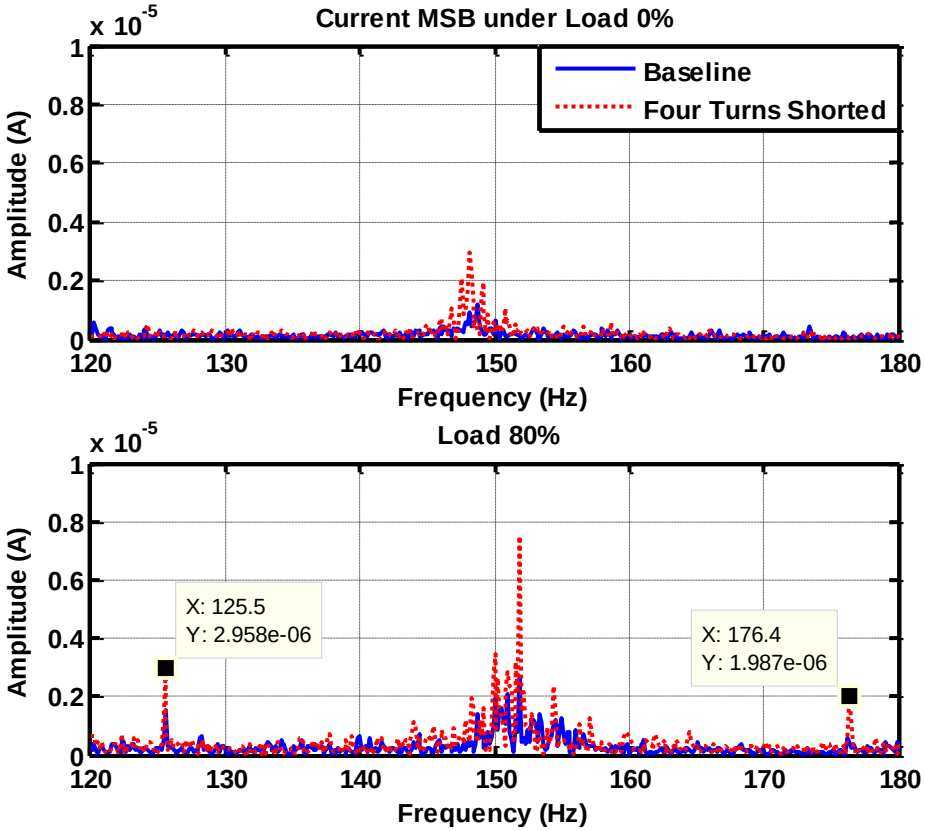

Figure 7.6 A-phase current MSB for healthy motor and motor with a four inter-turn short circuit fault at zero and 80% of full load using sensorless control mode

Figure 7.7 depicts the output voltage power spectra from the drive to the motor terminals. The sidebands of the voltage increase in amplitude with increase in load and introduction of the fault increase. The voltage spectrum demonstrates slightly

better performance than the motor current spectrum because the VSD regulates the voltage to adapt to changes in the electromagnetic torque caused by the fault.

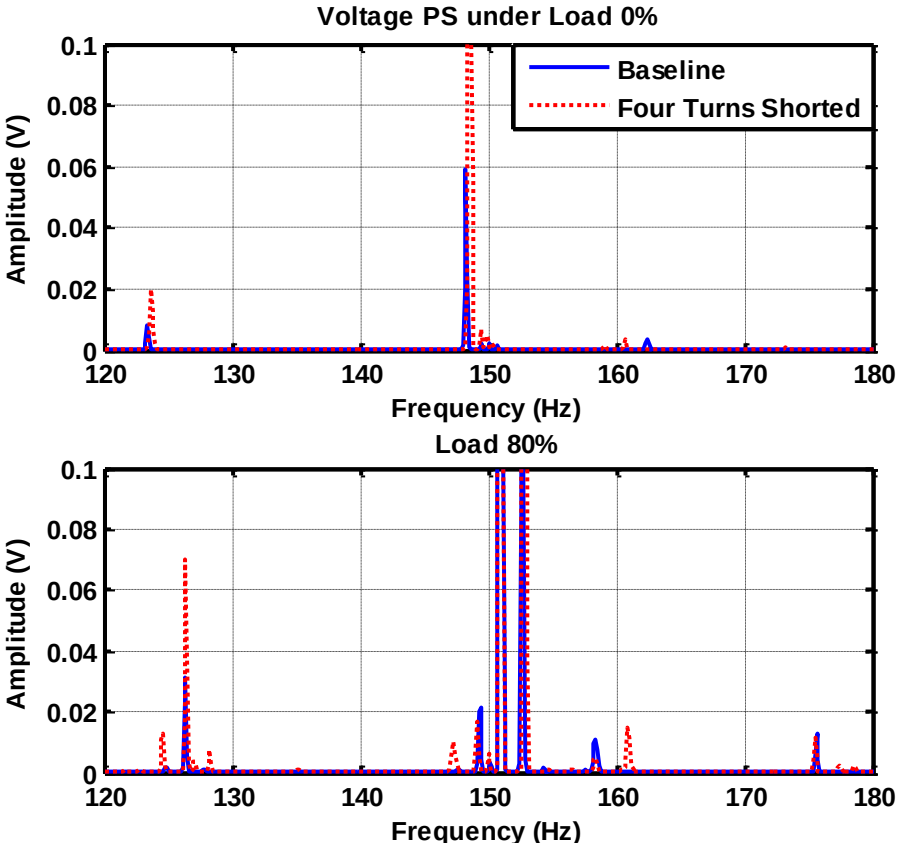

Figure 7.7 Voltage power spectra for healthy motor and motor with a four inter-turn short circuit fault at zero and 80% of full load using sensorless control mode

Fig. 7.8 presents typical MSB results from the voltage signal for healthy motor and motor with four inter-turn short circuit faults under two loads and with respect to the sensorless control mode. As it can be seen in Fig. 7.8 the MSB shows the larger changes in amplitudes with introduction of the fault, and this demonstrated that MSB has more effective noise reduction, which allows small amplitude signals to be assessed accurately, and hence can produce accurate modulation estimation.

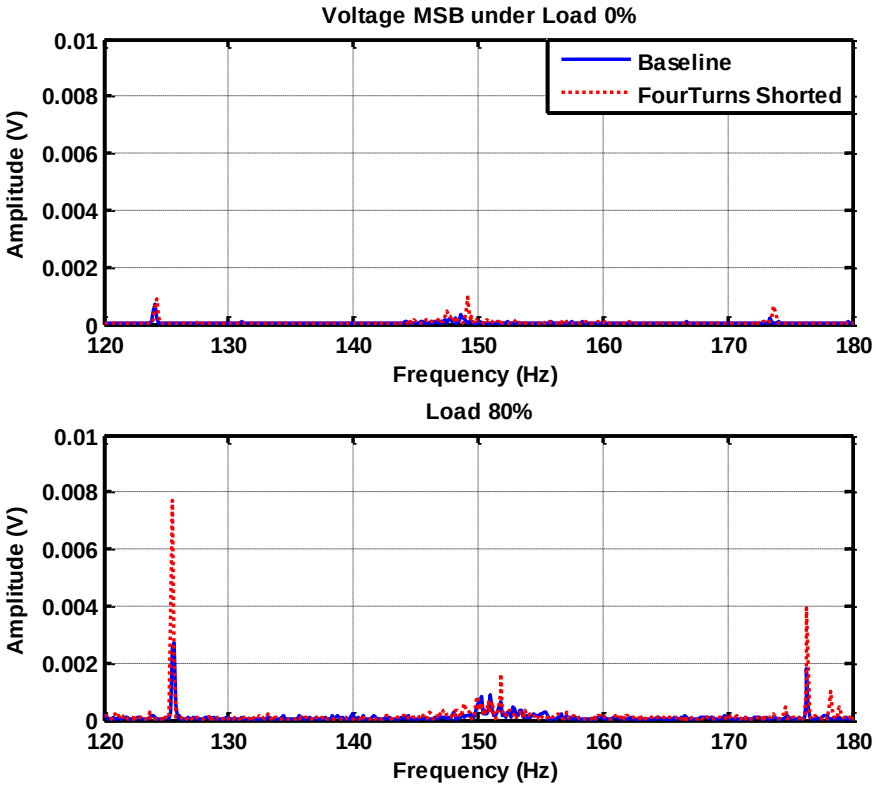

Figure 7.8 Voltage MSB for healthy motor and motor with a four inter-turn short circuit fault at zero and 80% of full load using SL control

Alwodai, et al., [96] and Cusido, et al., [97] used an alternative formula to detect and diagnose the presence of shorted turns in the stator windings of an induction motor. Stator faults cause uneven distribution of the airgap flux waveform around the stator cross section, which allows the stator currents to be modulated by rotor slot frequency, and the features frequency f_{sf} for the stator fault is identified according to [96, 97] using electrical signals analysis and is given by:

$$f_{sf} = f_S\left[1 \pm mN_b\left[\frac{1-s}{p}\right]\right] \tag{7.2}$$

where f_s denotes the supply frequency, N_b is the number of rotor bars, p the number of pole-pairs, s is the motor per unit slip, and m = 1, 2, 3… is the harmonic order. As the rotor frequency f_r is given by:

$$f_r = \frac{1-s}{p} f_S \tag{7.3}$$

Equation (7.2) therefore can be rewritten as:

$$f_{sf} = f_s \pm mN_b f_r \tag{7.4}$$

The per unit slip ***s*** is calculated as:

$$s = \frac{f_{slip}}{f_{sync}} = \frac{f_s/p - f_r}{f_s/p} \tag{7.5}$$

Fig. 7.9 shows typical power spectra for the current signals collected under zero and 80% full load, using sensorless control mode. For the healthy case, the characteristic frequency values shift lower and the peak amplitude increases with increase in loads. The existence of the characteristic frequencies in the healthy case is due to inevitable manufacturing tolerances or inherent errors that lead to a clear asymmetric distribution between the three-stator phases.

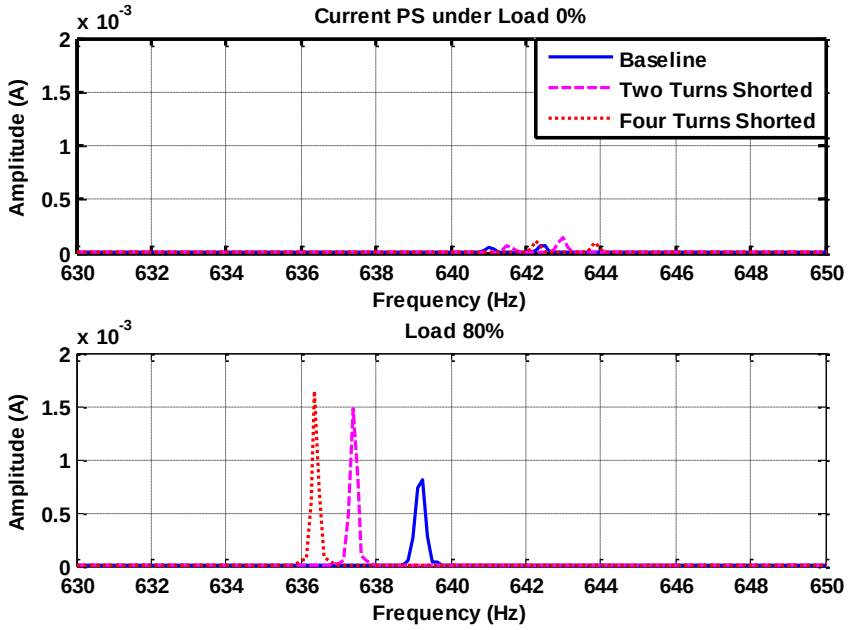

Figure 7.9 A-phase current power spectra for healthy motor and motor with two and four inter-turn short circuit fault at 0 and 80% of full load using SL control

However, as the asymmetry becomes worse due to the presence of the fault, the amplitude of the peaks increases slightly with the level of the fault, and the frequency

shifts downwards, with a shift that increases with the level of the fault. Both these observations are consistent with the faults resulting in a weaker magnetic field and more rotor slip. Thus, these changes could be used for separating different fault levels.

Typical stator current MSB are shown in Fig. 7.10 for the current signals from different loads and motor with two and four inter-turn short circuit faults. Similar to the characteristics observed from power spectra in Fig. 7.9, MSB analysis shows peak amplitudes at the characteristics frequencies which increase, while the frequencies shift lower as the load increases. In addition, bispectral peaks in Fig.7.10 appear at frequency values that have a 50 Hz difference from that of the power spectrum, showing the effect of MSB demodulation.

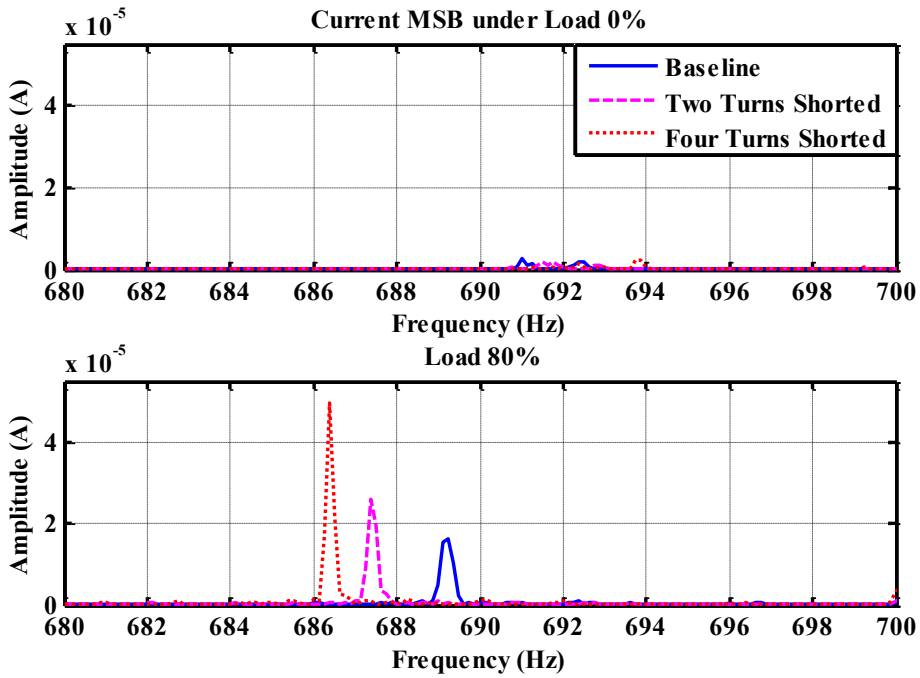

Figure 7.10 A phase current MSB for healthy motor and motor with two and four inter-turn short circuit fault at 0 and 80% of full load using SL control

No changes was found in the motor voltage signature with respect to the open loop control mode that can be used to identify stator faults [73]. This is due to the fact that in the open loop mode the drive feeds the motor with a supply of a constant V/Hz ratio regardless of the changes in the motor electromagnetic torque and current.

Oscillations in the motor torque due to the fault are not seen by the drive as there is no feedback. The V/Hz ratio is kept constant even when the slip changes either due to the load or the fault. No compensation action is taken by the drive as long as the reference speed stays the same.

Fig. 7.11 shows the power spectrum of voltage signature under healthy motor (BL) and motor with two and four inter-intern short circuit faults at loads of 0% and 80% of full load, with respect to sensorless control mode. It is clear that the amplitude of the sidebands increases with both severity of the fault and increases in load, as shown in Fig. 7.11, and the fault can be best detected under higher load. This demonstrates that the sensorless technique produces more accurate and efficient results as compare to the open loop technique.

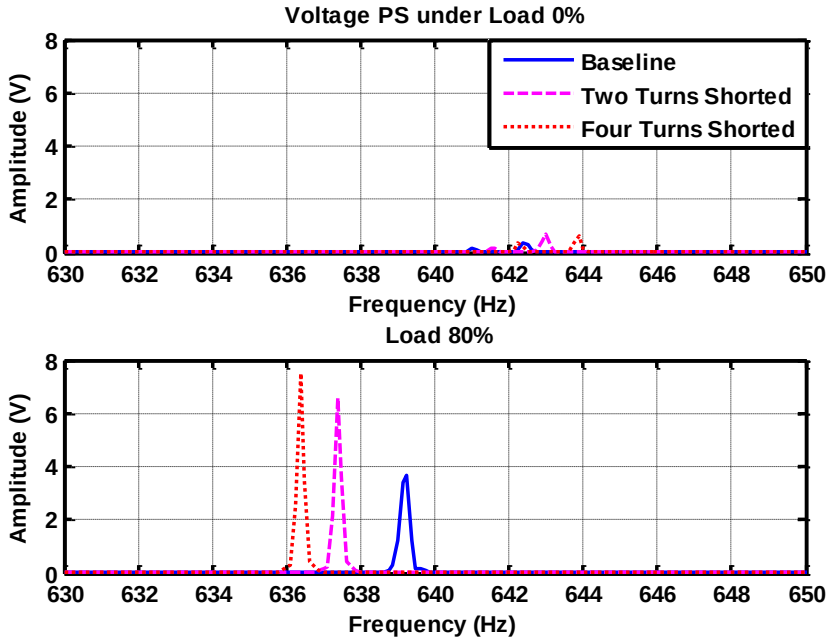

Figure 7.11 Voltage power spectra for healthy motor and motor with two and four inter-turn short circuit fault at 0 and 80% of full load using SL control

Typical stator voltage MSB is shown in Fig. 7.12 for the voltage signals with 0% and 80% full load and with two and four inter-turn short circuit faults. As with the power spectrum, the healthy case exhibits a frequency shift towards a lower value and an amplitude increase, as the load increases. However, for the faulty cases, as the fault

severity increases, the MSB amplitudes increase substantially and the frequency peaks shifts to lower frequencies. The larger change in amplitudes observed with the fault cases, demonstrates that MSB provides very effective noise reduction, which allows small amplitudes to be estimated accurately and hence produces accurate modulation estimation. In addition, the bispectral peaks in Fig. 7.12 appear at frequency values that have a 50 Hz difference from that of the power spectrum.

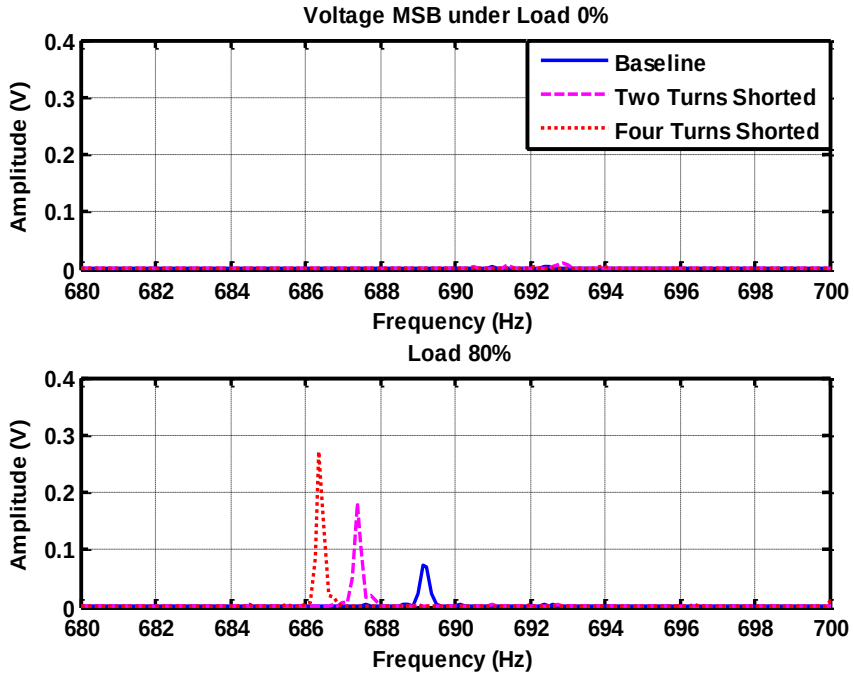

Figure 7.12 Voltage MSB under healthy motor and motor with two and four inter-turn short circuit fault at 0 and 80% of full load using SL control

7.4 Summary

This chapter presents the development and the practical implementation of a system for detection and diagnosis of a short-circuit fault in the winding of an induction motor. To diagnose the shorted winding fault, PS and MSB analysis have been used.

The following summary is deduced from the observations of results obtained by the experiments. The results presented in Fig.7.5 to Fig. 7.8 agree with those obtained by Thomson and Gilmore [9] and Abdelhamid [3] using the equation

$f_t = \left[\frac{n}{p}(1-s) \pm q \right] f_s$ and the results presented in Fig. 7.9 to Fig.7.12 agree with those obtained by Alwodai, et al., [96] and Cusido, et al., [97] using the equation $f_{sf} = f_s \pm mN_b f_r$, from which it was decided that both equations can be used for detection and diagnose of a short-circuit fault, it is concluded that:

- ✓ The stator faults cause an increase in sideband amplitudes and this increase can be observed in both the current and voltage signals under the sensorless control mode.
- ✓ If the degree of the faults increased, then the magnitude of spectral peaks at the fault frequencies increased, thus severe short-circuit winding faults can be easily identified.
- ✓ It is easy to diagnose the short-circuit winding fault under high load conditions because the magnitude of spectral peaks at the fault frequencies increases with increase of load. The frequency peaks with high magnitude can be easily identified.
- ✓ The implemented test methods demonstrated efficient fault diagnosis and CM of an induction motor. The results obtained present with a high degree of reliability, which enables the proposed methods to be used as monitoring tools for diagnosis of short-circuit winding faults of similar motors.
- ✓ MSB has a better performance in diagnosing stator faults and has very effective noise reduction, which allows small amplitudes to be estimated accurately and hence produce accurate modulation estimation.

The next chapter will focus on developing advance signal processing techniques using both motor current and voltage signals for detection and diagnosis of compound motors faults (both rotor and stator) under sensorless control mode.

Chapter 8

Modulation Signal Bispectrum Analysis of Electric Signals for the Detection and Diagnosis of Compound Faults in Induction Motors with Sensorless Drives

This chapter presents a new method for fault detection of stator winding asymmetry combined with a broken rotor bar with different degrees of severity, using MSB analysis of motor current and voltage signals under sensorless control modes. The results of motor current and voltage signals using PS and MSB analysis are compared. The MSB is shown to provide very effective noise reduction, more than that of the PS. In a power spectrum the faults exhibit as asymmetric sidebands around the supply frequency. These sidebands are shown to be quantified more accurately using a new MSB-SE estimator which leads to more consistent and accurate diagnosis of the fault severity.

8.1 Introduction

Recently, the challenge of detecting and identifying compound faults in induction motors has been taken up by researchers such as Messaoudi and Sbita [48] and Carcia-Perez, et al., [155] who have used high- resolution analysis of the motor current spectrum. The exposure of the motor to an unbalanced supply, combined with broken rotor bar fault reduces the efficiency, significantly increases the temperature with consequent likely damage to the induction motor [99, 156]. Higher order spectra (HOS) are useful signal processing tools that have shown significant benefits over traditional spectral analyses because HOS have unique properties of nonlinear system identification, phase information retention and Gaussian noise elimination [19, 49]. Therefore, HOS analysis has received considerable attention in the condition monitoring of real machines. A study by Gu, et el., [19] investigated the use of motor current signals for the diagnosis of different faults in reciprocating compressors using a new data processing method, the modulation signal bispectrum (MSB), to suppress random noise. This work resulted in a more accurate diagnosis than that obtained by using only the power spectrum (PS).

More details on current signature analysis have been presented in [52] on improved broken rotor bar (BRB) diagnosis based on MSB analysis without the use of close loop control modes. The characteristics of the current signals of the healthy motor and with a BRB are explained. The ideal electromagnetic relationship of the driving motor both healthy and with a BRB were investigated. The results showed that for the case of the BRB there was an additional sinusoidal current component with frequency $2sf_s$ (where s is the slip and f_s is the supply frequency).

The use of MSB analysis of the motor current signals for detection of stator faults is presented in [51]. These faults can cause winding temperature to increase which may affect the current signal. Results presented in [51] demonstrated that MSB analysis

has the potential to accurately and efficiently extract signal modulation due to the presence of motor faults and eliminate non-modulated and random components.

All the above mentioned works focus on fault detection of induction motors directly connected to the power line supply and did not examine the effects of a closed loop variable speed drive system on the power supply parameters, i.e. current and voltage in the case of induction motor faults. However, closed-loop variable speed drive (VSD) systems can induce strong noise into voltage and current measurements.

To evaluate MSB analysis for detection of combined faults, an experimental study was conducted based on a three-phase induction motor (two-pole pairs) with rated output power of 4 kW, as shown in Fig. 5.2. For a full description of the test rig, with photos and figures, see Chapter 5.

In order to evaluate the performance of MSB analysis, current and voltage signals were collected for five diverse motor conditions: a healthy motor (baseline, BL), one broken rotor bar (1BRB), two broken rotor bars (2BRB), see Fig. 5.10. They were induced by drilling carefully into the bars along their height in such a way that the hole cut the bar completely to simulate the broken rotor bar fault. Subsequently, the tests were further carried out when the 1BRB is compounded with a phase winding resistance increment (R_{fs} = 0.4Ω) and 2BRB bar with (R_{fs} = 0.4Ω), in which the resistance increments were realised by an external resistor bank connected into one of the three winding phases, as shown in Fig. 5.19.

For all test cases, the motor ran under five successive loads: 0%, 20%, 40%, 60%, and 80% of full load, which lets the investigative performance to be inspected at different loads and avoids any possible damages of the test system that might occur if the full load was applied immediately. As shown in Fig.8.1, each of the five load increments was repeated three times, making a total of 15 load steps, a current-load plot is also shown. This test step diagram also indicates how the test results are presented. Where vertical lines are shown in any plot, these represent the start of each new load test cycle.

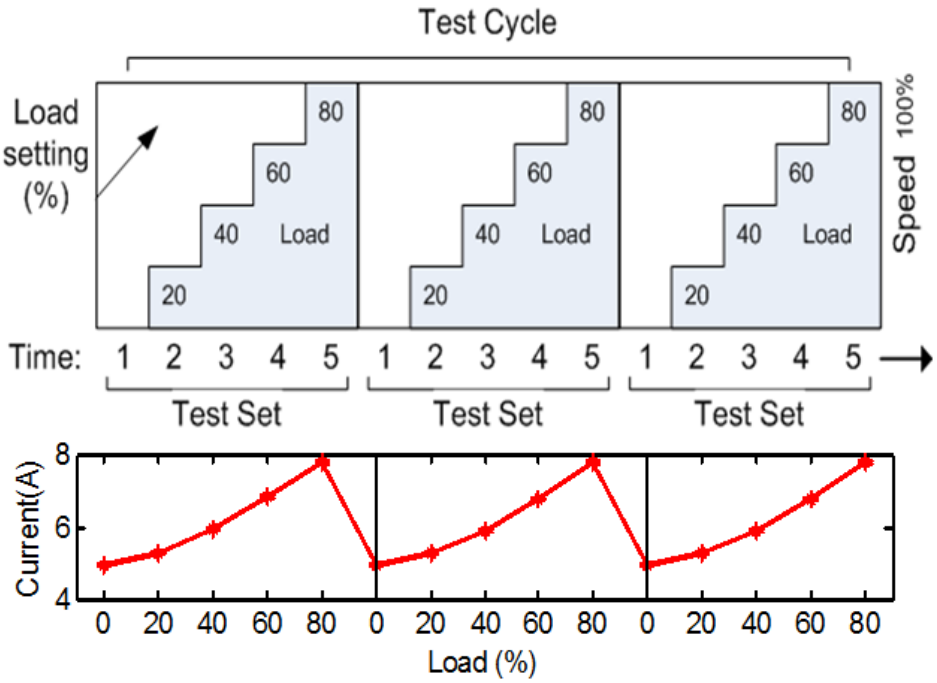

Figure 8.1 Load cycle for three repeat tests

8.2 Broken Rotor Bar with Phase Winding Resistance Increments ($R_{fs} = 0.4\Omega$)

The current and voltage readings show that there is a noticeable difference in current and voltage imbalances when the fault resistance is introduced. The maximum is 1.068V at 80% loading for the 0.4Ω fault resistance. Fig. 8.2 indicates the results of calculating motor voltage and current imbalances across all phases in accordance with the NEMA definition.

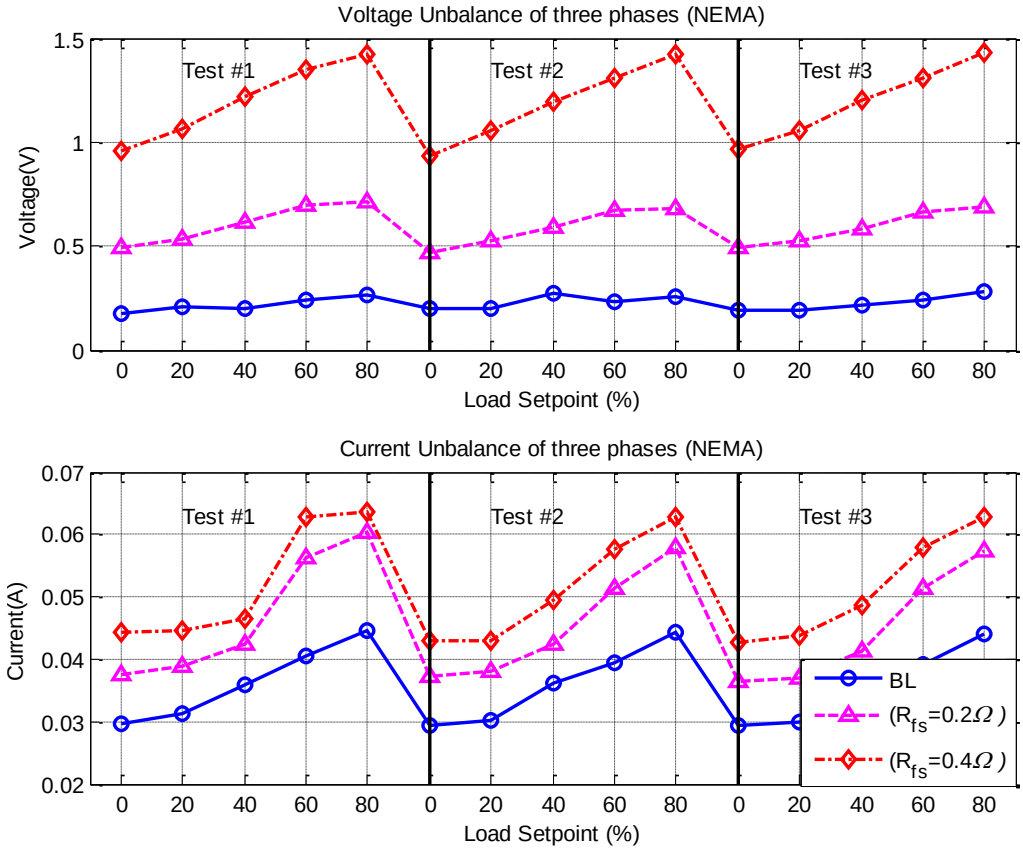

Figure 8.2 Voltage and current imbalances by NEMA definitions

Fig. 8.3 and Fig. 8.4 show a direct comparison between a MSB slice at the supply frequency and PS for the current and voltage signals under 40% load at full speed for the healthy motor. MSB shows very good noise reduction compared with PS, see Fig.8.3 (a) and Fig. 8.4 (a). The 50 Hz supply component present in the PS is largely eliminated in the MSB. This makes for easier and more reliable observation of components that relate to motor health conditions. The sideband components $(f_s - f_r)$ and $(f_s + f_r)$ around f_s shown by the power spectra of Fig. 8.3 (b) and Fig. 8.4 (b) are represented by a single component at 24.88 Hz in the plot of the MSB. This makes spectral peaks such as those due to eccentricity faults in the high frequency range to be estimated more accurate with better diagnostic results.

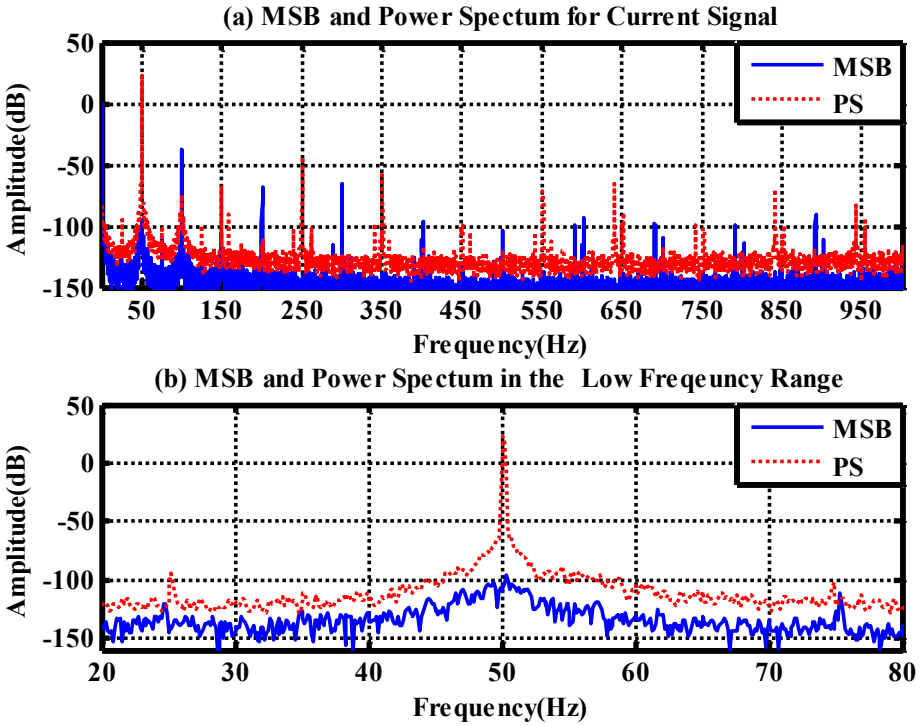

Figure 8.3 MSB and power spectrum characteristics for current signals

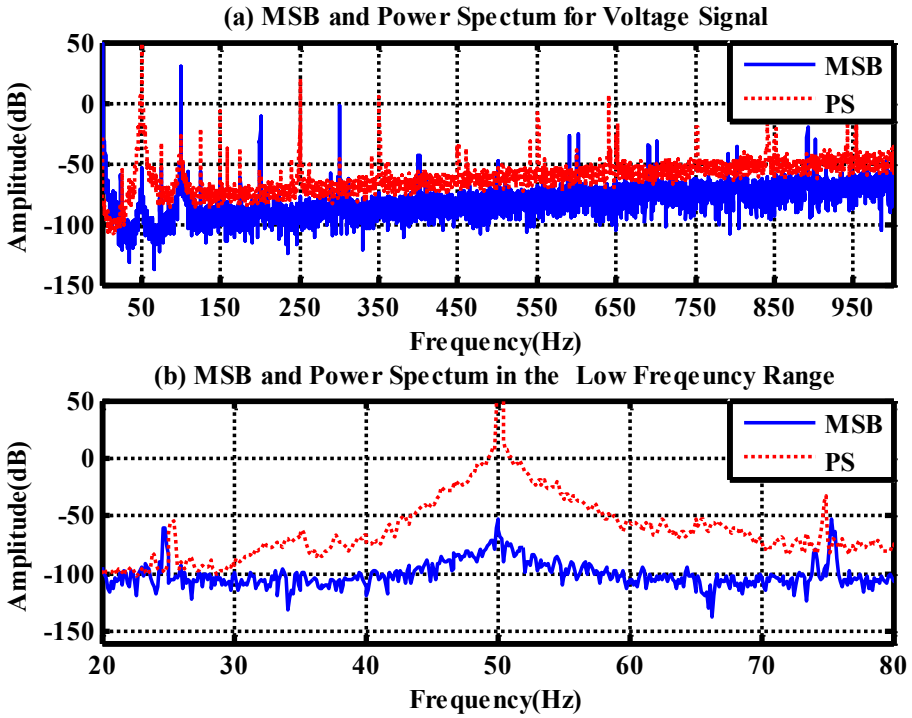

Figure 8.4 MSB and power spectrum characteristics for voltage signals

Fig. 8.5 presents the experimental results of the stator current spectrum when the motor is operated under stator winding asymmetry. New components at frequencies *(1+2k).fs*, occur in the current spectrum. These harmonic components are induced by the unbalance in the supply voltage. The rise in the amplitude of the sidebands created by the stator winding asymmetry is clearest at the supply frequency third harmonic (150 Hz).

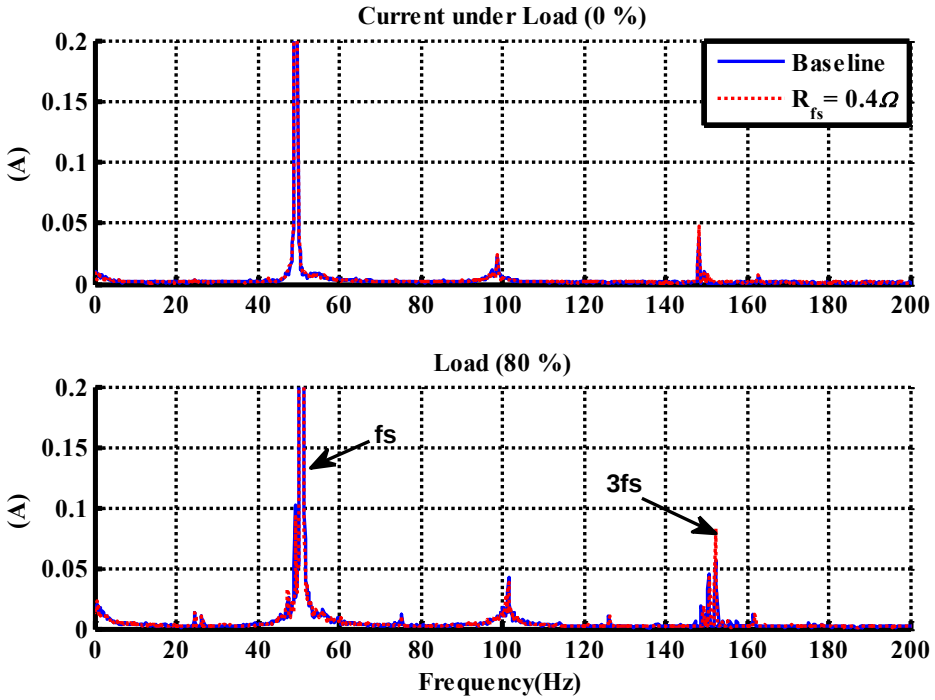

Figure 8.5 Phase current spectra for baseline and R_{fs} = 0.4 Ω

Fig. 8.6 shows the spectrum of stator current with only a rotor fault at zero load and 80% full load. No sidebands can be seen for the broken rotor bar under 0% motor load because the slip is too small to have a measurable effect. It is clear that the amplitude of sideband increased at higher load, so the presence of this fault is best detected under high load.

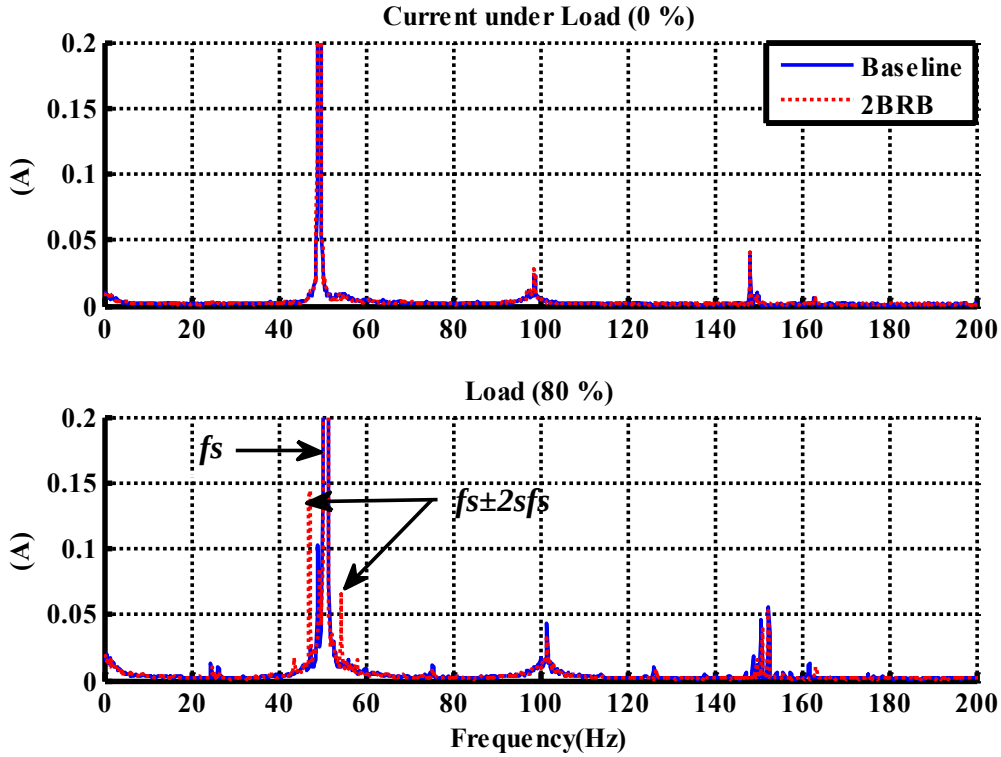

Figure 8.6 Phase current spectra for BL and 2BRB with different loads

Fig. 8.7 shows the spectrum of stator current under healthy motor at full speed and under loads of 0% and 80% with 2BRBs and 0.4Ω winding asymmetry. It can be seen that there are no visible sidebands for broken rotor bar under 0% motor load since, again, the slip is too small to have a measurable effect, see Fig. 8.7. It is clear that the amplitude of sidebands increased at higher load, so the presence of this fault is best detected under high load.

Fig. 8.7 clarifies that the additional increase of the sidebands at $f_s(1\pm 2ks)$ is due to the stator winding asymmetry that has an amplitude increase at *3fs*.

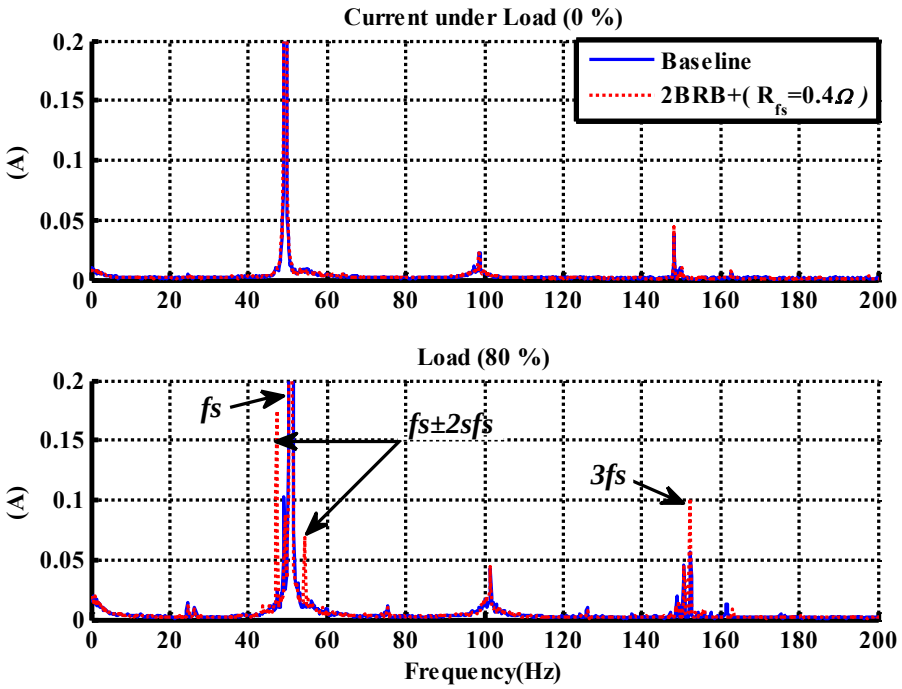

Figure 8.7 Phase current spectra for baseline, and 2BRB with R_{fs} = 0.4 Ω

Fig. 8.8 and Fig. 8.9 shows the spectra of the stator current for the healthy motor, motor with one and two BRB and motor with 1 BRB and 2BRB plus 0.4Ω winding asymmetry, at full speed. In this case five loads were applied; 0%, 20%, 40%, 60% and 80% of full load. It can be seen that there are no visible sidebands for loads of 0% and 20% since the slip is too small to be identified.

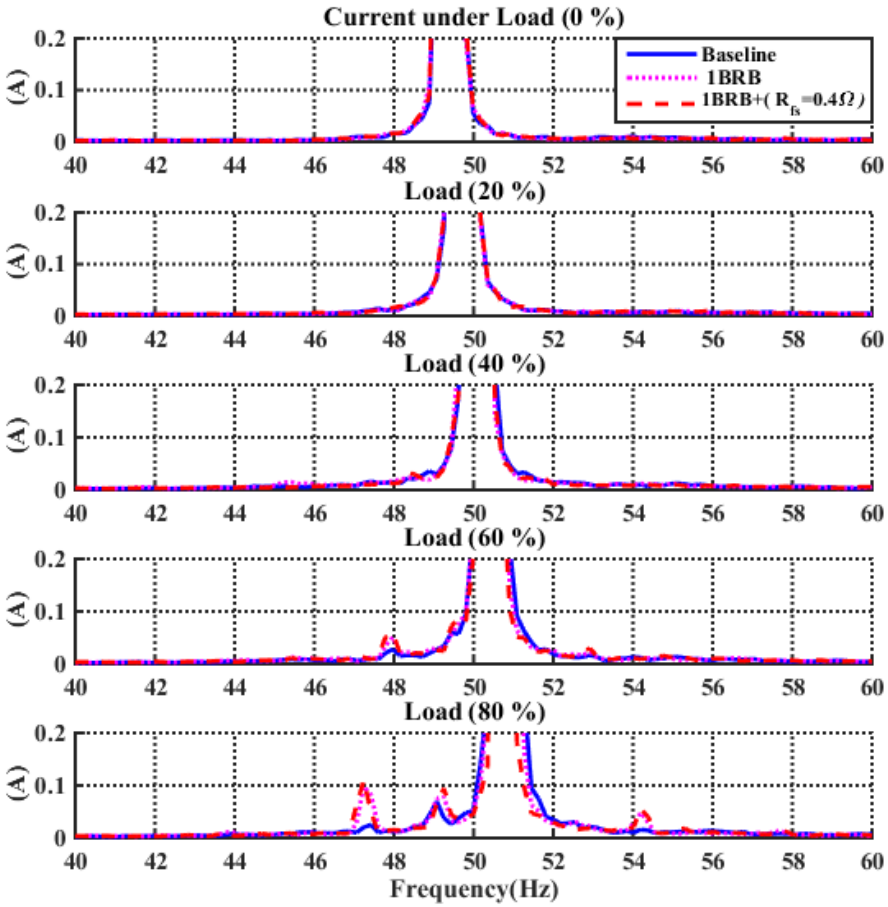

Figure 8.8 Phase current spectra for BL, 1BRB and 1BRB with R_{fs} = 0.4 Ω under different loads

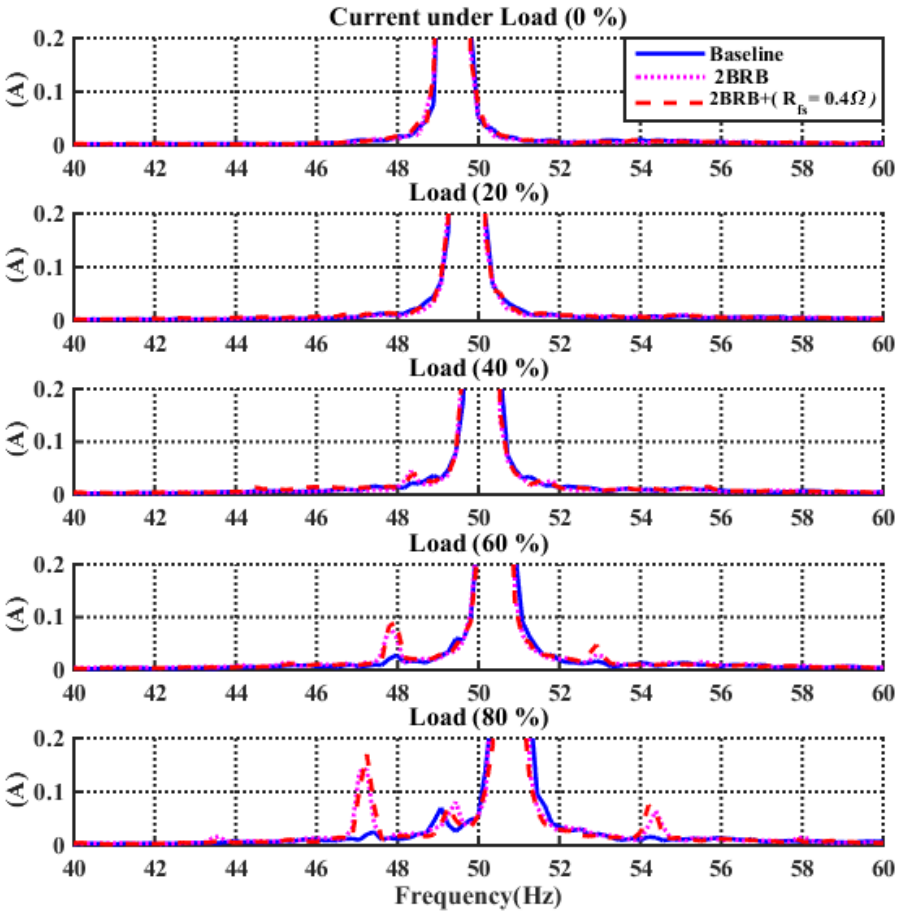

Figure 8.9 Phase current spectra for BL, 2BRB and 2BRB with $R_{fs} = 0.4\ \Omega$ under different loads

However, sidebands are visible for the same broken rotor bar fault under 40% motor load, and clearly visible when the motor load is increased to 60% load. The maximum amplitude of the current sidebands is significantly increased by introducing the resistor imbalance. It is also clear that the amplitude of sideband increases as the severity of the fault and load increases as shown in Fig.8.9 and the fault can be best detected under higher load.

Fig. 8.10 and Fig. 8.11 depict the output voltage spectra from the drive to the motor terminals. The sidebands of voltage increase in amplitude with load and severity of the fault. The main concern here is how effective is motor voltage signature analysis when it comes to analysing and detecting faults that occur in an induction motor. The

sensorless control mode gives measurable indication of the fault as soon as load reaches 40%, and at 80% load the graph shows prominent increases in sidebands and the results show some notable and inevitable changes see Fig. 8.11. This proves that sensorless control mode allows more accurate and efficient detection.

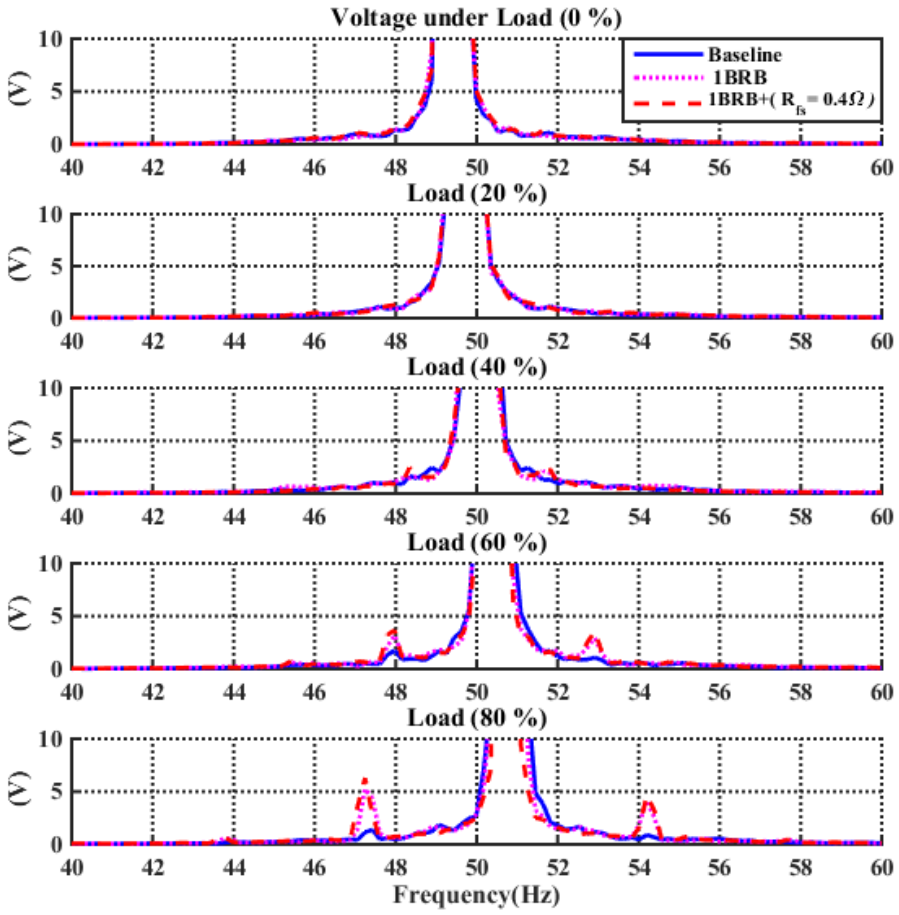

Figure 8.10 Voltage spectra for BL, 1BRB and 1BRB with R_{fs}= *0.4 Ω* under different loads using SL control

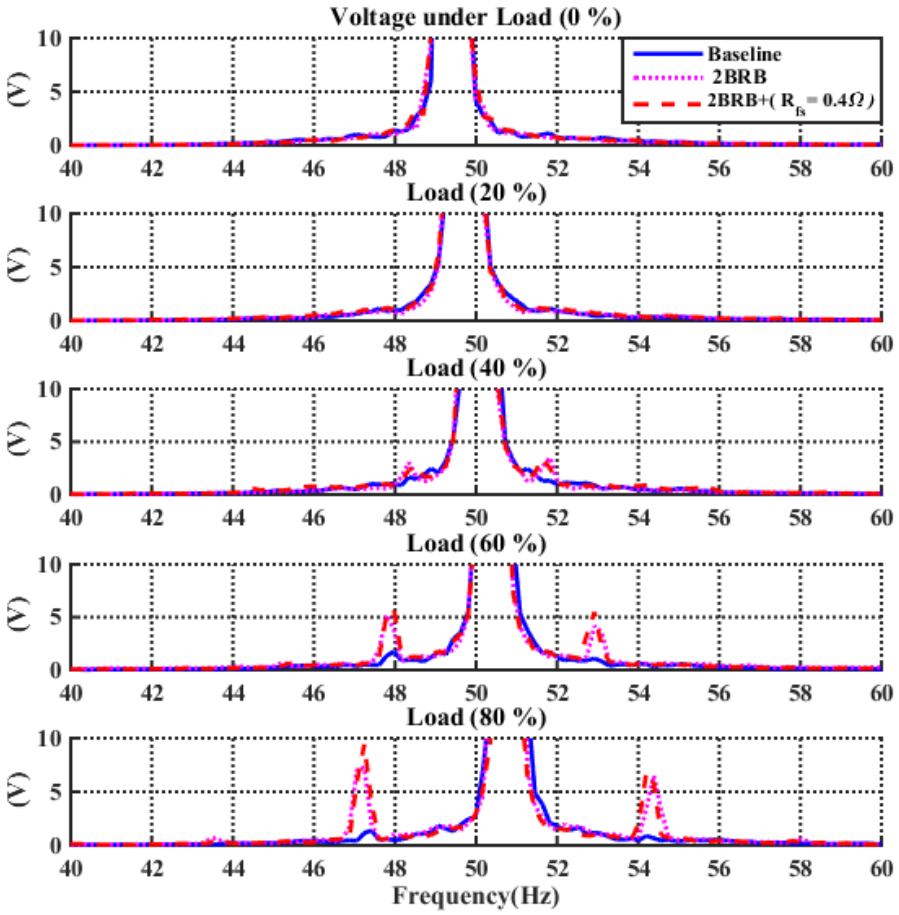

Figure 8.11 Voltage spectra for BL, 2BRB and 2BRB with R_{fs} = *0.4 Ω* under different loads using SL control modes

8.3 Characteristics of MSB

Fig. 8.12 presents typical MSB results (MSB magnitude and MSB coherence) from the current signal for a motor with 2 BRBs and phase winding resistance increment (R_{fs} = *0.4 Ω*) under 60% load with respect to sensorless control mode. As it can be seen in Fig.7.12 the MSB shows two distinctive peaks at bifrequencies (2.56, 50.0) Hz and (24.54, 50.0) Hz. Clearly, the first one relates to $2sf_s$ and can be relied on to detect and diagnose BRB without doubt, whereas the second one relates to oscillation in the rotor speed. Moreover, these two peaks are also clear and distinctive in the MSB coherence, confirming that they stem from modulation processes between $2sf_s$ and f_s,

and f_r and f_s respectively, and that these modulations have good signal to noise ratio which can be relied on to ensure the diagnosis.

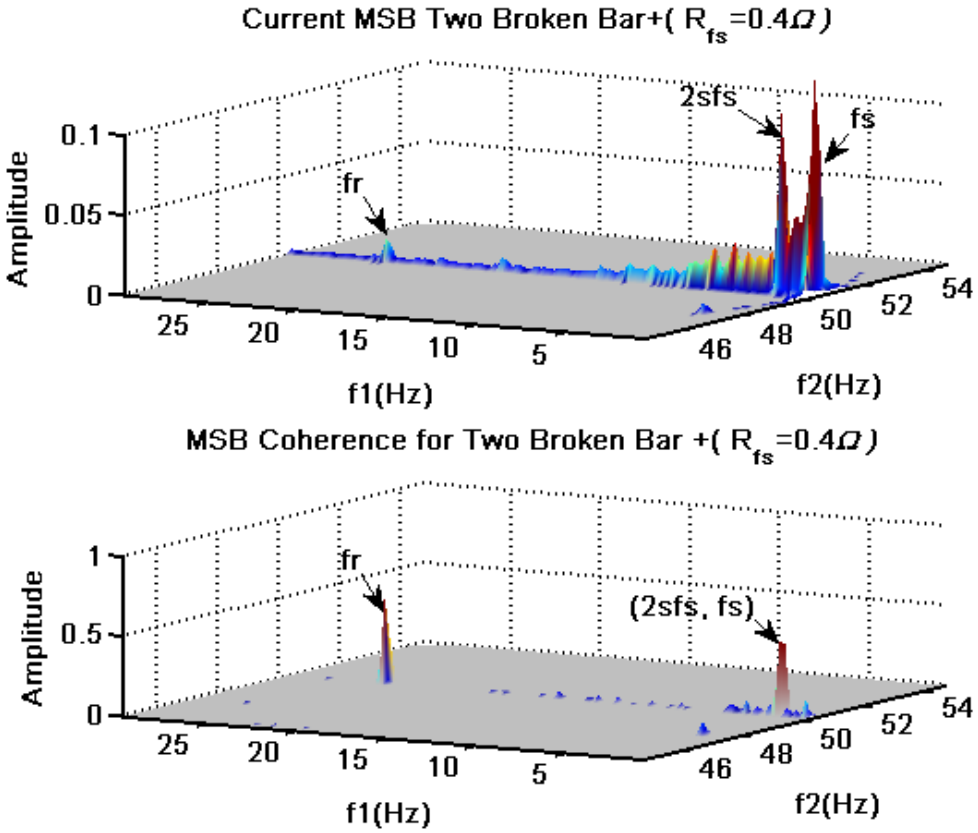

Figure 8.12 Characteristics of current MSB for 2BRB with asymmetry resistance 0.4Ω under 60% load

Figure 8.13 presents MSB results from the voltage signal under the same conditions as shown in Fig.8.12. Similarly, the two distinctive peaks at bifrequency (2.56, 50.0) Hz and (24.54, 50.0) Hz can be used to diagnose the BRB and the winding asymmetry respectively, showing that the voltage signals also contains information on the presence of the faulty.

Moreover, comparing the MSB coherences between the current and voltage signals, it can be seen that the coherence amplitudes of the voltage signals are clearly higher than those of the current signals (larger than 0.5). This means that the voltage signal

has a higher signal to noise ratio with respect to the two fault components. Therefore, in closed loop systems the MSB based on voltage signals is more sensitive to these faults and hence produces more accurate and reliable results than the current signals. This because the VSD regulates the voltage to adapt changes in the electromagnetic torque caused by these faults.

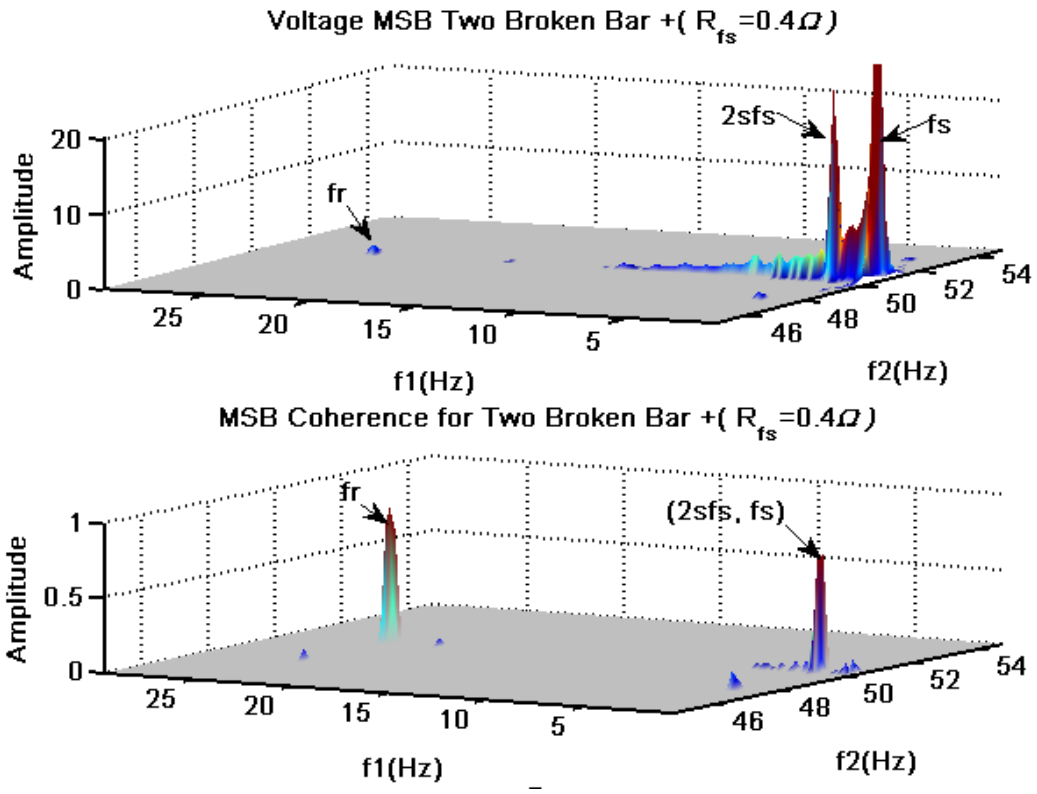

Figure 8.13 Characteristics of voltage MSB for 2BRB with asymmetry resistance 0.4Ω under 60% load

8.4 Comparison between Techniques

A comparative study of different condition monitoring techniques which includes the MSB and PS based on current and voltage signals has investigated both healthy and combined fault conditions. Fig.8.14 shows the comparative diagnostic performance of current signals under different faults and different loads with respect to the sensorless

control mode. The performance parameters are the peak magnitudes at $2sf_s$, extracted from spectra analysis.

It is significant that the amplitude of the sideband increases with both load and severity of the fault, and both PS and MSB peaks are better at detecting the fault under high loads (60% and 80% of full load). However, MSB gives gradual, and hence better, severity separation and also avoids incorrect diagnosis under the low load conditions (e.g. 20% full load) where the PS may give a false diagnosis of the healthy condition due to its significant noise content.

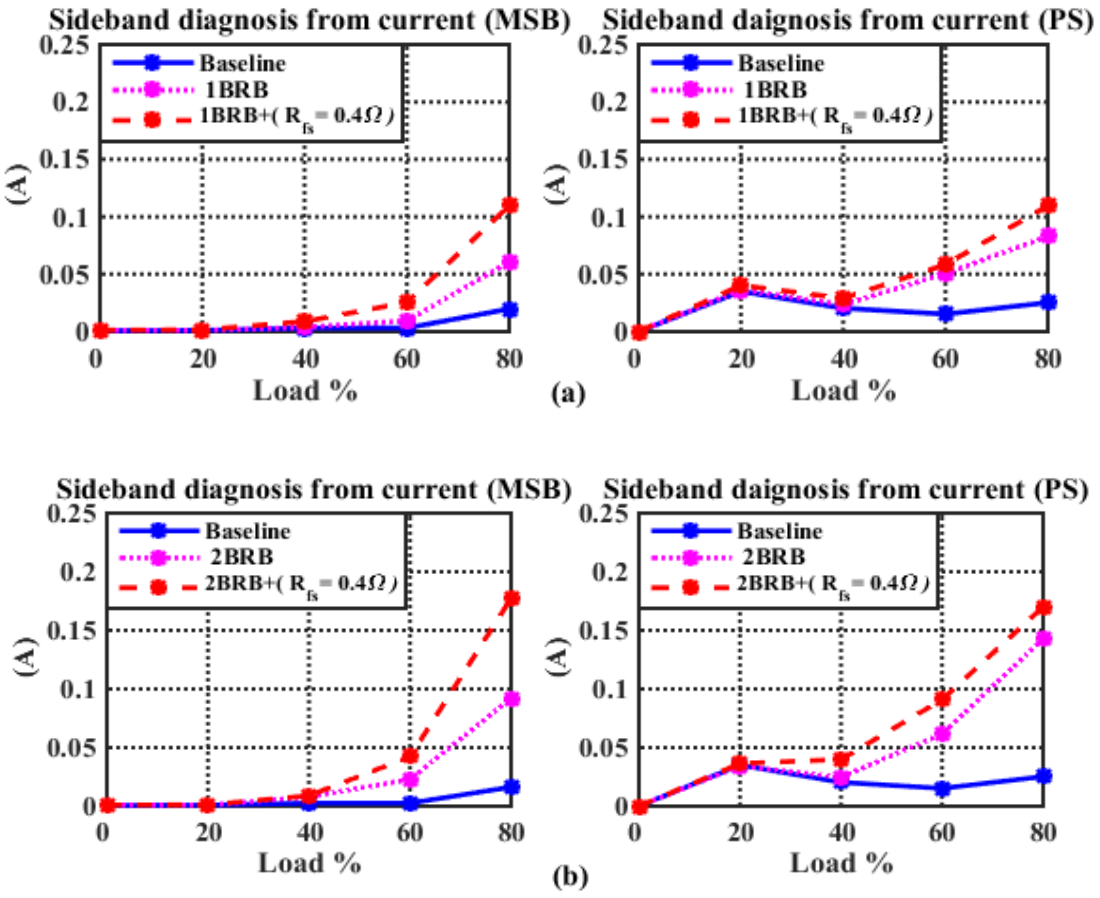

Figure 8.14 Current signal based diagnosis comparison between MSB and PS

Similar to the current signal based diagnosis shown in. Fig.8.14, the voltage based diagnosis shown in Fig.8.15 is provide more support for the proposal that MSB

provides better diagnostic performances in that it separates the fault severity better under high loads and avoids misdetection under low loads. In addition, the MSB diagnosis based on voltage signals show more sensitive detection at the lower load of 40% of full load as its peak values are clearly higher than the baseline, compared with the current signals.

In general, this experimental evaluation shows that the MSB based diagnosis performs better than the PS, and the voltage signals give significantly better results than the current signals.

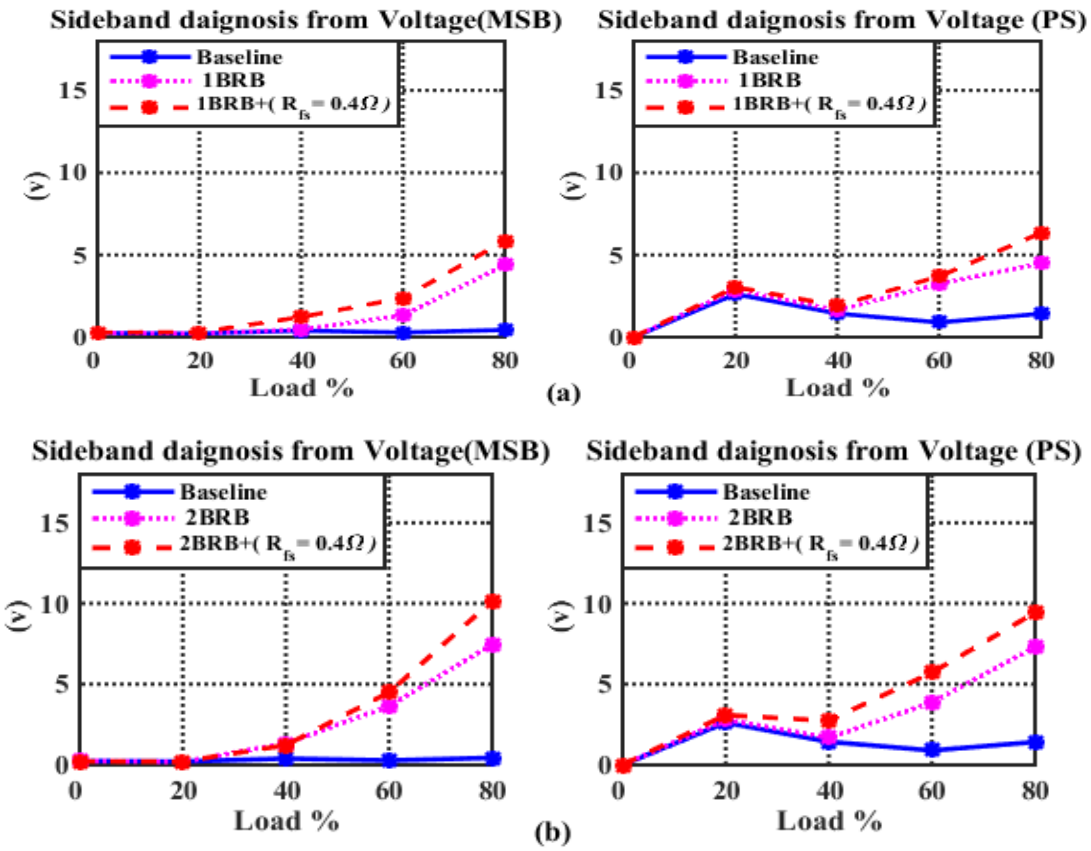

Figure 8.15 Voltage signals based diagnosis comparison between MSB and PS

8.5 Summary

This chapter has shown the effectiveness of using both motor current and voltage signals for detection and diagnosis of compound motor faults combining both BRB and stator winding asymmetry under sensorless control mode.

The effects of combined faults on the motor current and voltage spectrum of an induction motor have been experimentally investigated using analysis techniques such as PS and MSB.

The key factor that influences detection and diagnosis is to accurately extract small sidebands from noisy measurements of both current and voltage signals. This chapter has shown that using MSB to suppress the noise provides more accurate sideband estimation and thus better diagnostic results, compared with conventional power spectrum analysis.

The results show that the additional increase in the amplitude of the sidebands at $2sf_s$ is due to stator winding asymmetry and can be observed in both the current and voltage signals.

MSB coherence results have confirmed that voltage signals under sensorless control mode have a higher signal to noise ratio with respect to the faults. In the PS the faults show as asymmetric sidebands around the supply frequency.

These sidebands can be quantified more accurately using a new MSB-SE estimator as shown in Fig.8.14 and Fig.8.15, which results in more consistent detection and accurate diagnosis of the fault severity.

Chapter 9

Conclusions and Future Work

This chapter presents the final conclusions for the entire research project and provides an overview of the main achievements. In addition, an explicit summary of the contributions of the research conducted by the author is detailed. Finally, recommendations for future work on the CM of induction motors with VSDs are given.

9.1 Review of the Aims, Objectives and Achievements

This section describes how well this research project has met its original aim and objectives, and the new contributions to knowledge that it has made. The main achievements of this research are explained and linked with the original aim and objectives set out in Section 1.3.

Aim: The aim of the research in this thesis was to detect and diagnose faults in an induction motor using electrical signals from VSDs. The aim has been met, and it has been demonstrated that motor current and voltage signals are possible means to detect and distinguish between common faults in an induction motor. A novel procedure for induction motor fault detection based on modulation signal bispectrum (MSB) analysis of electrical signals from VSDs has been developed, leading to more accurate diagnostics.

The key achievements of the research work recognised in this thesis are:

Objective one: To develop a three-phase induction motor test facility capable of simulating a range of motor faults of varying degrees of severity and obtain relevant experimental data. To change the open loop configuration of the test rig into a closed loop configuration in order to increase the system performance and accuracy of the test results.

Achievement One: Experimental tests play an important role in CM research and Chapter 5 fully described the test rig facility used in this research. Importantly, the speed of the motor could be changed using a digital variable speed controller which could be set is in either open loop (V/Hz) or sensorless modes which are commonly used in industry. The experimental rig was used to perform tests on a healthy motor, a motor with either stator or rotor faults and a motor with a combination of faults. Motor current and voltage signals data were collected under the different fault conditions for different loads and different speeds, and signal processing techniques were applied with respect to the open loop and sensorless control modes.

Objective Two: To investigate the effect on the performance of a three phase squirrel cage induction motor with; broken rotor bars and stator winding asymmetry separately; and stator winding asymmetry combined with a broken rotor bars.

Achievement Two: The sources and causes of these faults were reviewed. This review showed that electrical faults have many effects on the performance on induction motors, including pulsation in the rotating magnetic field which, in turn, causes increased vibration, acoustic noise, speed oscillation, an increase in motor temperature and oscillatory running conditions. These all result in a reduction in motor efficiency and shortening of the motor life.

Objective Three: To investigate the capability of electric signals from the VSD for detection and diagnosis of induction motor faults with a high degree of accuracy.

Achievement Three**:** Chapter 3 explains the operation of modern inverter control systems include open loop and close loop modes. It was demonstrated that different conventional techniques can be applied to control the speed and torque of induction motors. Little work was found that explored the diagnostic performance of electric signals of motors with sensorless VSDs, which are increasingly used in industry for obtaining better dynamic response, higher efficiency and lower energy consumption. The review further demonstrated that sensorless VSD gives reliable and accurate fault diagnosis, and can be employed effectively for CM and control simultaneously.

Objective Four: To apply and investigate the use of signal processing methods and techniques to collected data and attempt to detect, diagnose and assess the relative fault severity of the seeded faults.

Achievement Four: Time and frequency domain signal processing methods were applied to the collected data in attempts to detect and diagnose the seeded faults. A comparative study has been carried out to examine the detection and diagnosis performances of stator and rotor faults for a motor with and without a VSD drive. Evaluation results in Chapter 6 show that the electrical faults cause an increase in the

amplitude of the sidebands of the motor current signature when the motor is under the open loop control. However, the increase in sidebands can be observed in both the current and voltage signals under the sensorless control mode. It shows that the both current and voltage signatures from VSD drives can give effective indication of the faults. Sensorless control shows some promising and efficient results that were more accurate than the results achieved through open loop control and was more sensitive in identifying the faults.

Objective Five: To apply more advanced signal processing techniques to extract weak fault signals from noise contaminated current and voltage measurements obtained using sensorless drives.

Achievement Five**:** The MSB method, which uses HOS, has been investigated for analysis of motor current and voltage signals from sensorless drive, in order to extract weak fault signals, when they present in noisy current and voltage measurements. The technique developed was carefully applied, demonstrating its efficiency in detecting and diagnosing stator faults as shown in Chapter 7. It was found that motor current and voltage signals analysis using the MSB method can be effectively used in fault detection more consistently than the other conventional techniques used.

Objective Six: To present a new method for combined fault detection of stator winding asymmetry and broken rotor bar based on MSB-SE analysis of motor current and voltage signals with different degrees of severity and under sensorless control (closed) mode.

Achievement Six: Chapter 8 examines the diagnostic performance under closed-loop control of asymmetric stator winding and broken rotor bar faults. It examines the effectiveness of conventional diagnosis features in both motor current and voltage signals using PS and MSB analysis. Evaluation of the results showed that combined faults caused an additional increase in the sideband amplitude and this increase can be observed in both the current and voltage signals under the sensorless control mode.

These sidebands can be quantified more accurately using the new MSB-SE estimator, which results in more consistent detection and accurate diagnosis of the fault severity.

Objective Seven: To provide useful information and guide lines for future research in this field.

Achievement Seven: Section 9.4, suggests several useful paths for future work on CM of induction machines using different seeded faults and using the same technique as developed in this research.

9.2 Conclusions

This research investigated sensorless variable speed behaviour in the case of induction motor faults. The key conclusions from this study can be summarised as follows:

1. Open-circuit faults, inter-turn short-circuit faults, broken rotor bars, and combined stator winding asymmetry with broken rotor bars have been detected and diagnosed using electrical signals from VSD systems.
2. The comparative performance of motor current and terminal voltage spectra for fault detection have been assessed for a healthy motor, a motor with separate stator and rotor faults (with different degrees of severities), under different speeds and different loads using both open loop and sensorless control modes, which yields:

    - ✓ The spectrum of the stator current shows that the amplitude of sidebands increases with fault severity and load for both the open loop and sensorless operating modes.
    - ✓ The sidebands in the voltage spectrum appear only for the sensorless control mode, and increase in amplitude with both load and fault severity.
    - ✓ The voltage spectrum demonstrates slightly better performance than the motor current spectrum because the VSD regulates the voltage to adapt to changes in the electromagnetic torque caused by the fault.

- ✓ A significant increase in slip frequency has been noted as the fault severity and load increases in both sensorless and open loop modes.
- ✓ The sensorless control gives more reliable and accurate diagnostic result.

3. The stator fault causes the amplitude change and frequency shifts at the characteristic frequency which can be used as diagnostic features:

   - ✓ The MSB analysis has a good noise reduction capability and produces a more accurate and reliable diagnosis than the PS, in that it gives a more correct indication of the fault severity and location for stator faults for all operating conditions.
   - ✓ In the case of a power spectrum using electrical signals from the VSD, spectral peaks appear at ($fs \pm Nb*fr$) and increase as the load and fault increases. In addition, the frequency values decrease slightly as the fault severity increases because of changing flux due to motor temperature. In a similar way, the phase current and voltage bispectrum sidebands also increase in amplitudes with load but they appear at ($Nb*fr$).

4. This thesis examined the diagnosing of combined asymmetry stator winding on broken rotor bar (BRB) faults under sensorless (closed-loop) operation modes.

   - ✓ A new method for detecting and diagnosing compound faults of stator winding asymmetry and broken rotor bar using electrical signals from VSD has been presented.
   - ✓ It examines the effectiveness of conventional diagnostic features in both motor current and voltage signals using PS and MSB analysis.
   - ✓ Evaluation results show that the combined faults cause an additional increase in the sideband amplitude and this increase in sideband can be observed in both the current and voltage signals under the sensorless control mode.

- ✓ The MSB analysis has a good noise reduction capability and produces a more accurate and reliable diagnosis in that it gives a more correct indication of the fault severity in combination faults and their location for all operating conditions.
- ✓ In the case of the power spectrum, spectral peaks appear at frequencies at ($f_s \pm 2sf_s$) and increase as the load and fault increase. In a similar way, the phase current and voltage bispectrum also increase in amplitudes with load and fault severity but these peaks appear at ($2sf_s$).
- ✓ The MSB avoids incorrect diagnosis under lower load conditions (20% loads) where PS may provide an inadequate diagnosis due to its significant values, even for the healthy conditions.
- ✓ The MSB diagnosis based voltage signals can show more sensitive detection at the lower load of 40% as its peak values are clearly higher than the baseline, compared with that obtained from current signals.
- ✓ The power spectrum exhibits asymmetric sidebands around the supply frequency. These sidebands can be quantified more accurately using a new MSB-SE estimator, which results in more consistent detection and accurate diagnosis of the fault severity.
- ✓ MSB coherence results confirmed that voltage signals under sensorless control mode have a higher signal to noise ratio with respect to the faults.

5. The work presented in this thesis is extend to cover other combinations of faults to investigate the possibility of monitoring combinations of faults in a similar way to that used in this thesis. The influence of stator winding asymmetry combined with discharge valve leakage (DVL) significantly increases the temperature and reduces the motor efficiency and shorten the motor life.

   This work studies the use of motor current signals information to detect and diagnose the effect of the stator winding on different common reciprocating

compressor (RC) faults which create varying load to the induction motor [157, 158].

- ✓ The evaluation results show that the motor current signal contains sufficient information (average torque and dynamic torques) for diagnosing the simulated fault cases. In particular, the stator winding asymmetry combined with discharge pressure leakage cause an additional increase in the sideband amplitude.
- ✓ The results demonstrated that the MSB has a better performance in differentiating spectrum amplitudes caused by different faults especially the compound fault. Hence, the results illustrated show good agreement with the work presented in this thesis.

9.3 Contributions to Knowledge

- **First Contribution:**

The diagnostic features extracted from motor current and voltage signatures under rotor faults using both the open loop and sensorless control mode based on time and frequency domains are new in the field of condition monitoring of induction machines.

- **Second Contribution:**

The detection and diagnosis of open phase circuit faults using motor current and voltage spectrum analysis under open loop and sensorless control mode is another important contribution and is entirely novel. No work has been found describing, in any detail, the detection and diagnosing such open circuit fault using electric signals from VSDs under different load and different speed.

- **Third Contribution:**

There are no previous reports in the literature of using MSB analysis based on electric signals for the detection and diagnosis of an inter-turn short-circuit with

sensorless drive. The author believes that the use of MSB technique to analyse motor current and voltage for CM of an inter-turn short-circuit under sensorless drive is novel.

- **Fourth Contribution:**

  No study has been found using the MSB analysis based on electric signals from a sensorless drive for combination fault detection and diagnosis, it is believed that the use of MSB analysis for combination fault detection of stator winding asymmetry and broken rotor bar is unique.

- **Fifth Contribution:**

  The application of MSB-SE to electric signals from the VSD for detection and diagnosis of combination faults has not been undertaken before and hence the research work developed in this thesis is believed to be the first to present this new method for combination fault detection of stator winding asymmetry and broken rotor bar based on MSB-SE analysis and which compared this new method with conventional PS.

9.4 Recommendations for Future Work

The results presented in this work have shown the effectiveness of using MSB analysis with respect to VSDs in study of induction motors. This area will become more important in time as the popularity of VSDs increases. The interest in the practical implementation of CM systems will also increase as companies try to further improve productivity by decreasing unscheduled outages. The author of this thesis now makes a number of recommendations for research to enhance the CM of induction motors using electrical signals from VSDs.

- **Recommendation One:**

  To perform additional experiments for simulating different types of faults with different levels of severity based on electrical signals from VSDs.

- **Recommendation Two:**

The research should be extended to other motor driven machinery such as pumps, fans, gearboxes, machine tools etc.

- **Recommendation Three:**

Here MSB analysis has been applied on electrical signals from VSD to detect and diagnose induction motor faults, as shown in Chapters 7 and 8. It is recommended that this method be applied on electrical signals from VSD to diagnose other motor faults such as eccentricity and bearing faults.

- **Recommendation Four:**

To evaluate the possibilities of model-based fault detection and diagnosis using a mathematical model and it is recommended that the model should be extended to include electrical and mechanical faults with VSD model.

References

[1] Rao, B. *Handbook of condition monitoring*, 1996: Elsevier.

[2] Payne, B.S. *Condition monitoring of electrical motors for improved asset management*, PhD Thesis, School of Engineering, 2003, University of Manchester, Manchester.

[3] Saleh, A.F. *Detection and diagnosis of electrical faults in induction motors using instantaneous phase variation*, School of Engineering, PhD Thesis, 2005, University of Manchester, Manchester.

[4] Benbouzid, M. E. H., Nejjari, H., Beguenane, R., & Vieira, M. *Induction motor asymmetrical faults detection using advanced signal processing techniques.* IEEE Transactions on Energy Conversion, 1999. 14(2): p. 147-152.

[5] Motor Reliability Working Group. *Report of large motor reliability survey of industrial and commercial installations, Part I.* IEEE Transactions on Industry Applications, 1985. IA-21(4): p. 853-864.

[6] Albrecht, P.F., Appiarius, J. C., Cornell, E. P., Houghtaling, D. W., McCoy, R. M., Owen, E. L., & Sharma, D. K. *Assessment of the Reliability of Motors in Utility Applications - Updated.* IEEE Transactions on Energy Conversion, 1986. EC-1(1): p. 39-46.

[7] Gaeid, K. S., Ping, H. W., Khalid, M., & Salih, A. L. *Fault diagnosis of induction motor using MCSA and FFT.* Electrical and Electronic Engineering, 2011. 1(2): p. 85-92.

[8] Benbouzid, M. E. H., Vieira, M., & Theys, C. *Induction motors' faults detection and localization using stator current advanced signal processing techniques.* IEEE Transactions on power electronics, 1999, 14(1): p. 14-22.

[9] Thomson, W.T. & Gilmore, R. J. *Motor current signature analysis to detect faults in induction motor drives-fundamentals, Data interpretation, and industrial case histories*. In Proceedings of 32nd Turbo machinery Symposium, A&M University, 2003,Texas, USA.

[10] Hussein, N. A., Mahmood, D. Y., & Abdul-Baki, E. M. *3-phase Induction motor bearing fault detection and isolation using MCSA technique based on neural network algorithm.* Int. J. Appl. Eng. Res., no. 5, 2011: p. 581–591.

[11] Alwodai, A., Gu, F., & Ball, A. D. *A comparison of different techniques for induction motor rotor fault diagnosis.* In Journal of Physics: Conference Series (Vol. 364, No. 1, p. 012066). IOP Publishing, 2012.

[12] Cabal-Yepez, E., Osornio-Rios, R. A., Romero-Troncoso, R. J., Razo-Hernandez, J. R., & Lopez-Garcia, R. *FPGA-based online induction motor multiple-fault detection with fused FFT and wavelet analysis*. In Reconfigurable Computing and FPGAs,2009. International Conference on. IEEE.

[13] Zaggout, M., Tavner, P., Crabtree, C., & Ran, L. *Detection of rotor electrical asymmetry in wind turbine doubly-fed induction generators.* IET Renewable Power Generation, 2014: p. 878-886.

[14] Saad, S.A.A. *The utilisation of information avalable in the sensorless control system of an AC induction motor for condition monitoring*, PhD Thesis, in *Engineering*, 2015, University of Huddersfield, Huddersfield.

[15] Bose, B. K. *Modern power electronics and AC drives*, Vol. 123. 2002, Prentice Hall USA.

[16] Ong, C. M. M. O. *Dynamic simulation of electric machinery: using MATLAB/SIMULINK*. Vol. 5, 1998. Prentice-Hall PTR.

[17] Polka, D. *Motors and Drives: A Practical Technology Guide*, 2003: ISA.

[18] Buja, G.S. and & Kazmierkowski, M. P. *Direct torque control of PWM inverter-fed AC motors-a survey.* Industrial Electronics, IEEE Transactions on, 2004. 51(4): p. 744-757.

[19] Gu, F., Shao, Y., Hu, N., Naid, A., & Ball, A. D. *Electrical motor current signal analysis using a modified bispectrum for fault diagnosis of downstream mechanical equipment.* Mechanical Systems and Signal Processing, 2011. 25(1): p. 360-372.

[20] Shaeboub, A., Gu, F., Lane, M., Haba, U., Wu, Z., & Ball, A. D. *Modulation signal bispectrum analysis of electric signals for the detection and diagnosis of compound faults in induction motors with sensorless drives.* Systems Science & Control Engineering, 2017. 5 (1). pp. 252-267. ISSN 2164-2583.

[21] Sasi, A.Y.B. *The exploitation of instantaneous angular speed for machinery condition monitoring*, PhD Thesis, School of Engineering, 2005, University of Manchester, Manchester.

[22] Rgeai, M.N. *Helical gearbox fault detection using motor current signature analysis*, PhD Thesis, School of Engineering, 2007, University of Manchester, Manchester.

[23] Slemon, G.R. & Straughen, A. *Electric machines*, 1980: Addison-wesley New York.

[24] Yeh, C. C., Sizov, G. Y., Sayed-Ahmed, A., Demerdash, N. A., Povinelli, R. J., Yaz, E. E., & Ionel, D. M. *A reconfigurable motor for experimental emulation of stator winding interturn and broken bar faults in polyphase induction machines*. IEEE Transactions on Energy Conversion, 2008.

[25] Pandey, K. K., Zope, P. H., & Suralkar, S. R. *Review on fault diagnosis in three-phase induction motor*. Proceedings published by International Journal of Computer Applications® (IJCA), 2012.

[26] Bhowmik, P.S., Pradhan, S., & Prakash, M. *Fault diagnostic and monitoring methods of induction motor: A Review*. International Journal of Applied Control, Electrical and Electronics Engineering (IJACEEE), 2013.

[27] Sin, M. L., Soong, W. L., & Ertugrul, N. *Induction machine on-line condition monitoring and fault diagnosis-A survey*. In Australasian Universities Power Engineering Conference, 2003.

[28] Starr, A., & Rao, B. K. N. *Condition monitoring and diagnostic engineering management*, 2001: Elsevier.

[29] McCully, P. J., & Landy, C. F. *Evaluation of current and vibration signals for squirrel cage induction motor condition monitoring*, 1997.

[30] Liu, Z., Yin, X., Zhang, Z., Chen, D., & Chen, W. *Online rotor mixed fault diagnosis way based on spectrum analysis of instantaneous power in squirrel cage induction motors.* Energy Conversion, IEEE Transactions on, 2004. 19(3): p. 485-490.

[31] Abdalla, G. *Planetary gearbox condition monitoring based on modulation analysis*, PhD Thesis, 2017, University of Huddersfield, Huddersfield.

[32] Lei, Y., Zuo, M. J., He, Z., & Zi, Y. *A multidimensional hybrid intelligent method for gear fault diagnosis.* Expert Systems with Applications, 2010. 37(2): p. 1419-1430.

[33] Ozturk, H. *Gearbox health monitoring and fault detection using vibration analysis*, PhD Thesis, 2006, School of Natural and Applied Sciences of Dokuz Eylul University, Turkey.

[34] Drury, C. G., & Watson, J. *Good practices in visual inspection.* Human factors in aviation maintenance-phase nine, progress report, FAA/Human Factors in Aviation Maintenance.@ URL: http://hfskyway. faa. gov, 2002.

[35] Singh, G. K. *Induction machine drive condition monitoring and diagnostic research—a survey*. Electric Power Systems Research, 2003. 64(2): p. 145-158.

[36] Ellison, A. J., & Moore, C. J. *Acoustic noise and vibration of rotating electric machines*. In Proceedings of the Institution of Electrical Engineers, 1968. IET.

[37] Goldman, S. *Vibration spectrum analysis: a practical approach*. 1999: Industrial Press Inc.

[38] Rehab, I., Tian, X., Zhang, R., Gu, F., & Ball, A. *A study of the diagnostic amplitude of rolling bearing under increasing radial clearance using modulation signal bispectrum.* The 29th International Congress on Condition Monitoring and Diagnostic Enginering Management, 20th-22nd August 2016, Empark Grand Hotel, China.

[39] Sasi, A.B., Payne, B., Gu, F., & Ball, A. *The exploitation of instantaneous an gular speed for condition monitoring of electric motors*. Condition Monitoring and Diagnostic Engineering Management, 2001.

[40] Yousef Ben Sasi, A., Gu, F., Payne, B., & Ball, A. *Instantaneous angular speed monitoring of electric motors.* Journal of Quality in Maintenance Engineering, 2004, 10(2): p. 123-135.

[41] Naid, A. *Fault detection and diagnosis of reciprocating compressors using motor current signature analysis*, PhD Thesis, 2009, University of Huddersfield, Huddersfield.

[42] Blakeley, B., Lewis, B., & Lees, A. *Audio acoustic plant condition monitoring of spiral bevel gearbox.* Ironmaking & steelmaking, 2001, 28(3): p. 225-229.

[43] Benbouzid, M. E. H. *A review of induction motors signature analysis as a medium for faults detection.* Industrial Electronics, IEEE Transactions on, 2000, 47(5): p. 984-993.

[44] Ferree, D.V., & Burstein, N. *Electric signature analysis.* Maintenance and Asset Management, 2003, 18(3): p. 11-15.

[45] Sharifi, R., & Ebrahimi, M. *Detection of stator winding faults in induction motors using three-phase current monitoring.* ISA transactions, 2011, 50(1): p. 14-20.

[46] Vamvakari, A., Kandianis, A., Kladas, A., Manias, S., & Tegopoulos, J. *Analysis of supply voltage distortion effects on induction motor operation.* Energy Conversion, IEEE Transactions on, 2001, 16(3): p. 209-213.

[47] Kersting, W. H. *Causes and effects of unbalanced voltages serving an induction motor.* Industry Applications, IEEE Transactions on, 2001, 37(1): p. 165-170.

[48] Messaoudi, M., & Sbita, L. *Multiple faults diagnosis in induction motor using the MCSA method.* International Journal of Signal and Image Processing, 2010, 1(3): p. 190-195.

[49] Zhang, R., Gu, F., Mansaf, H., Wang, T., & Ball, A. D. *Gear wear monitoring by modulation signal bispectrum based on motor current signal analysis.* Mechanical Systems and Signal Processing, 2017, 94: p. 202-213.

[50] Chen, Z., Wang, T., Gu, F., Haram, M., & Ball, A. *Gear transmission fault diagnosis based on the bispectrum analysis of induction motor current signatures.* Journal of Mechanical Engineering, 2012, 48(21): p. 84-90.

[51] Alwodai, A., Yuan, X., Shao, Y., Gu, F., & Ball, A. D. *Modulation signal bispectrum analysis of motor current signals for stator fault diagnosis*. In Automation and Computing (ICAC), 2012, 18th International Conference on. IEEE.

[52] Gu, F., Wang, T., Alwodai, A., Tian, X., Shao, Y., & Ball, A. D. *A new method of accurate broken rotor bar diagnosis based on modulation signal bispectrum analysis of motor current signals.* Mechanical Systems and Signal Processing, 2015, 50: p. 400-413.

[53] Obaid, R. R., Habetler, T. G., & Tallam, R. M. *Detecting load unbalance and shaft misalignment using stator current in inverter-driven induction motors*. In Electric Machines and Drives Conference, 2003. IEEE International (Vol. 3, pp. 1454-1458).

[54] Wang, L. *Induction motor bearing fault detection using a sensorless approach*, PhD Thesis, 2007, Texas A&M University.

[55] Zhu, H. Y., Hu, J. T., Gao, L., & Huang, H. *Practical aspects of broken rotor bars detection in PWM voltage-source-inverter-fed squirrel-cage induction motors.* Journal of Applied Mathematics, 2013.

[56] Haram , M., Wang, T., Gu, F., & Ball, A. *An Investigation of the electrical response of a variable speed motor drive for mechanical fault diagnosis*. COMADEM, 2011.

[57] Benghozzi , A., Shao, Y., Shi, Z., Gu, F., & Ball, A. D. *The diagnosis of a gearbox transmission system using electrical control parameters*. In Automation and Computing (ICAC), 2012 18th International Conference on. IEEE.

[58] Lane , M., Ashari, D., Gu, F., & Ball, A. D. *Investigation of Motor Current Signature Analysis in Detecting Unbalanced Motor Windings of an Induction Motor with Sensorless Vector Control Drive*. In Vibration Engineering and Technology of Machinery, 2015, Springer. p. 801-810.

[59] Abusaad, S., Benghozzi, A., Shao, Y. M., Gu, F. S., & Ball, A. *Utilizing data from a sensorless AC variable speed drive for detecting mechanical misalignments*. In Key Engineering Materials. Vol. 569. Trans Tech Publications, 2013.

[60] Hamad, N., Brethee, K. F., Gu, F., & Ball, A. D. *An investigation of electrical motor parameters in a sensorless variable speed drive for machine fault diagnosis*. In Automation and Computing (ICAC), 2016 22nd International Conference on (pp. 329-335). IEEE.

[61] Liang, B. *Condition Monitoring and Fault Diagnosis of Three-Phase Induction Motors*, PhD Thesis, 2001, in Science and Engineering,University of Manchester, Mnchester.

[62] Mustafa, M.O. *Faults Detection and Diagnosis for Three Phase Induction Machines*, PhD Thesis, 2012, Luleå University of Technology, Sweden.

[63] Kastha , D., & Bose, B. K. *Investigation of fault modes of voltage-fed inverter system for induction motor drive.* Industry Applications, IEEE Transactions on, 1994. 30(4): p. 1028-1038.

[64] Hughes , A., & Drury, W. *Electric motors and drives: fundamentals, types and applications*, 2013, Newnes.

[65] Parekh, R. *AC Induction Motor Fundamentals.* Microchip Technology Inc, 2003.

[66] Kovács, P.K. *Transient phenomena in electrical machines*. Vol. 100, 1984, Elsevier Amsterdam.

[67] Hughes, A. *Electric motors and drives: fundamentals, types and applications*, 1993, London, Butterworth-Heinemann.

[68] Say, M.G. *Alternating current machines*, 1986, Harlow, Longman Scientific and Technical.

[69] Hughes, E. and Smith, I. M. *Hughes electrical technology*, 1987, Harlow: Longman Scientific & Technical.

[70] Alwodai, A. *Motor Fault Diagnosis Using Higher Order Statistical Analysis of Motor Power Supply Parameters*, PhD Thesis, 2015, University of Huddersfield, Huddersfield.

[71] Lane, M. *Using the AC Drive Motor as a Transducer for Detecting Electrical and Electromechanical Faults*, 2011, University of Huddersfield.

[72] Malik , S., and Kluge, D. *ACS1000 world's first standard AC drive for medium-voltage applications.* ABB Review, 1998, 2(98): p. 4-11.

[73] Shaeboub , A., Abusaad, S., Hu, N., Gu, F., & Ball, A. D. *Detection and diagnosis of motor stator faults using electric signals from variable speed drives*. In Automation and Computing (ICAC), 2015 21st International Conference on (pp. 1-6). IEEE.

[74] Yu, Z., and Figoli, D. *AC Induction Motor control using constant V/Hz principle and Space Vector PWM technique with TMS320C240*. Texas Instruments Application Report SPRA284A, 1998.

[75] Xu, X., and Novotny, D. W. *Selection of the flux reference for induction machine drives in the field weakening region.* IEEE transactions on industry applications, 1992. 28(6): p. 1353-1358.

[76] Rashid, M.H. *Power electronics handbook: devices, circuits and applications*. Academic press, 2010.

[77] Crowder, R. *Electric Drives and Electromechanical Systems:* Applications and Control, Newnes, 2006.

[78] Bose, B.K. *Power electronics and variable frequency drives: technology and applications.* IEEE Press, 1997.

[79] El-Hawary, M. E. *Principles of electric machines with power electronic applications* IEEE Press, 2002.

[80] Skibinski , G., Maslowski, W., & Pankau, J. *Installation considerations for IGBT ac drives*. In Textile, Fiber, and Film Industry Technical Conference, IEEE 1997 Annual (pp. 6-12).

[81] Bernet, S., Teichmann, R., Zuckerberger, A., & Steimer, P. K. *Comparison of high-power IGBT's and hard-driven GTO's for high-power inverters.* Industry Applications, IEEE Transactions on, 1999. 35(2): p. 487-495.

[82] Turkel, S. S., and Solomon, S. *Understanding variable speed drives.* Engineering, Construction and Maintenance, 1997.

[83] Hiremath, C., and Kaur, P. *Implementation of sensorless vector control technique based on mras speed estimator for parallel connected induction motors.* International Journal of Scientific Research and Education, 2015.

[84] Zerdali, E., and Barut, M. *MRAS based real-time speed-sensorless control of induction motor with optimized fuzzy-PI controller*. International Symposium on Sensorless Control for Electrical Drives and Predictive Control of Electrical Drives and Power Electronics (SLED/PRECEDE), 2013. IEEE.

[85] Luo, Y., Wang, Z., Wei, G., & Alsaadi, F. E. *Robust $\mathscr{H}_\infty$ Filtering for a Class of Two-Dimensional Uncertain Fuzzy Systems With Randomly Occurring Mixed Delays.* IEEE Transactions on Fuzzy Systems, 2017, *25*(1): p. 70-83.

[86] Ahmed, A.H.O. *Speed sensorless vector control of induction motors using rotor flux based model reference adaptive system.* Journal of Engineering and Computer Science, 2015**.**

[87] ABB, *Technical Guide No. 100. High performance drives-speed and torque regulation*, in High Performance Drives-speed and torque regulation, 1996, ABB Industrial Systems.

[88] Stone, G. C. *A perspective on online partial discharge monitoring for assessment of the condition of rotating machine stator winding insulation.* IEEE Electrical Insulation Magazine, 2012. 28(5): p. 8-13.

[89] Sabaghi, M., & Farahani, H. F. *Monitoring of induction motor temperature under unbalanced supplying by stator resistance estimation.* Indian Journal of Science and Technology, 2012. 5(3): p. 2354-2359.

[90] Motor Reliability Working Group. *Report of large motor reliability survey of industrial and commercial installations, Part II.* IEEE Transactions on Industry Applications, 1985. IA-21(4): p. 865-872.

[91] Siddique, , A., Yadava, G. S., & Singh, B. *A review of stator fault monitoring techniques of induction motors.* Energy Conversion, IEEE Transactions on, 2005. 20(1): p. 106-114.

[92] Ye, Z., & Wu, B. *Simulation of electrical faults of three phase induction motor drive system.* In Power Electronics Specialists Conference (PESC), 2001 32nd Annual (Vol. 1, pp. 75-80). IEEE.

[93] Mehala, N. *Condition monitoring and fault diagnosis of induction motor using motor current signature analysis*, PhD Thesis, 2010, National Institute of Technology Kurukshetra, India.

[94] Henao, H., Martis, C., & Capolino, G. A. Capolino. *An equivalent internal circuit of the induction machine for advanced spectral analysis.* Industry Applications, IEEE Transactions on, 2004. 40(3): p. 726-734.

[95] Nandi, S., Toliyat, H. A., & Li, X. *Condition monitoring and fault diagnosis of electrical motors-a review.* Energy Conversion, IEEE Transactions on, 2005. 20(4): p. 719-729.

[96] Alwodai, A., Shao, Y., Yuan, X., Ahmed, M., Gu, F., & Ball, A. D. *Inter-turn short circuit detection based on modulation signal bispectrum analysis of*

motor current signals. In Automation and Computing (ICAC), 2013 19th International Conference on (pp. 1-6). IEEE. Brunel University.

[97] Cusidó, J., Romeral, L., Ortega, J. A., Garcia, A., & Riba, J. *Signal injection as a fault detection technique.* Sensors, 2011, 11(3): p. 3356-3380.

[98] Kalpana , K., and Agarawal, A. *Fault diagnosis of three phase induction motor using fuzzy logic controller and sequence analyzer*. MIT International Journal of Electrical and Instrumentation Engineering, 2012, 2(2), p. 112-118.

[99] Sridhar, S., and Rao, K. U. *Detection of simultaneous unbalanced under-voltage and broken rotor fault in induction motor*. In Condition Assessment Techniques in Electrical Systems (CATCON), 2013 1st International Conference on (pp. 48-53). IEEE.

[100] Mirabbasi, D., Seifossadat, G., & Heidari, M. *Effect of unbalanced voltage on operation of induction motors and its detection*. In Electrical and Electronics Engineering, 2009. IEEE.

[101] Alwodai, A., Wang, T., Chen, Z., Gu, F., Cattley, R., & Ball, A. *A study of motor bearing fault diagnosis using modulation signal bispectrum analysis of motor current signals.* Journal of Signal and Information Processing, 2013. 4(03), 72.

[102] Shrivastava , A., & Wadhwani, S. *Condition monitoring for inner raceway fault of induction motor ball bearings.* International Journal of Electrical Engineering, 2012. 5(3): p. 239-244.

[103] Stack, J. R., Habetler, T. G., & Harley, R. G. *Fault classification and fault signature production for rolling element bearings in electric machines.* Transactions on Industry Applications, 2004. 40(3): p. 735-739. IEEE.

[104] Blodt, M., Granjon, P., Raison, B., & Rostaing, G. *Models for bearing damage detection in induction motors using stator current monitoring.* IEEE Transactions on Industrial Electronics, 2008. 55(4): p. 1813-1822.

[105] Akin, B., Orguner, U., Toliyat, H. A., & Rayner, M. *Low order PWM inverter harmonics contributions to the inverter-fed induction machine fault diagnosis.* IEEE Transactions on Industrial Electronics, 2008. 55(2): p. 610-619.

[106] Ibrahim, A., El Badaoui, M., Guillet, F., & Bonnardot, F. *A new bearing fault detection method in induction machines based on instantaneous power factor.* IEEE Transactions on Industrial Electronics, 2008. 55(12): p. 4252-4259.

[107] Schoen, R. R., Habetler, T. G., Kamran, F., & Bartfield, R. G. *Motor bearing damage detection using stator current monitoring.* IEEE Transactions on Industry Applications, 1995. 31(6): p. 1274-1279.

[108] Yang, D. M. *Induction motor bearing fault diagnosis using Hilbert-based bispectral analysis*. In Computer, Consumer and Control (IS3C), 2012 International Symposium on (pp. 385-388). IEEE.

[109] Lau, E. C., & Ngan, H. W. *Detection of motor bearing outer raceway defect by wavelet packet transformed motor current signature analysis.* IEEE Transactions on Instrumentation and Measurement, 2010. 59(10): p. 2683-2690.

[110] Vas, P. *Parameter estimation, condition monitoring, and diagnosis of electrical machines*. Vol. 27, 1993, Oxford University Press.

[111] Dorrell, D. G., Thomson, W. T., & Roach, S. *Analysis of airgap flux, current, and vibration signals as a function of the combination of static and dynamic airgap eccentricity in 3-phase induction motors.* IEEE Transactions on Industry applications, 1997. 33(1): p. 24-34.

[112] Morinigo -Sotelo, D., García-Escudero, L. A., Duque-Perez, O., & Perez-Alonso, M. *Practical aspects of mixed-eccentricity detection in PWM voltage-source-inverter-fed induction motors.* IEEE Transactions on Industrial Electronics, 2010. 57(1): p. 252-262.

[113] Nandi, Nandi, S., Toliyat, H. A., & Parlos, A. G. *Performance analysis of a single phase induction motor under eccentric conditions*. In Industry Applications Conference, 1997. Thirty-Second IAS Annual Meeting. IEEE.

[114] Hong, J., Hyun, D., Lee, S. B., & Kral, C. *Offline monitoring of airgap eccentricity for inverter-fed induction motors based on the differential inductance.* IEEE Transactions on Industry Applications, 2013. 49(6): p. 2533-2542.

[115] Ghoggal, A., Zouzou, S. E., Razik, H., Sahraoui, M., & Khezzar, A. *An improved model of induction motors for diagnosis purposes–Slot skewing effect and air–gap eccentricity faults.* Energy Conversion and Management, 2009. 50(5): p. 1336-1347.

[116] Faiz, J., & Ojaghi, M. *Different indexes for eccentricity faults diagnosis in three-phase squirrel-cage induction motors: A review.* Mechatronics, 2009. 19(1): p. 2-13.

[117] Sahraoui M., Ghoggal, A., Zouzou, S. E., & Benbouzid, M. E. *Dynamic eccentricity in squirrel cage induction motors–Simulation and analytical study of its spectral signatures on stator currents.* Simulation Modelling Practice and Theory, 2008. 16(9): p. 1503-1513.

[118] Guldemir, H. *Detection of airgap eccentricity using line current spectrum of induction motors.* Electric Power Systems Research, 2003. 64(2): p. 109-117.

[119] Drif, M. H., & Cardoso, A. M. *Airgap-eccentricity fault diagnosis, in three-phase induction motors, by the complex apparent power signature analysis.* IEEE Transactions on Industrial Electronics, 2008. 55(3): p. 1404-1410.

[120] Bellini, A., Filippetti, F., Franceschini, G., Tassoni, C., & Kliman, G. B. *Quantitative evaluation of induction motor broken bars by means of electrical signature analysis.* IEEE Transactions on Industry Applications, 2001. 37(5): p. 1248-1255.

[121] Martins , J. F., Pires, V. F., & Amaral, T. *Induction motor fault detection and diagnosis using a current state space pattern recognition.* Pattern Recognition Letters, 2011. 32(2): p. 321-328.

[122] Filippetti, F., Franceschini, G., Tassoni, C., & Vas, P. *AI techniques in induction machines diagnosis including the speed ripple effect.* IEEE Transactions on Industry Applications, 1998. 34(1): p. 98-108.

[123] Cerna, M., & Harvey, A. F. *The fundamentals of FFT-based signal analysis and measurement.* National Instruments, Junho, 2000.

[124] Mehala, N., & Dahiya, R. *A comparative study of FFT, STFT and wavelet techniques for induction machine fault diagnostic analysis*. In Proceedings of the 7th WSEAS International Conference on Computational Intelligence, Man-Machine Systems and Cybernetics, Cairo, Egypt, 2008.

[125] Engineering, R. A. O. *The Study of Root Mean Square (RMS).* Royal Academy of Engineering, 2011.

[126] Bin Hasan, M. M. A. *Current based condition monitoring of electromechanical systems*, PhD Thesis, 2012, University of Bradford.

[127] Jardine, A. K., Lin, D., & Banjevic, D. *A review on machinery diagnostics and prognostics implementing condition-based maintenance.* Mechanical Systems and Signal Processing, 2006. 20(7): p. 1483-1510.

[128] Tandon, N., & Choudhury, A. *A review of vibration and acoustic measurement methods for the detection of defects in rolling element bearings.* Tribology International, 1999. 32(8): p. 469-480.

[129] Iorgulescu, M., & Beloiu, R. *Vibration and current monitoring for fault's diagnosis of induction motors.* Annals of the University of Craiova, electrical engineering series, 2008, 57(32): p. 102-107.

[130] Heckbert, P. *Fourier Transforms and the Fast Fourier Transform (FFT) Algorithm.* Comp. Graph 2, 1995: 15-463.

[131] Kalaskar, C. S., & Gond, V. J. *Motor Current Signature Analysis to Detect the Fault in Induction Motor*. International Journal of Engineering Research and Applications, 2014. Vol. 4(6): p. 58-61.

[132] Treetrong, J. *Fault Detection of Electric Motors Based on Frequency and Time- Frequency Analysis using Extended DFT*. International Journal of Control and Automation, 2011, 4(1): 49-58.

[133] Hongxi, W., & Weidong, Y. *Rotor bar fault feature extraction of induction motor base on FFT and MUSIC*. In *Mechatronic Science, Electric Engineering and Computer (MEC), 2011*. IEEE.

[134] McInerny, S. A., & Dai, Y. *Basic vibration signal processing for bearing fault detection.* IEEE Transactions on education, 2003. 46(1): p. 149-156.

[135] Liang, B., Iwnicki, S. D., & Zhao, Y. *Application of power spectrum, cepstrum, higher order spectrum and neural network analyses for induction motor fault diagnosis.* Mechanical Systems and Signal Processing, 2013. 39(1): p. 342-360.

[136] Mehala, N., & Dahiya, R. *Condition monitoring methods, failure identification and analysis for Induction machines.* International Journal of Circuits, Systems and Signal Processing, 2009. 3(1): p. 10-17.

[137] Habu, U., Brethee, K., Hassin, O., Gu, F., & Ball, A. *Detection and Diagnosis of Reciprocating Compressor Faults Based on Modulation Signal Bispectrum Analysis of Vibrations.* In: COMADEM 2017, University of Central Lancaster.

[138] Hassin, , O., Yao, A., Gu, F., & Ball, A. *Journal bearing condition monitoring based on the modulation signal bispectrum analysis of vibrations*. In: Proceedings of the International Conference on Power Transmissions (ICPT), 2016. Taylor & Francis, pp. 907-912. ISBN 9781138032675.

[139] Tian, X., Abdallaa, G. M., Rehab, I., Gu, F., Ball, A. D., & Wang, T. *Diagnosis of combination faults in a planetary gearbox using a modulation signal bispectrum based sideband estimator*. In Automation and Computing (ICAC), 2015 .IEEE.

[140] Cochran, P. *Polyphase Induction Motors, Analysis: Design, and Application*. 1989, CRC Press.

[141] Raharjo, P. *An Investigation of Surface Vibration, Airbourne Sound and Acoustic Emission Characteristics of a Journal Bearing for Early Fault Detection and Diagnosis*, PhD Thesis, 2013, University of Huddersfield.

[142] Rehab, I.A. *The Optimization of Vibration Data Analysis for the Detection and Diagnosis of Incipient Faults in Roller Bearings*, PhD Thesis, 2016, University of Huddersfield.

[143] Milimonfared, J., Kelk, H. M., Nandi, S., Minassians, A. D., & Toliyat, H. A. *A novel approach for broken-rotor-bar detection in cage induction motors.* IEEE Transactions on Industry Applications, 1999. 35(5): p. 1000-1006.

[144] Shaeboub, A., Lane, M., Haba, U., Gu, F., & Ball, A. D. *Detection and diagnosis of compound faults in induction motors using electric signals from variable speed drives*. In Automation and Computing (ICAC), 2016. IEEE.

[145] Lane, M., Shaeboub, A., Gu, F., & Ball, A. D. *Investigation of Reductions in Motor Efficiency caused by Stator Faults when operated from an Inverter Drive*. In Automation and Computing (ICAC), 2016. IEEE.

[146] Haba, U., Feng, G., Shaeboub, A., Peng, X., Gu, F., & Ball, A. *Detection and Diagnosis of Compound Faults in a Reciprocating Compressor based on Motor Current Signatures.* In: COMADEM 2016, the 29th International Congress on Condition Monitoring and Diagnostic Engineering Management, Empark Grand Hotel in Xi'an, China.

[147] Korde, A. *Online Condition Monitoring of Motors Using Electrical Signature Analysis.* Recent Advances in Condition-Based Plant Maintenance. In Seminar Organized by Indian Institute of Plant Engineers, Mumbai, India. Vol. 1718. 2002.

[148] Penman, J., Sedding, H. G., Lloyd, B. A., & Fink, W. T. *Detection and location of interturn short circuits in the stator windings of operating motors.* IEEE Transactions on Energy Conversion, 1994. 9(4): p. 652-658.

[149] Thomson, W.T. *On-line MCSA to diagnose shorted turns in low voltage stator windings of 3-phase induction motors prior to failure*. In Electric Machines and Drives Conference (IEMDC), 2001. IEEE.

[150] Joksimovic, G. M., & Penman, J. *The detection of inter-turn short circuits in the stator windings of operating motors.* IEEE Transactions on Industrial Electronics, 2000. 47(5): p. 1078-1084.

[151] Duan, F. *Diagnostics of rotor and stator problems in industrial induction motors*. School of Electrical and Electronic Engineering, 2010, The Unversity of Adelaide, Australia.

[152] Stone, G. C., Boulter, E. A., Culbert, I., & Dhirani, H. *Electrical insulation for rotating machines: design, evaluation, aging, testing, and repair* (Vol. 21), 2004. John Wiley & Sons.

[153] Jonathan, S. *Finite element and electrical circuit modelling of faulty induction machines: Study of internal effects and fault detection techniques*, PhD Thesis, 2007, University Libre de Bruxelles.

[154] Bonnett, A. H., & Soukup, G. C. *Cause and analysis of stator and rotor failures in three-phase squirrel-cage induction motors.* IEEE Transactions on Industry applications, 1992. 28(4): p. 921-937.

[155] Garcia-Perez, A., de Jesus Romero-Troncoso, R., Cabal-Yepez, E., & Osornio-Rios, R. A. *The application of high-resolution spectral analysis for identifying multiple combined faults in induction motors.* IEEE Transactions on Industrial Electronics, 2011.

[156] Constantine, R.A.E. *Effects of Mixed Faults on the Stator Current Spectrum of the Induction Machine,* 2014, WSEAS, Conference/ELECT-06, Istanbul.

[157] Haba, U., Feng, G., Shaeboub, A., Peng, X., Gu, F., & Ball, A. D. *Motor Current Signature Analysis for the Compound Fault Diagnosis of Reciprocating Compressors.* International Journal of COMADEM, 2017, 20(3). ISSN: 1363-7681.

[158] Haba, U., Shaeboub, A., Mones, Z., Gu, F., & Ball, A. *Diagnosis of Compound Faults in Reciprocating Compressors Based on Modulation Signal Bispectrum of Current Signals*. In Proceedings of the 2nd International Conference on Maintenance Engineering, IncoME-II 2017, University of Manchester.

Appendix A

Time Domain Features Using Open Loop Control and Sensorless Control Modes for Detection and Diagnosis Stator Fault

This section presents time domain features of MCSA , voltage signature analysis and vibration analysis for healthy motor and motor with stator fault at 0% and 80% of full load and 50% full speed using open loop and sensorless control modes.

Figure A.1 shows healthy motor and motor with stator fault at 50% motor speed with different loads under open loop and sensorless control modes. It can be seen that the motor speed decrease as motor fault and load increase using open loop and the speed approximately constant with respect to sensorless control.

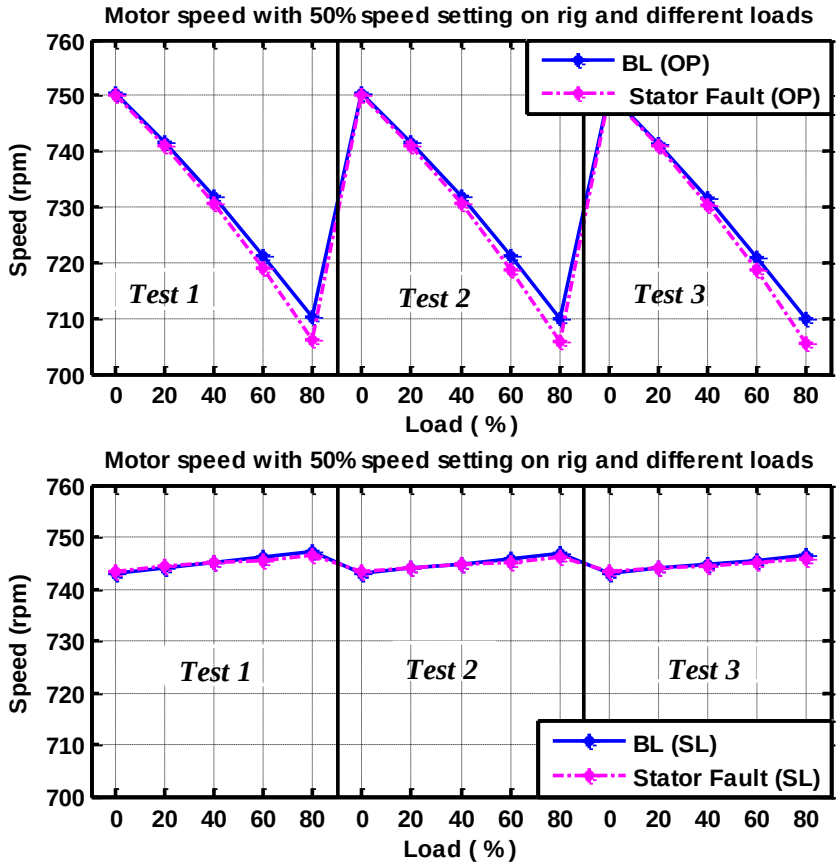

Figure A. 1 A healthy motor and motor with stator fault at 50% motor speed with different loads under OP and SL control modes.

Figure A. 2 shows stator phase current for healthy motor and motor with stator fault condition at 50% motor speed with 0% and 80% of full load under open loop and sensorless control modes. It seems clear from the Fig A.2 the current value changes with load. This means that increasing in load leads to increase in motor current and also there is a difference between healthy motor and motor with stator fault with respect to open loop and sensorless control mode.

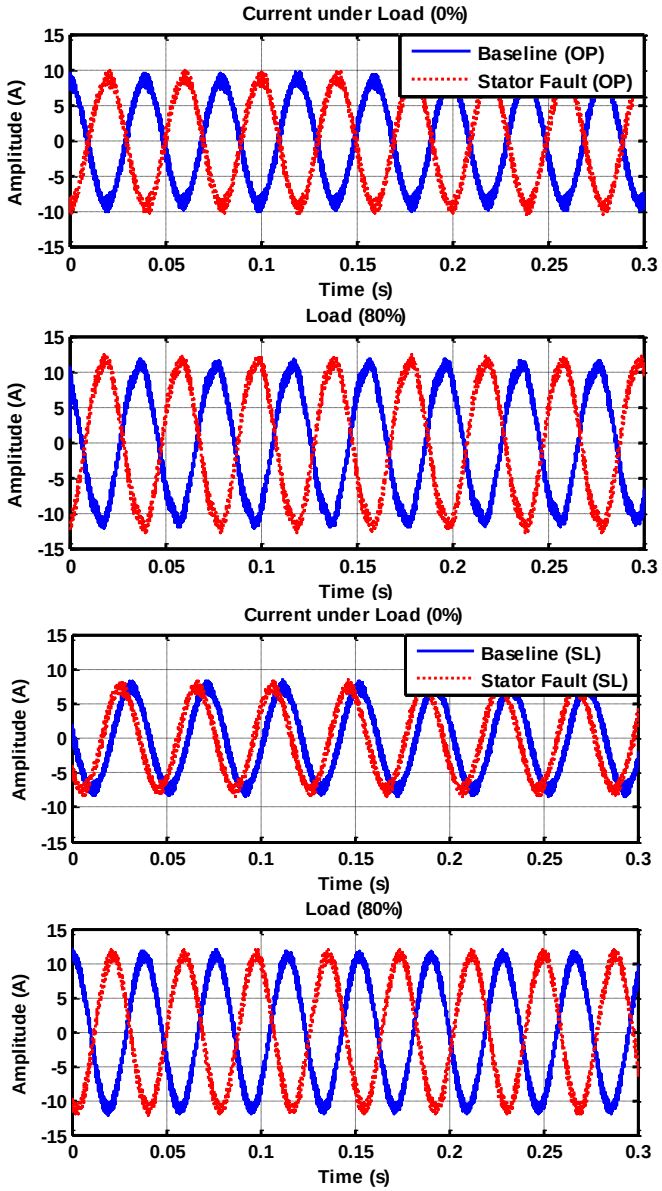

Figure A. 2 A stator phase current for healthy motor and motor with stator fault condition at 50% motor speed with 0% and 80% full load under OP and SL control modes.

Figure A. 3 shows motor voltage signature analysis for healthy and motor with stator fault at 50% motor speed with different loads, 0% and 80% full load under open loop control and sensorless control modes.

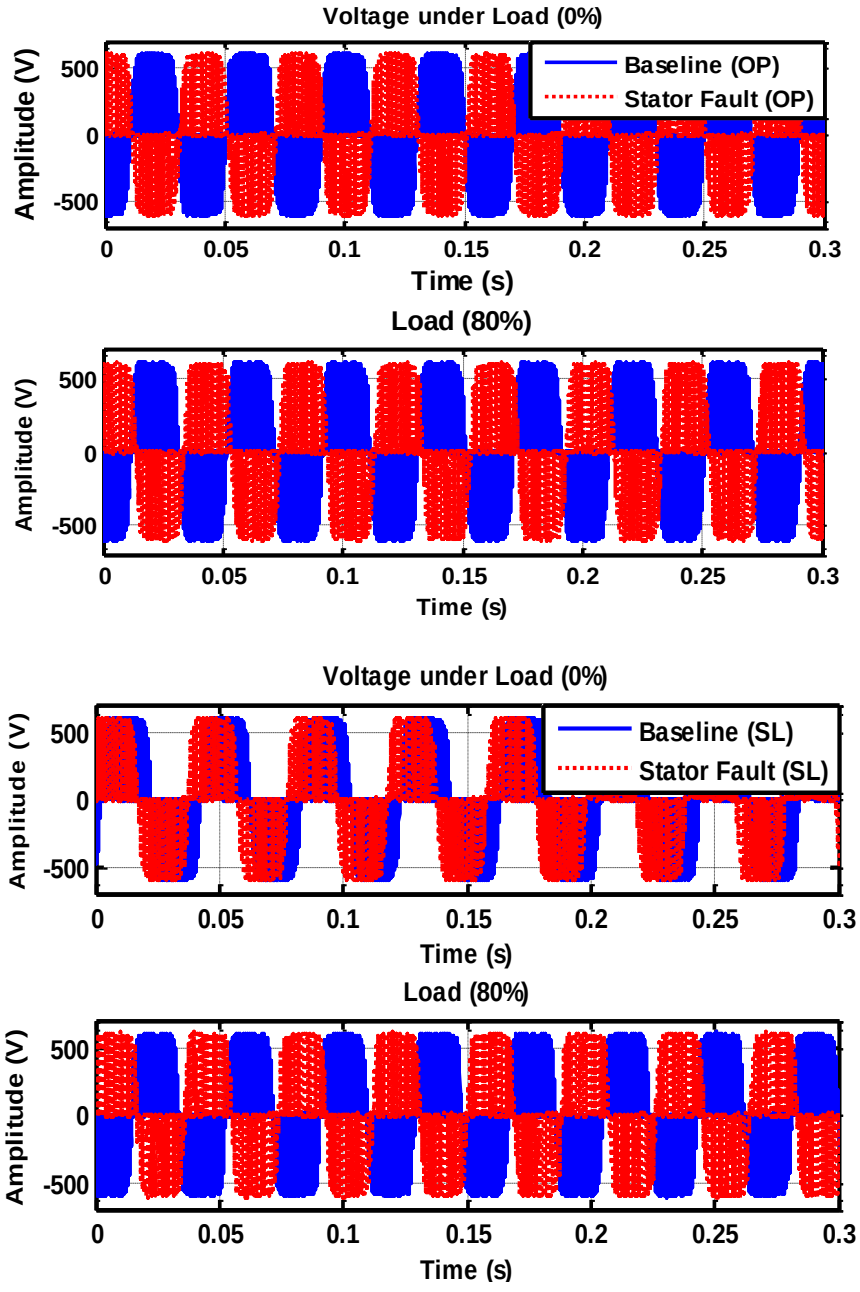

Figure A . 3 A stator phase voltage for healthy motor and motor with stator fault at 50% motor speed with 0% and 80% full load under OP and SL control modes.

Figure A. 4 shows motor vibration signature analysis for healthy motor and motor with stator fault at 50% motor speed with 0% and 80% of full load under open loop and sensorless control modes. It can be seen that there is a difference between healthy motor and motor with stator fault in signature analysis of vibration with respect to open loop and sensorless control operations and also this difference can be seen with different loads.

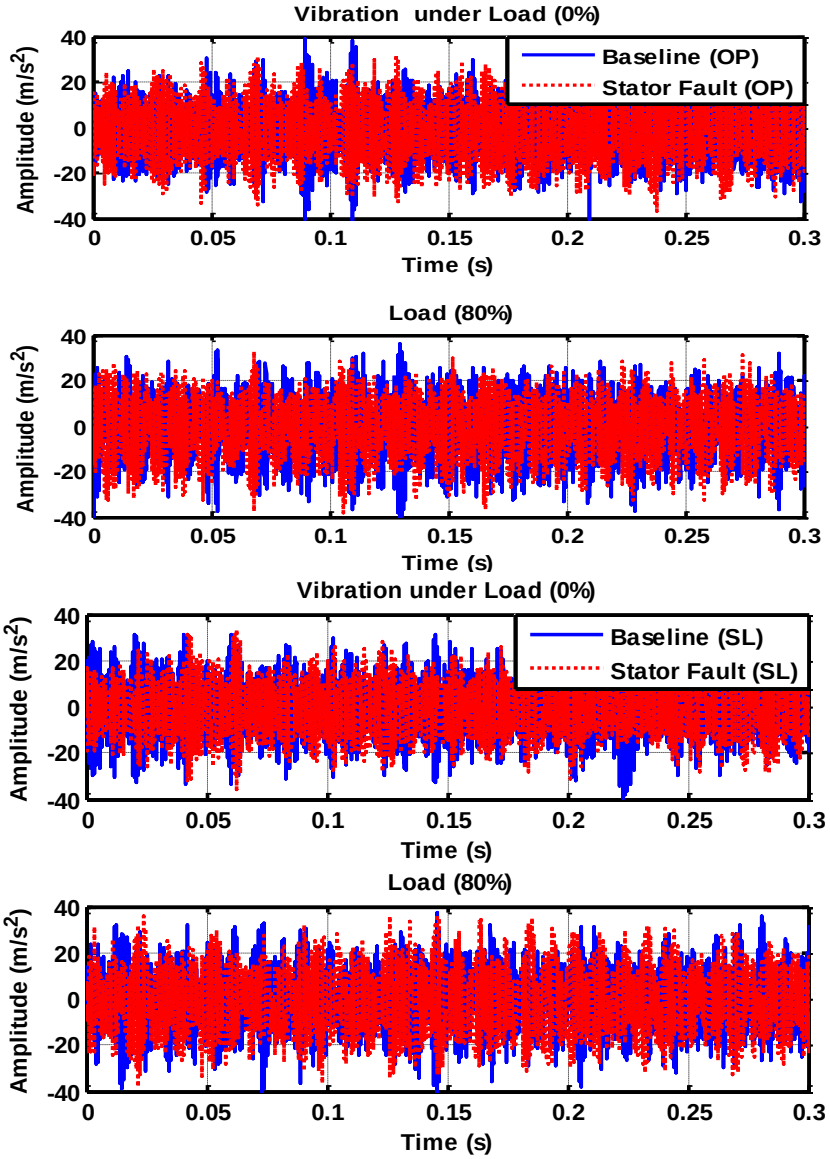

Figure A. 4 Motor vibration signature analysis for healthy motor and motor with stator fault at 50% motor speed with 0% and 80% full load under OP and SL control modes

Appendix B

Time Domain Features Using Open Loop Control and Sensorless Control Mode for Detection and Diagnosis Rotor Fault

This section presents time domain features of MCSA, voltage signature analysis and vibration analysis for healthy motor and motor with rotor fault at 75% full motor speed under 0% and 80% full load and using open loop and sensorless control modes.

Figure B. 1 show healthy motor and motor with stator fault at 75% motor speed with different loads under open loop and sensorless control modes. It can be seen that the motor speed decrease as motor fault and load increase in open loop. However, small changes can be seen with sensorless operatin.

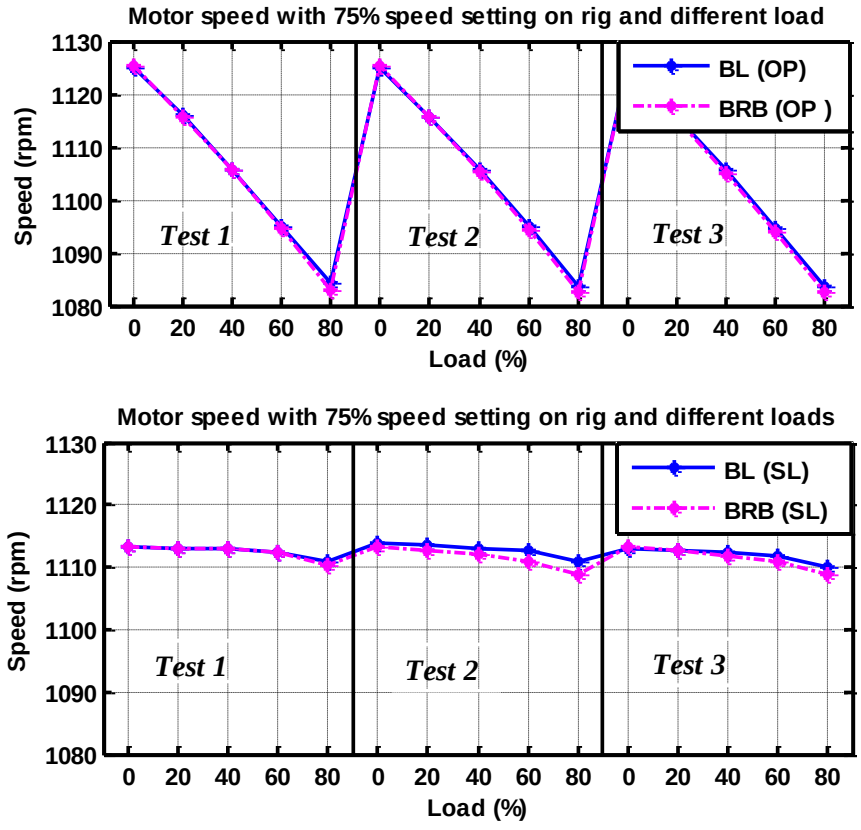

Figure B.1 A healthy motor and motor with rotor fault at 75% motor speed with different loads using OP and SL control modes

Figure B. 2 shows stator phase current for healthy motor and motor with rotor fault condition at 75% motor speed and at 0% and 80% full load using open loop and sensorless control modes. It seems clear from the Fig B 2 the current value changes with load. This means that increasing in load leads to increase in motor current. Also there is different in the current values from open loop and sensorless operations.

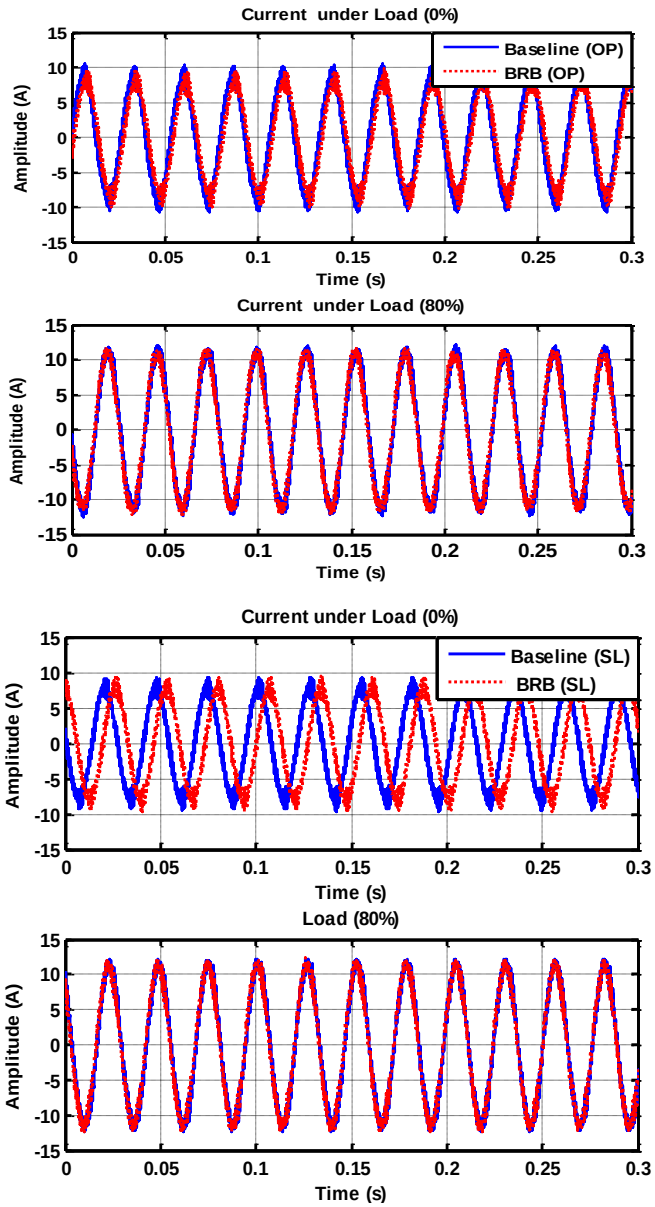

Figure B. 2 Stator phase current for healthy and motor with rotor fault at 75% motor speed with 0% and 80% full load under OP and SL control mode

Figure B. 3 shows motor voltage signature analysis for healthy motor and motor with rotor fault at 75% motor speed under 0% and 80% full load using open loop and sensorless control mode.

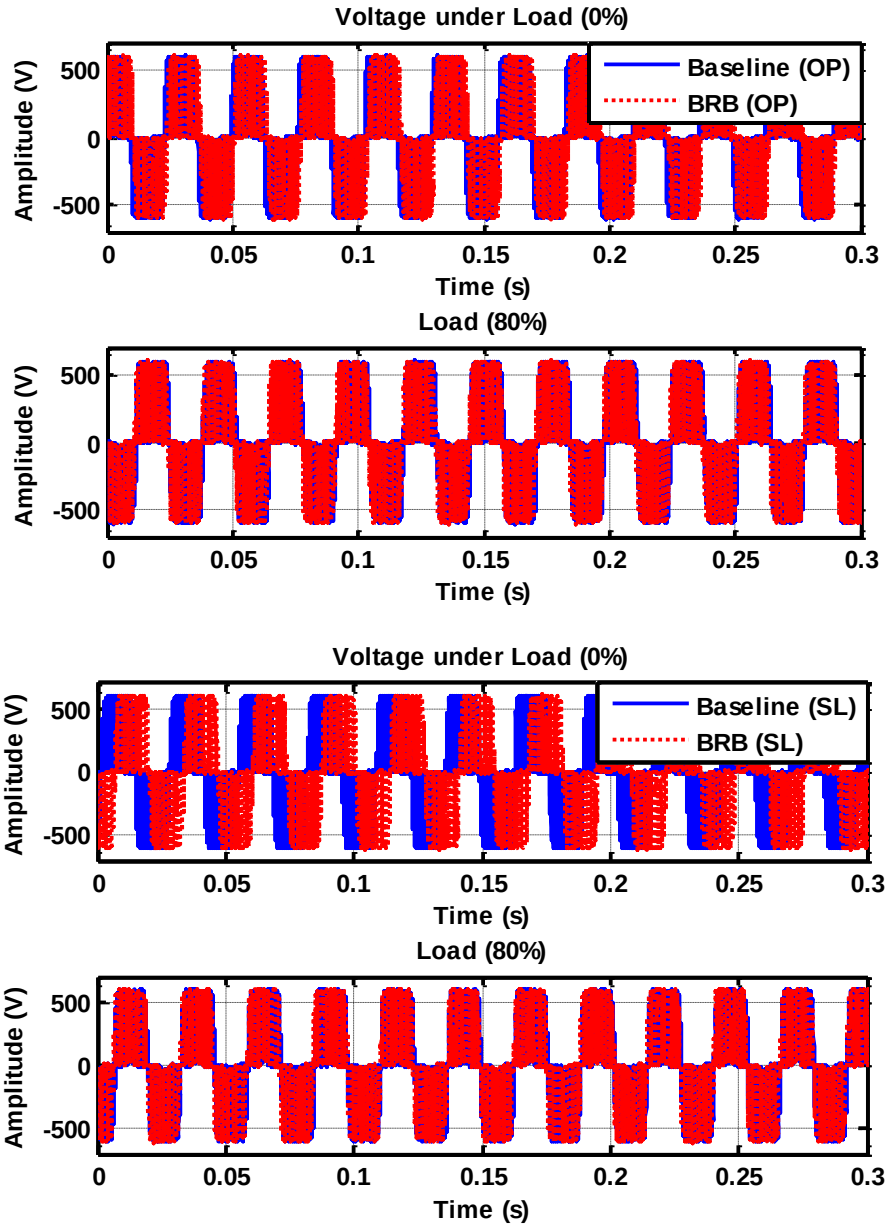

Figure B. 3 Motor voltage signature analysis for healthy motor and motor with rotor fault at 75% motor speed with 0% and 80% full load under OP and SL control modes

Figure B. 4 shows motor vibration signature analysis for healthy motor and motor with rotor fault at 75% motor speed with 0% and 80% of full load under open loop

control and sensorless control modes. It can be seen that there is a difference between healthy motor and motor with rotor fault in signature analysis of vibration and also this difference can be seen with different loads and different speeds.

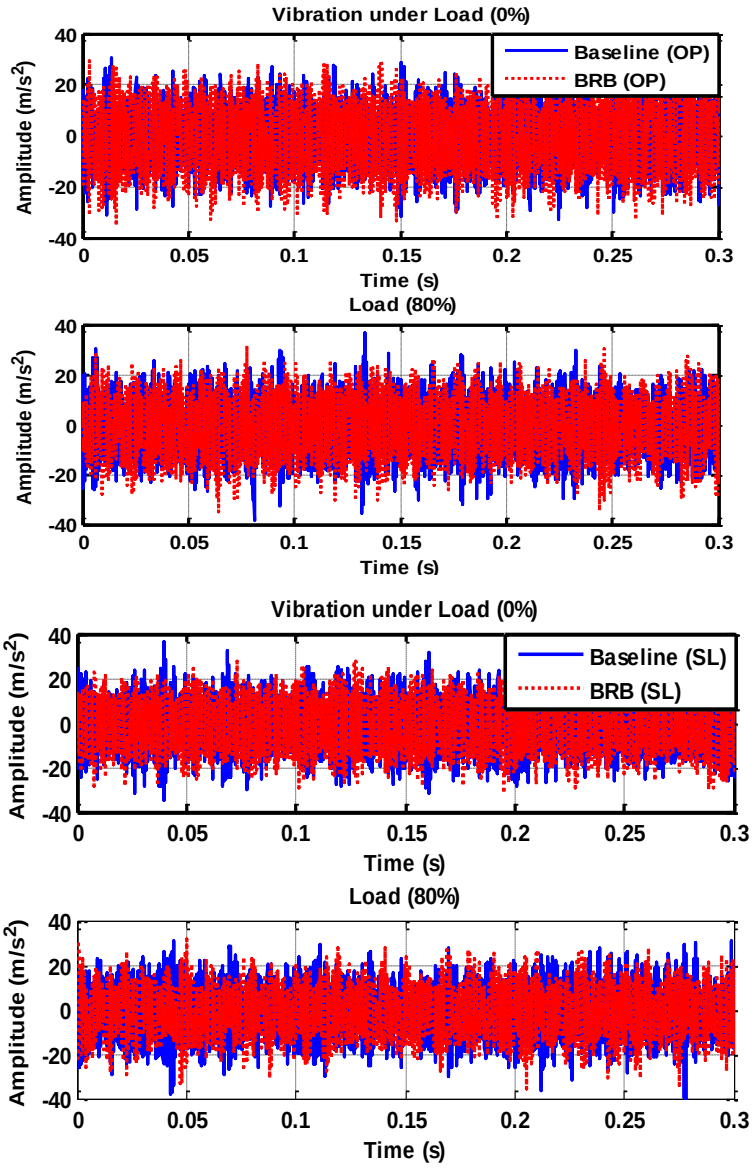

Figure B. 4 Motor vibration signature analysis for healthy and motor with rotor fault at 75% motor speed with 0% and 80% of full load under OP and SL control mode